Doctoral Thesis ETH No. 16353

The Structure-Function Relationship of Stathmin and EB1- Two Key Proteins Regulating Microtubule Dynamics

A dissertation submitted to the
SWISS FEDERAL INSTITUTE OF TECHNOLGY ZURICH
for the degree of
Doctor of Natural Sciences

presented by

Honnappa Srinivas
MSc. (Biochemistry), UAS, Bangalore
born May 12th, 1975
citizen of India

accepted on the recommendation of
Prof. Fritz K. Winkler, examiner
Prof. Joachim Seelig, co-examiner
Dr. Michel O. Steinmetz, co-examiner

Paul Scherrer Institut, Villigen, 2005

Table of contents

List of Original Publications

This thesis comprises the following original publications.

Honnappa, S., Cutting, B., Jahnke, W., Seelig, J. and Steinmetz M.O. 2003. Thermodynamics of the Op18/stathmin-tubulin interaction. *J. Biol. Chem.* **278**, 38926-38934.

Honnappa, S., John, C.M., Kostrewa, D., Winkler, F.K. and Steinmetz M.O**.** 2005. Structural insights into the EB1-APC interaction. *EMBO J.* **24**, 261-269.

Honnappa, S., Jahnke, W., Seelig, J. and Steinmetz M.O. 2005. Control of intrinsically disordered stathmin function by multisite phosphorylation. *Submitted*

I. Zusammenfassung

Mikrotubuli (MTs) sind Polymere aufgebaut aus αβ-Tubulin Heterodimere, welche zwischen Wachstums- und Schrumpfphasen wechseln können und deshalb dynamische Strukturen darstellen. Sie sind für eine Reihe von biologischen Prozessen wie Mitose, Zellbewegung, neuronale Differenzierung und Cargo Transport wichtig. Die dynamischen Eigenschaften der MTs sind durch stabilisierende und destabilisierende, zelluläre Faktoren reguliert. Meine Doktorarbeit hat das Verstehen der Struktur-Funktionsbeziehung von zwei Schlüsselproteinen, Stathmin und EB1 (end binding protein 1), welche in der Regulation der Dynamik von MTs eine Rolle spielen zum Ziel. Ich bin spezifische Fragen betreffend der Stathmin Struktur und des Wirkungsmechanismus der Tubulin-Stathmin Wechselwirkung in Abhängigkeit von Phosphorylierung angegangen. Meine Doktorarbeit liefert zudem Einsichten in Strukturbestimmende Elemente der EB1-Adenomateous Polyposis Coli Tumor Suppressor (APC) Wechselwirkungen.

Stathmin ist ein intrinsisch unstrukturiertes, kleines Protein, welches ternäre Komplexe mit Tubulin bildet, um die MT Polymerisation zu inhibieren. Obwohl die MT destabilisierende Aktivität von Stathmin etabliert ist, fehlen uns Einsichten in den darunter liegenden molekularen Mechanismus. Meine Doktorarbeit liefert eine detaillierte thermodynamische Analyse der Tubulin-Stathmin Wechselwirkung.

Die Aktivität von Stathmin ist über Phosphorylierung von vier Serinen (Ser16, Ser25, Ser38 und Ser63) reguliert. Um Einsichten in die Auswirkung von Phosphorylierung auf die Funktion von Stathmin zu erlangen, habe ich für die Produktion von sieben Stathmin Phosphoisoformen in milligramm Mengen Protokolle entwickelt. Mittels kalorimetrischen und spektroskopischen Methoden, zusammen mit der kürzlich veröffentlichten Kristallstruktur von einem Tubulin-Stathmin Komplex dokumentiere ich in meiner Doktorarbeit die molekulare Basis, um den Effekt von multipler Stathmin Phosphorylierung zu verstehen. Wir haben herausgefunden, dass Phosphorylierung von Ser16 und Ser63 am stärksten zur Inaktivierung der Stathmin Aktivität beiträgt, konsistent mit den publizierten *in vivo* Daten. Die Phosphorylierung von Ser16 hindert sterisch die Wechselwirkung der Aminosäure Seitenkette mit der α-Tubulin Untereinheit. Die Phosphorylierung von Ser63

zerstört die Struktur der Stathmin Helix, ohne die Berührungsfläche von Stathmin mit Tubulin zu beeinflussen.

EB1 ist ein Mitglied der so genannten plus Ende Proteinen (+TIP), welches als Schlüsselspieler für die Modulation der MT Dynamik in allen eukaryotischen Zellen aufgekommen ist. Voraussetzung für die räumliche und temporäre Ansammlung von +TIP Proteinen sind Protein-Protein Wechselwirkungen am wachsenden MT plus Ende. Das Kernstück dieses Netzwerkes ist EB1 und seine Familienmitglieder. Obwohl grosse Fortschritte dazu geführt haben, dass wir die Wechselwirkungsnetzwerke zwischen +TIP Proteine kennen, fehlen uns Einblicke in die strukturelle Basis deren Wirkungsweise.

Meine Doktorarbeit hat das Ziel mittels eines integrierten biophysikalischen und biochemischen Ansatzes, EB1-vermittelte Wechselwirkungsnetzwerken im atomaren Detail zu verstehen. Wir habe herausgefunden, dass EB1 als stabiles Homodimeres mit einem parallelem Coiled Coil vorliegt, und dass die Dimerisation unablässig für die Faltung der C-terminalen EB1 Domäne ist. Zudem berichtet meine Doktorarbeit die erste Kristallstruktur der C-terminalen EB1 Domäne. Diese Domäne besitzt ein einzigartiges, EB1-ähnliches Sequenzmotiv, welches als Wechselwirkungsstelle für andere +TIP Proteine zu Funktionieren scheint. Die dimere Domäne weist einen hoch konservierten Oberflächenbereich mit einer tiefen hydrophoben Furche in der Mitte auf. Meine Doktorarbeit dokumentiert ferner, dass zwei Aminosäuren (Ile2805 und Pro2806) von APC für die Wechselwirkung mit EB1 unablässig sind. Gestützt durch die strukturellen Erkenntnisse schlage ich vor, dass die Isoleucin Seitenkette die hydrophobe Furche besetzt.

Die vorliegende Doktorarbeit liefert ein Beispiel eines experimentellen Ansatzes für die Erforschung von mechanistischen Fragen betreffend intrinsisch unstrukturierten Proteinen, für die Untersuchung der funktionellen Rolle von multipler Proteinphosphorylierung und für die Bestimmung der Affinität und Eigenheiten von dynamischen Protein-Protein Wechselwirkungen.

I. Summary

Microtubules (MTs) are polymers made of αβ-tubulin heterodimers that can switch between growing and shrinking phases and thus represent dynamic structures. They are important for widely different processes, which include mitosis, cell migration, neuronal differentiation and transport of cargo. The dynamic properties of MTs are regulated by many stabilizing and destabilizing cellular factors. This thesis aims to understand the structure-function relationship of two key proteins stathmin and EB1 (end binding protein 1) involved in regulating MT dynamics. In particular, I wanted to address specific questions concerning the structure of stathmin and the mechanism of action of the phosphorylation-controlled stathmin-tubulin interaction. In addition, the thesis aimed to investigate structural determinants of the EB1-ademato us polyposis coli tumor suppressor (APC) interaction.

Stathmin is an intrinsically disordered small protein that forms ternary complexes with tubulin to inhibit MT polymerization. Although the MT-destabilizing activity of stathmin is well established, the exact molecular mechanism has not been fully resolved. My thesis provides the first detailed thermodynamic analysis of the tubulin-stathmin interaction. The thesis establishes that stathmin primarily regulates MT dynamics by sequestering tubulin subunits.

The activity of stathmin is tightly regulated by phosphorylation of four serine residues (Ser16, Ser25, Ser38, and Ser63). In order to gain insights into the consequences of phosphorylation, I established protocols for the preparation of milligram amounts of seven stathmin phosphoisoforms. Using calorimetric and spectroscopic methods in addition to the recently published X-ray crystal structure of a tubulin-stathmin complex, the thesis provides a molecular basis for understanding the down-regulating effect of multisite stathmin phosphorylation. We found that phosphorylation of Ser16 and 63 contribute most to the inactivation of stathmin consistant with *in vivo* data. Phosphorylation of Ser16 sterically hinders the interaction of the residue side chain with the α-tubulin subunit, and phosphorylation of Ser63 disrupts the stathmin helix structure without compromising the contact interface between the two molecules.

EB1 is a member of so called plus-tip proteins (+TIPs) that emerged as a key player in the modulation of MT dynamics in eukaryotic organisms. Protein-protein interactions at the growing MT plus ends create a dynamic network that is required for spatial and temporal accumulation of +TIP proteins. The core element of this network is EB1 and its family members. Despite the substantial progress that has been made in identifying the interaction networks among +TIP proteins, we still lack insight into the structural basis of their mode of action.

Using an integrated biophysical and biochemical approach, this thesis aims to understand EB1-mediated interaction networks at the atomic level. We found that EB1 is a stable homodimer with a parallel coiled-coil, and showed that dimerization is essential for the folding of its C-terminal domain. In addition, the thesis reports the first crystal structure of the EB1 C-terminal domain. It harbors a unique sequence motif, which is seen to shape a binding site for other +TIP proteins. The highly conserved surface patch displays a deep hydrophobic cavity at its centre. I demonstrate that two residues (Ile2805 and Pro2806) of APC are essential for the interaction with EB1 and based on these structural insights, I propose that the isoleucine side chain occupies this cavity.

The thesis exemplifies experimental approaches for exploring mechanistic questions regarding intrinsically disordered proteins, for studying the role of multi-site phosphorylation and to determine the strength and nature of dynamic protein-protein interactions.

II. Introduction

1. The Cytoskeleton

The cytoskeleton is a network of protein fibers in the cytoplasm that gives shape to a cell and mediates cell movement. The cytoskeleton provides a scaffold to structure the cytoplasm, lends the cell mechanical stability, serves as tracks for the transport of proteins and vesicles within the cell, and directs intracellular organization by positioning organelles. The cytoskeleton also plays an essential role when cells rearrange their internal components as they grow, divide, or adapt to changing circumstances. These processes are accompanied and driven by a rearrangement of the cytoskeleton. Generally, the cytoskeleton consists of protein subunits that polymerise into fibre-like structures.

There are three major types of cytoskeleton in cells: actin filaments, microtubules and intermediate filaments. In addition, a growing body of evidence indicates that septins constitute a fourth component of the cytoskeleton. These cytoskeletal networks assemble by incorporating small building blocks (actin, tubulin or intermediate filament proteins, respectively) into filamentous polymers. Intermediate filaments assemble through the association of antiparallel dimers into apolar filaments. The incorporation of actin and tubulin subunits, by contrast, occurs in a head-to-tail fashion and generates polar fibres. Furthermore, actin and tubulin subunits hydrolyse phosphate bonds after incorporation. In the case of microtubules, energy is stored in the fibre and released on disassembly. Whereas intermediate filaments mainly confer strength to a cell, actin filaments and microtubules are used to sustain and adapt cellular shape. The polarized nature of the latter two cytoskeletal systems allow a cell to generate asymmetry.

1.1 Actin

Actin is a 43 kDa monomeric protein that polymerizes into double-helical filaments. Actin filaments are highly dynamic polymers of about 6 nm in diameter that form by the polymerization of globular G-actin monomers. The filaments consist of two intertwined helical strands that form a left-handed helix. Actin is an ATPase that binds ATP in a cleft buried deep inside the molecule facing the minus end of the polymer. It uses the energy gained from hydrolysing ATP to rapidly polymerise and depolymerise. The two ends of the

polymer show different dynamic behaviour, with the plus (or barbed) end exhibiting higher polymerisation and depolymerisation rates than the minus (or pointed) end (Kabsch and Vandekerckhove, 1992;Steinmetz *et al.*, 1997).

Actin is present in all cells, but is most abundant in muscle cells where it is responsible for muscle contraction. In contraction, thick filaments containing the motor protein myosin use ATP hydrolysis to slide along thin actin fibres. In other cells, actin is essential for many motile processes that affect morphogenesis. It is involved in membrane pushing during cell movement, vesicle and organelle transport, exo- and endocytosis, and the separation of the daughter cells at the end of mitosis through constriction of the cytokinetic ring. Myosin is also present in unpolymerised form in nonmuscle cells, where it acts as a motor transporting cargo such as vesicles, organelles or RNA along actin filaments. It also serves to exert force by contracting actin fibres, for example in the cytokinetic ring (Sellers, 1999).

1.2 Intermediate filaments

Intermediate filaments (IFs) are rope-like fibres with a diameter of about 11 nm. In contrast to the molecular structure of actin and microtubules, which are highly conserved in evolution, the proteins forming intermediate filaments have considerably diverged and their expression varies among different cell types (Herrmann *et al.*, 2003). IF-like proteins have also been found in budding yeast (Mayordomo and Sanz, 2002). The subunits of intermediate filaments are themselves elongated and fibrous; they form dimers of two α-helical chains that are intertwined in a coiled-coil rod, which then associate into linear arrays (Strelkov *et al.*, 2003). Intermediate filaments can spontaneously self-assemble and do not require the energy gained from ATP or GTP hydrolysis for polymerisation. Unlike actin or microtubules, they are not intrinsically polar, because the subunits are arranged symmetrically. They can form a meshwork extending across the cytoplasm or the nucleus. Because of their high stability *in vitro*, intermediate filaments have long been assumed to form static networks *in vivo*, providing mechanical stability and resistance to shear stress. However, increasing evidence shows that intermediate filaments are often very dynamic and motile (Helfand *et al.*, 2004).

1.3 Septins

Septins are conserved filament-forming proteins that assemble into cortical cytoskeletal structures in animal and fungal cells. The septin assembly was originally discovered by electron microscopy as "mother-bud neck filaments" in budding yeast (Byers and Goetsch, 1976). Electron-dense striations, approximately 10nm thick, run circumferentially between a mother cell and the bud; these were later identified with the "septin rings" observed by fluorescence microscopy. Since septin mutants are commonly defective in cytokinesis and formation of the neck filaments/septin rings, septins have been considered the primary constituents of the neck filaments (Field and Kellogg, 1999; Longtine et al., 1996). To date, genetic and cytological studies have revealed that the septin rings may serve as (i) a spatial landmark to establish and/or maintain cell polarity for budding, (ii) a diffusion barrier to segregate cortical molecules between mother and bud, and (iii) a scaffold for anchoring other proteins or higher-order subcellular structures (Kusch *et al.*, 2002).

Septins form heteromeric septin–septin complexes and bind and hydrolyze GTP. In addition, recombinant septins and septin complexes purified from yeast, *Drosophila* or mammalian cells form filaments *in vitro*. Thus, it seems likely that the filament formation of septins and GTP binding and hydrolysis are important for their function. The specific role of GTP binding and hydrolysis is, however, not yet clear. Some data are consistent with a role of GTP binding or hydrolysis in regulating the formation of septin filaments, whereas other data suggest that septin filament formation does not require associated GTP hydrolysis. It is also possible that GTP binding or hydrolysis is involved in regulating the interaction of septins with non-septin proteins or in regulating the interaction of septins with phospholipids possibly involved in the association of septins with membranes. Although rapid progress has been made in understanding the functions of septins, the mechanisms governing their localization and organization remain mysterious (Longtine and Bi, 2003).

Septins have a conserved domain structure with a variable length amino (N)-terminal region, a conserved central GTP-binding region and, in most family members, a carboxy (C)-terminal region that is predicted to form a coiled-coil structure. Within and between species, septins typically show at least 30% overall amino acid sequence identity.

1.4 Microtubules

Microtubules (MTs) are indispensable for the proper functioning of eukaryotic cells. In non-dividing cells, MTs form a network throughout the cytoplasm that underlies and helps maintain the structure of organelles such as the Golgi and ER. In addition, MTs serve as the tracks for organelle and vesicle movement. As the major component of axonemes and the mitotic spindle, MTs also play fundamental roles in motility and cell division. During mitosis, MTs form the mitotic spindle to which chromosomes attach and which is ultimately responsible for the migration of the duplicated chromosomes to each spindle pole (Brinkley, 1997).

Because of the fundamental role that MTs and associated proteins play in cells, disruption of MT functioning often has detrimental effects. Severe perturbation of MT processes may hamper normal growth and development and result in the death of the organism. Impairment of cell motility and division may manifest in conditions such as infertility, Down's syndrome and the development of some cancers. In order to understand how disruption of MT functioning can have such a detrimental impact on cells, it is important to understand how MT processes are controlled. Insight into the regulation of MT-associated processes will not only help elucidate the mechanisms that lead to a disease state, but may also affect the diagnosis and treatment of such devastating diseases.

1.4.1 Tubulin

The αβ-tubulin heterodimer is the structural subunit of MTs. The α- and β-tubulins share 40% amino-acid sequence identity; both exist in several isotype forms and undergo a variety of post-translational modifications (Luduena, 1998). Each tubulin monomer binds a guanine nucleotide, which is non-exchangeable when bound to the α-subunit, or N site, and exchangeable when bound to the β-subunit, or E site. The atomic model of the αβ-tubulin dimer was fitted to a 3.7-Å density map obtained by electron crystallography of zinc-induced tubulin sheets (Nogales *et al.*, 1998). The structures of α- and β-tubulins are basically identical; each monomer is formed by a core of two β-sheets surrounded by α-helices. The monomer structure is very compact, but can be divided into three functional domains: the amino-terminal domain containing the nucleotide-binding region, an intermediate domain

containing the taxol-binding site, and the carboxy-terminal domain, which probably constitutes the binding surface for motor proteins.

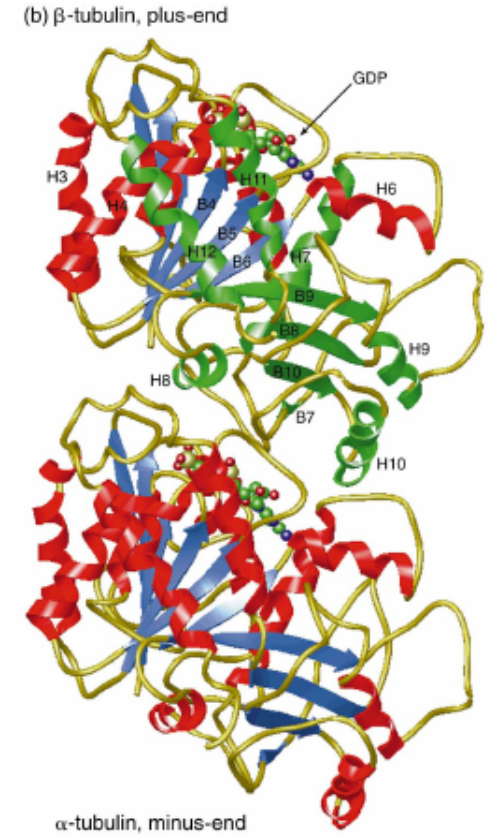

Figure 1. Cartoon representation of Tubulin heterodimer

The N-terminal nucleotide-binding domain (residues 1–206) is formed by the alternation of parallel beta strands (B1 B6) and helices (H1 H6). The nucleotide-binding pocket is formed by the loops connecting each strand and helix (loops T1–T6) and the N-terminal end of the core helix (H7). After the core helix is a smaller, second domain that is formed by three helices (H8 H10) and a mixed beta sheet (B7 B10). The C-terminal region is formed by two antiparallel helices (H11 and H12) that cross over the previous two domains. In the dimer the GTP nucleotide in the α-subunit is buried at the intradimer interface, explaining the nonexchangeability of the site (figure 1). This position of the N site also explains the control exerted on the structural stability of the tubulin dimer by a magnesium bound with high-affinity at this site (Menendez *et al.*, 1998). In contrast, the nucleotide at the E site is partially exposed on the surface of the dimer, allowing its exchange in solution. The binding of GTP at the E-site is likely to have three effects (Wang and Nogales, 2005) during MT assembly: first, to reduce the dimer−dimer bending by locally changing the conformation around the

nucleotide at the interface (figure 1); second, to straighten the dimer, a long-range allosteric change that could involve helix H7 and the following T7 loop in β-tubulin which link the intra-dimer and inter-dimer interfaces; and third, to fine-tune the conformation of the monomer so as to strengthen lateral contacts within the protofilaments. These three effects may permit the partial straightening of protofilaments able to form lateral contacts that are otherwise inhibited in the more curved GDP state.

1.4.2 Assembly and Polarity of Microtubules

Microtubules are long, straight, hollow cylinders of 25 nm diameter that are more rigid than actin filaments. MT filaments form as a consequence of the polymerisation of tubulin globular subunits (Downing and Nogales, 1998). Each ~100 kDa tubulin heterodimer is composed of the closely related α–and β–tubulin polypeptides. Both monomers can bind GTP, but only β-

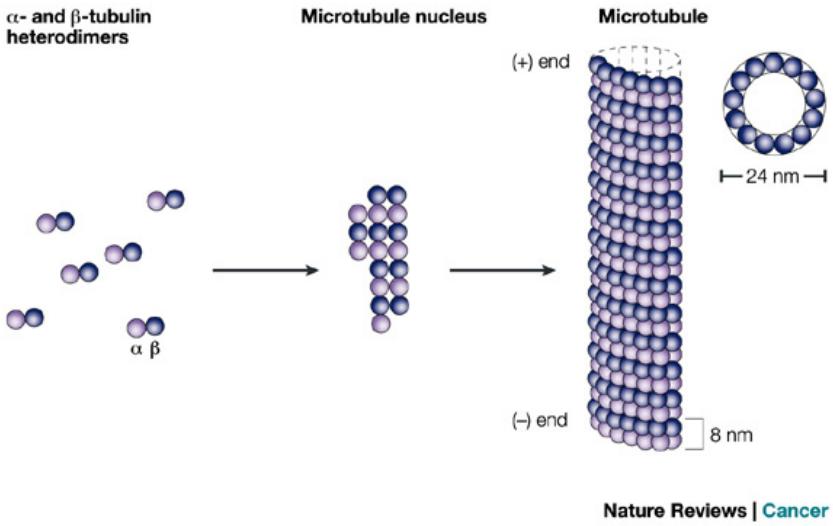

Figure 2. Oligomerization of microtubules (adapted from Wilson, 2004 423 /id). Heterodimers of α- and β-tubulin assemble to form a short MT nucleus. Nucleation is followed by elongation of the MT at both ends to form a cylinder that is composed of tubulin heterodimers arranged head-to-tail in 13 protofilaments. Each MT has a so-called plus (+) end, with β-tubulin facing the solvent, and a minus end (-), with α-tubulin facing the solvent.

tubulin has GTP hydrolysing activity. Linear protofilaments formed by heterodimers associate laterally to form the hollow MT cylinder. Within a protofilament, the tubulin heterodimers associate head-to-tail (figure 2). This makes MTs intrinsically polar, resulting in structural

and kinetic differences at the two different ends, designated plus and minus. The β-tubulin within the dimer is oriented toward the plus end, and the α-tubulin subunit toward the minus end. Most MTs form from the association of 13 protofilaments into a tube (figure 2).

MT nucleation occurs at specific structures called MT organising centres (MTOCs). MTOCs prevent the random formation of MTs throughout the cell by restricting nucleation to specific locations. The MT minus ends are embedded within the MTOC, while the plus ends extend into either the cytoplasm or the nucleus (Heidemann and McIntosh, 1980;Dammermann *et al.*, 2003). The structure of the MTOCs varies considerably between species and cell types. Studies of various organisms have established that γ-tubulin, which shows some homology to α- and β-tubulin, is a universal component of MTOCs and essential for microtubule nucleation. It exists in a large complex that forms an open ring structure of 25nm diameter called the γ-tubulin ring complex or γTuRC, which functions as a capping factor at the minus end for microtubule nucleation(Pereira and Schiebel, 1997;Moritz and Agard, 2001). The complex is also present in the cytosol but must be recruited by the MTOC to become active, despite the fact that it can nucleate microtubules *in vitro*. The γTuRC proteins have been proposed to constitute a scaffold on which 13 γ-tubulin proteins are arranged to serve as adaptors for tubulin binding to form the 13 protofilaments of a microtubule. Thus, the γ-tubulin complex not only nucleates microtubules but also stabilises their minus ends

1.4.3 Microtubule Dynamic Instability

MTs frequently switch between periods of growth and shrinking. The dynamically unstable behavior (Desai and Mitchison, 1997) is thought to be a consequence of the delayed hydrolysis of GTP after tubulin assembly. *In vitro,* both ends show this behavior, with the plus end growing and shrinking faster than the minus end. However, the dynamic behavior of the minus ends might not be relevant *in vivo*, because they are generally capped and thus stabilized in cells (Dammermann *et al.*, 2003). The observation of MT assembly *in vivo* and the behavior of purified tubulin *in vitro* led to the formulation of the dynamic instability model (figure 3) (Mitchison and Kirschner, 1984). This model assumes that both the phases of polymerization and

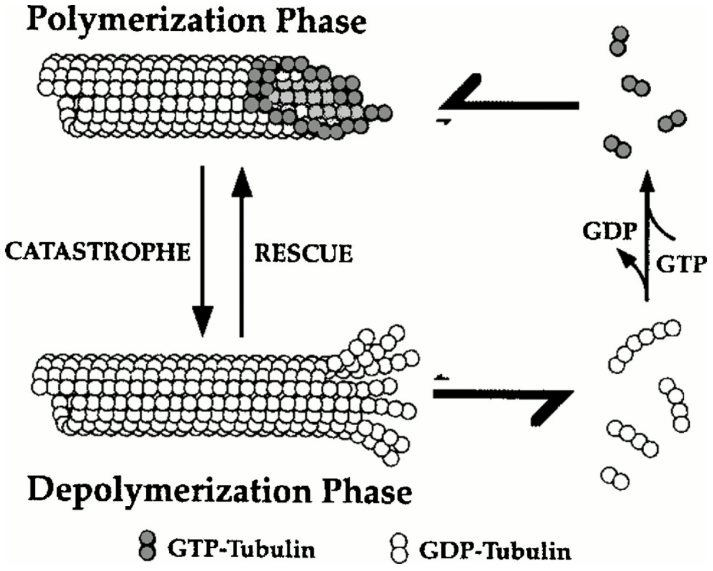

Figure 3. Microtubule Dynamic Instability. Dynamic instability is characterized by the coexistence of polymerising and depolymerising MTs. GTP-tubulin is incorporated at polymerising MT ends. The bound GTP is hydrolysed during or soon after polymerisation, and Pi is subsequently released. Thus the MT lattice is predominantly composed of GDP-tubulin. Polymerising MTs infrequently transform to the depolymerisation phase (catastrophe). Depolymerising MTs can also occasionally transform back to the polymerisation phase (rescue). This representation incorporates the notions of a small GTP cap acting as a stabilising structure at polymerising ends and different conformational configurations at polymerising and depolymerising ends (adapted from Desai and Mitchison, 1997).

depolymerisation are persistent, with occasional transitions between states. The transition from growth to shrinkage is termed catastrophe, and from shrinkage to growth, rescue. Both catastrophes and rescues occur abruptly, infrequently and stochastically. Four parameters are used to describe microtubule behaviour: the two rates of polymerization and depolymerisation, and the two frequencies for catastrophes or rescues. *In vitro*, the growth rate is a function of the concentration of free tubulin dimers but not the shrinkage rate. The relationships between catastrophe or rescue frequencies and the concentration of free tubulin are more complex and not well understood: for example, the catastrophe frequency seems to decrease with increasing amounts of free tubulin because catastrophes take place less often at higher polymerisation rates (Walker *et al.*, 1988). However, there are also conditions where the two parameters are uncoupled. For example, when the Mg2+ concentration is increased, the polymerisation rate goes up as well, but the catastrophe frequency does not change (Erickson and O'Brien, 1992).

Although a population of microtubules can maintain a stable amount of polymerised tubulin over time, individual microtubules never reach a steady state. Instead, they consume energy from GTP hydrolysis to maintain a state of dynamic instability. The GTPase activity of β-

tubulin is strongly activated through binding of the adjacent α-tubulin when a tubulin heterodimer is inserted into a microtubule. Due to this, there might be only a single layer of dimers containing GTP, the so-called GTP cap, at the plus end while all other dimers inside the microtubule contain GDP.

GTP hydrolysis is not needed for assembly since microtubules still form from the tubulin dimers if GMPCPP, a nonhydrolysable homologue of GTP, is used for the *in vitro* polymerisation reaction. GMPCPP microtubules are more stable than those formed with GTP and do not show dynamic instability (Mickey and Howard, 1995), which implicates hydrolysis in the depolymerisation of microtubules. These observations have led to the hypothesis that microtubules containing GDP-tubulin are intrinsically unstable, and that the GTP cap at the plus end is needed to stabilise microtubules. This proposal was supported by the outcome of experiments in which microtubules were cut in the middle, creating new plus ends without GTP caps from which the microtubules depolymerised rapidly(Walker *et al.*, 1989). Electron micrographs show that MTs depolymerising from their plus ends disintegrate into individual protofilaments that curl away from the cylinder, so that the ends look frayed (Chretien *et al.*, 1995). Hydrolysis of GTP to GDP appears to induce a structural change in tubulin so that the protofilaments have a tendency to bend. Since they cannot curl within a MT, this change results in a mechanical strain that weakens the stability of the microtubule. The strain is released when GDP-tubulin is exposed at the plus end, leading to rapid depolymerisation.

EM studies have also suggested that polymerising tubulin at the plus end first yields a flat sheet that later closes into a cylinder. It has been proposed that sheet closure lags behind the site where new subunits are added and that catastrophe occurs when the closing tube manages to catch up with the polymerising end. The special structure at the plus end during polymerization and depolymerisation probably explains why microtubule growth and shrinkage phases both persist for extended periods of time. The respective roles of the GTP cap and the closing sheet in stabilising microtubule plus ends are not quite clear, however. In addition to phases of growth and shrinkage, microtubules can also remain for some time in a suspended state in which they neither add nor loose dimers, suggesting an intermediate state in which the plus end has a fully closed tube, but no protofilament curling occurs(Tran *et al.*, 1997).

2. Microtubule-Associated Proteins

The first microtubule binding proteins identified were the classical microtubule-associated proteins (MAPs), for example the tau in neuronal or MAP4 in non-neuronal cells. They suppress catastrophes as well as promote rescues, binding to the microtubule lattice by electrostatic interactions in a way insensitive to the nucleotide. Tau and MAP4 are thought to act by cross- linking adjacent tubulin subunits, thereby preventing their dissociation from the microtubule cylinder. Today, many additional MAPs regulating microtubule dynamics are known. They use different mechanisms to associate with microtubules and to stabilise or destabilise them. For example, adding XMAP215, a microtubule-stabilising MAP, and Xkcm1, a microtubule destabilising kinesin to purified tubulin reconstitutes nearly physiological microtubule dynamics. In this system, XMAP215 stimulates microtubule growth and also counteracts the catastrophe-inducing activity of Xkcm1 (Kinoshita *et al.*, 2001).

2.1 Microtubule Destabilising Factors

2.1.1 The Stathmin Family

Stathmin is a member of microtubule-destabilizing proteins that regulate the dynamics of microtubules. Stathmin promotes microtubule depolymerization during interphase and late mitosis. The microtubule-depolymerizing activity of stathmin is regulated by changes in its degree of phosphorylation occurring during cell cycle progression. These modifications play a critical role in regulating the dynamic equilibrium of microtubules during different phases of the cell cycle.

In higher eukaryotes, the stathmin family of microtubule regulators includes the ubiquitous cytosolic stathmin, also designated p19, oncoprotein18, Op18, pp17, 19K, prosolin, and metablastin (Sobel, 1991), and three closely related neural-specific and neural growth-associated gene products termed RB3 (rat brain-3), SCG10 (superior cervical ganglia protein 10), and SCLIP (SCG10-like protein). These proteins share a highly conserved stathmin-like

domain (SLD) (Mori and Morii, 2002) that display 65–75% amino acid identity with stathmin including the predicted α-helix (figure 4) (Charbaut *et al.*, 2001).

Stathmin is a 17kD protein expressed in all cell types ranging from 0.005% to 0.5% of total protein in the cell (Brattsand *et al.*, 1993). The highest proportions are found in fast-proliferating cells like cancer cells; the lowest are present in terminally differentiated cells like neurons (Rowlands *et al.*, 1995). In contrast to the ubiquitous cytosolic stathmin, the other stathmin family members, excluding SCLIP, are highly expressed in the nervous system (Ozon *et al.*, 1999) where they are found in the Golgi apparatus and the growth cone (Grenningloh *et al.*, 2004).

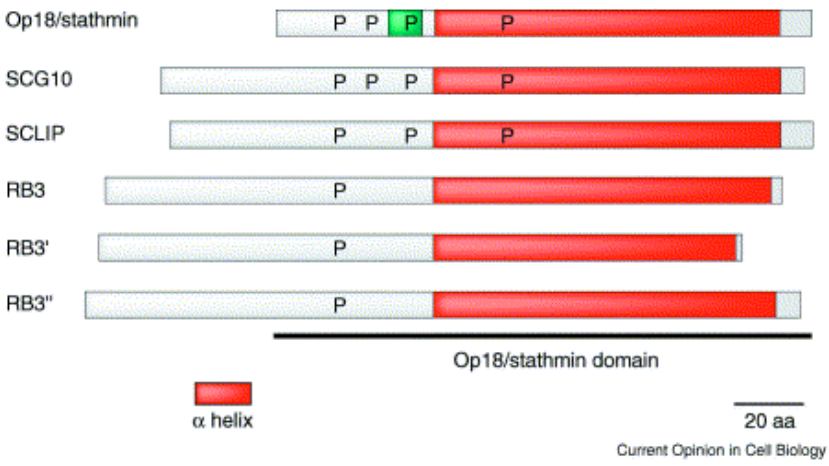

Figure 4. **Schematic diagram of stathmin and related proteins**. SCG10, SCLIP, RB3, RB3′ and RB3" are expressed in neurons and differ from stathmin by N-terminal extensions that probably target them to membranes. The stathmin domain is highly conserved among all family members (~70% identical). The N-terminal region of stathmin is unstructured (Ozon *et al*., 1997; Wallon *et al*., 1997). Most of the remaining protein is predicted to have an α-helical structure (Gigant *et al*., 2000; Ozon *et al*., 1998), shown in red. When not bound to tubulin, this region exhibits a disordered structure (Steinmetz *et al*., 2000; Steinmetz *et al*., 2001). The positions of serine phosphorylation sites in stathmin are shown. The conserved positions of serine residues are also present in the other family members (adapted from Cassimeris, 2002).

A characteristic feature of the neural family members is a hydrophobic N terminus that includes two Cys residues serving as palmitoylation sites. This N terminus mediates association to intracellular membranes, primarily at the Golgi apparatus but also within growth cones (Lutjens *et al.*, 2000). On the other hand, the ubiquitous stathmin protein lacks the hydrophobic part of the N terminus and exhibits a widespread cytosolic distribution.

Stathmin is an Intrinsically Disordered Protein

It has become evident that a significant fraction of eukaryotic genomes encode proteins with substantial regions of disordered structure. In spite of the lack of structure, these proteins are functional; many are involved in critical steps of the cell cycle and other regulatory processes. In general, intrinsically disordered proteins interact with a target ligand and undergo a structural transition to a folded state upon binding. Several features of intrinsically disordered proteins make them well suited to interact with multiple targets and mediate cell regulation. New algorithms developed to identify disordered regions have demonstrated their presence in cancer-associated proteins and in proteins regulated by phosphorylation.

Based on sequence prediction programmes stathmin contains three distinct regions: an unstructured N-terminus, N: 1-44; a region with high helix propensity, H 1: 44-89; and a region with low helix propensity, H 2: 90-142. In solution stathmin exists in rapid equilibrium between a disordered structure and one containing a long α-helical structure (Steinmetz *et al.*, 2000). Tubulin binding stimulates a large region of stathmin to fold into an extended α-helix, similar to that found in the RB3-tubulin crystal structure (Gigant *et al.*, 2000;Ravelli *et al.*, 2004).

The Tubulin- Stathmin Complex

Stathmin family members form ternary complex termed T_2S containing two tubulin dimers and one stathmin monomer (Belmont and Mitchison, 1996). These complexes display very different stabilities (Charbaut *et al.*, 2001), the T_2S complex formed with RB3-SLD, for example, is more stable than that formed with stathmin.

In the complex, RB3-SLD adopts a hook-like shape accommodating the two bound tubulin heterodimers (figure 5). RB3-SLD comprises three structural domains: an N-terminal ‘cap’ domain (residues 4 to 28) that is conserved in the stathmin family, a variable linker domain (residues 29 to 45) and a conserved helical carboxy-terminal domain (residues 46 to 145) (Maucuer *et al.*, 1993). Within the N-terminal cap domain, residues 7 to 23 form a β-hairpin (figure. 5b) that extends the β-sheet of the intermediate domain 4 of the α-tubulin subunit located at one end of the T_2R complex. This extension, together with nearby interactions

(figure. 5c), contributes significantly to the stability of the tubulin–colchicine: RB3-SLD complex. Interestingly, Ser 16, which is conserved in the stathmin family and phosphorylated in stathmin in response to a number of signals (Beretta *et al.*, 1993), is located in the tight turn of the β-hairpin (figure. 5c) and its phosphorylation could inhibit proper formation of the N-terminal cap structure. Furthermore, the residues of tubulin interacting with the N-terminal cap mediate longitudinal contacts between tubulin heterodimers assembled in protofilaments (Nogales *et al.*, 1999).

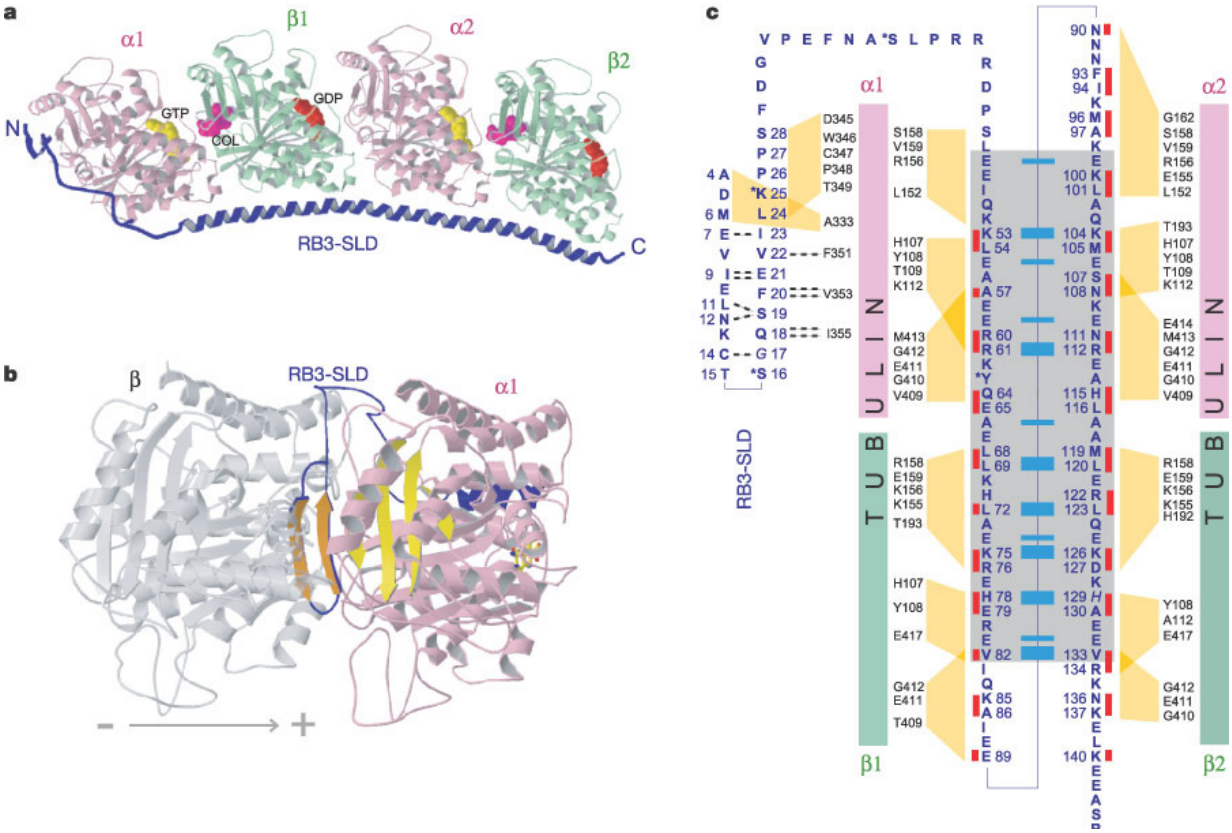

Figure 5. **The tubulin–colchicine:RB3-SLD complex**. **a**, The complex includes two tubulin αβ heterodimers, with colchicine bound to β subunits at the interface with α. The RB3-SLD connecting region (residues 29–45)as shown from the tubulin–podophyllotoxin:RB3-SLD complex where it is defined best (podophyllotoxin is a competitive inhibitor of colchicine that binds to tubulin). **b**, The β hairpin (orange) in the N-terminal domain of RB3-SLD caps the T2R complex, extending the β sheet (yellow) of the intermediate domain in the α1 subunit. The extensive overlap with a protofilament (+)-end β subunit (Nogales *et al*., 1999), preventing the addition of the T2R complex to a MT, is illustrated. **c**, Interactions of RB3-SLD residues with tubulin (except for the least-well-defined RB3-SLD connecting region and the extension of the tubulin intermediate domain β-sheet) represented by yellow connecting areas. Red bars designate residues of the α-helix pointing towards tubulin. Dashed lines denote mainchain hydrogen bonds in the extension of the intermediate domain β-sheet. Within the internal repeat (grey), identical residues are connected by blue lines; ; thick blue lines indicate side-chain pointing towards tubulin. Asterisks indicate positions of stathmin phosphorylation sites (adapted from Ravelli *et al*., 2004).

The SLD therefore sterically hinders the incorporation of the T_2R complex at the plus end of microtubules via its N-terminal cap. In addition, it enforces the curved heterodimer assembly

through its C-terminal helix 11. The SLD linker region involves a proline-rich sequence that is least conserved among SLDs of the stathmin family (Charbaut *et al.*, 2001). In the T_2R structure, the majority of the stathmin side-chains that point towards tubulin are defined and most of the previously proposed tubulin residues that interact with stathmin are confirmed (Ravelli *et al.*, 2004). The interacting SLD residues include the residues of the mostly hydrophobic seam proposed to be responsible for the interaction but also at least as many polar/charged residues. As hypothesized previously, the structure also shows that the internal repeat in the C-terminal α-helix is mirrored in an identical positioning relative to the corresponding tubulin heterodimer.

Stathmin as Regulator of Microtubule Dynamics

Originally, stathmin was described as a protein that binds to tubulin dimers and increases the catastrophe frequency of MT *in vitro* (Belmont *et al.*, 1996). Subsequent studies have identified two putative mechanisms: (i) sequestration of the tubulin heterodimers that slows MT growth rate (Jourdain *et al.*, 1997;Curmi *et al.*, 1999) and (ii) direct stimulation of MT plus-end catastrophes (Tournebize *et al.*, 1997;Segerman *et al.*, 2003) (figure 6).

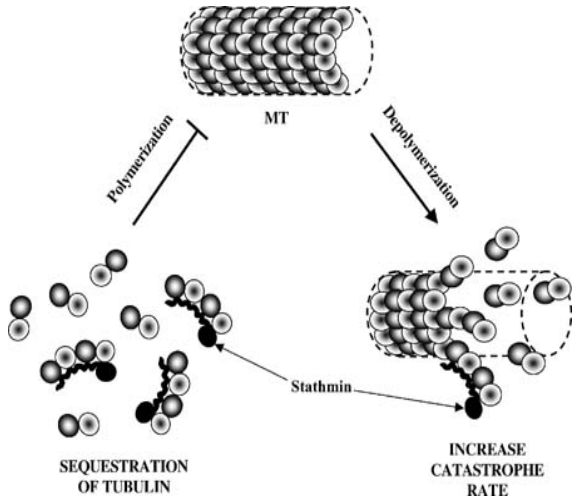

Figure 6. Model for the role of stathmin in the regulation of MT dynamics. MTs (MT) continuously switch between phases of polymerization and depolymerization. Stathmin can sequester unpolymerized tubulin by binding two α/β-tubulin heterodimers (represented by light and dark shaded circles), thus diminishing the pool of tubulin heterodimers available for polymerization. Stathmin can also bind to the end of polymerized MTs and increase the rate of catastrophe by inducing a conformational change that promotes MT depolymerization.(adapted from Rubin, 2004 402 /id).

Howell *et al.* (1999), who tried to distinguish between these mechanisms, found that stathmin has dual functional activity dependent on the pH. They found tubulin-sequestering activity at

pH 6.8, and catastrophe-enhancement with no sequestering activity at pH 7.5 (Howell *et al.*, 1999;Holmfeldt *et al.*, 2001). This view is supported by deletion mapping which indicated that the N terminus of stathmin is required for plus-end catastrophe promotion, whereas the C-terminal helical domain binds tubulin dimers ((Howell *et al.*, 1999;Segerman *et al.*, 2003).

The sequestering mechanism is largely supported by recent structural and biophysical studies (Steinmetz *et al.*, 2000;Gigant *et al.*, 2000;Wallon *et al.*, 2000;Muller *et al.*, 2001;Charbaut *et al.*, 2001;Amayed *et al.*, 2002). Electron microscopy (Steinmetz *et al.*, 2000) and the crystal structure of the RB3-tubulin complex (Gigant *et al.*, 2000;Ravelli *et al.*, 2004) suggest that the stathmin interaction with microtubules at tips could introduce curvature into the protofilaments that induces them to peel away from the microtubule. In addition it could disrupt lateral and longitudinal contacts of the individual protofilaments, destabilizing the microtubule tips.

Müller et al., (2001) showed using mass spectroscopy that stathmin links two tubulin heterodimers together by binding to helix 10 of α-tubulin, which is known to be involved in longitudinal tubulin-tubulin interaction within microtubule protofilaments. By interacting with this region, stathmin may also prevent the incorporation of the stathmin-tubulin complexes in the microtubules, preventing further polymerization. Thus, these studies demonstrate that stathmin is capable of binding both polymerized and unpolymerized tubulin and prevents polymerization of α/β heterodimers under some conditions or promote depolymerization of microtubules under others (Figure 6).

In contrast to the well characterized sequestering mechanism, the molecular details of how stathmin interacts with MT ends and triggers catastrophes are not clear.

Stathmin Activity is Negatively Regulated by Phosphorylation

Stathmin was initially identified as a protein phosphorylated in response to a number of extracellular signals (Sobel, 1991). Stathmin is phosphorylated at four Ser residues (Ser 16, 25, 38 and 63) by both cell cycle-regulating and signal-transducing kinase systems (Lawler, 1998). Modifications of these sites result in various degrees of functional inactivation (Marklund *et al.*, 1996;Larsson *et al.*, 1997;Horwitz *et al.*, 1997). Multisite phosphorylation of

stathmin at the start of mitosis is required for spindle formation (Larsson *et al.*, 1997), whereas phosphorylation by signal-transducing kinases has been shown to mediate regulation of the interphase array of MTs (Melander *et al.*, 1997). All four Ser phosphorylation sites of stathmin are conserved in SCG10 and SLIP, which may be of significance for regulation of the MT system during neural differentiation (Antonsson *et al.*, 1998). However, RB3 lacks three of the four sites and the remaining site, which corresponds to Ser-16 of stathmin, presents a nonconserved consensus sequence (Ozon *et al.*, 1997).

Phosphorylation of two serine residues (Ser 16 and 63) significantly reduces tubulin binding and inhibits the ability of stathmin to destabilize MTs *in vitro* (Di *et al.*, 1997;Holmfeldt *et al.*, 2001). This effect is further increased by phosphorylation at Ser 25 and 38. The effect of phosphorylation at Ser 16 and 63 was addressed by expressing mutants in which the serine residues were replaced by phosphorylation-mimicking aspartate residues in non-neuronal cells (Antonsson *et al.*, 1998). Analysis of the MT network in the transfected cells shows that the MT destabilizing activity of SCG10 is also efficiently regulated by phosphorylation.

PKA, MAPK, and CDK5 are good candidates to regulate stathmin *in vivo*. They are highly expressed in neurons and also present in growth cones (Pigino *et al.*, 1997). Many studies implicate in particular MAP kinases in neuronal differentiation (Fukunaga and Miyamoto, 1998). Moreover, both SCG10 and stathmin are found to be phosphorylated at all four serine residues in the developing brain (Antonsson *et al.*, 1998). These observations indicate that SCG10 and stathmin may link cell signaling mechanisms to changes in MT dynamics.

Stathmin Phosphorylation Regulates Cell Cycle Progression

The first hint that stathmin may play a role in the regulation of cell-cycle progression came from the observation that the level of phosphorylation of stathmin increases markedly when K562 erythroleukemia cells enter the mitotic phase of the cell cycle (Luo *et al.*, 1994). Brattsand *et al*. (Brattsand *et al.*, 1993) also showed that the level of stathmin phospohorylation peaks in mitosis in both Jurkat T cells and HeLa cells. In the same study it was shown that the level of stathmin phosphorylation is significantly lower in cells blocked in the G_1/S phases of the cell cycle compared to proliferating cells. Both studies also showed that stathmin is phosphorylated in vitro by $p34^{cdc2}$ kinase, the major protein kinase that

regulates entry of eukaryotic cells into mitosis. These observations provided circumstantial evidence that stathmin may play a role in the $p34^{cdc2}$-regulated pathway that controls entry into mitosis and progression through the rest of the cell cycle. The antisense RNA inhibition of stathmin expression in K562 leukemic cells results in decreased cellular proliferation and accumulation of cells in the G_2/M phases of the cell cycle. The study by Marklund *et al*. (1994) confirmed these observations and extended them by showing that overexpression of wild-type or $p34^{cdc2}$-target deficient mutants of stathmin in K562 cells also results in growth suppression and accumulation of cells in the G_2/M phases of the cell cycle. The fact that both overexpression and inhibition of stathmin expression results in mitotic arrest generated a paradox that was resolved two years later by the independent identification of stathmin as a cellular factor involved in the regulation of MT dynamics (Belmont *et al.*, 1996).

Role of Stathmin in Mitotic Spindle assembly

The mitotic spindle is a bipolar structure that plays a critical role in chromosome alignment and segregation during mitosis. During mitosis, stathmin becomes highly phosphorylated because of one or several factors present on mitotic chromatin (Andersen *et al.*, 1997). One factor has been identified as Polokinase1. Depletion of Polokinase1 inhibits chromatin-induced stathmin hyperphosphorylation and spindle assembly in mitotic *Xenopus* egg extracts (Budde *et al.*, 2001). This was originally demonstrated by Marklund *et al*., (1996) who studied the effect of overexpression of wild-type stathmin and $p34^{cdc2}$-target site phosphorylation deficient mutants on the mitotic phenotype of K562 cells. These studies showed that overexpression of wild-type stathmin depolymerizes interphase MTs but does not interfere with the formation of the mitotic spindle.

During interphase, stathmin is phosphorylated via the Rac1-Pak1 pathway (Daub *et al.*, 2001). Both proteins, Rac1 and Pak1, become activated at the leading edges of cells made motile by a wound in the monolayer or by exposure to growth factors (Sells *et al.*, 2000). The Rac1-Pak1 pathway mediates "pioneering" of MTs into the leading edge (Wittmann *et al.*, 2004). Thus, stathmin could be locally inactivated around mitotic chromosomes and at the leading edge of migrating cells, which would specifically promote localized MT growth. Chromosome segregation was not observed and the cells were arrested in the early stages of mitosis (i.e.,

prophase/prometaphase). Thus, the expression of a constitutively active form of stathmin arrests cells early in mitosis and prevents further progression through the cell cycle (Larsson *et al.*, 1997).

Stathmin has also been reported to be hyperphosphorylated in mitotic *Xenopus* egg extracts in the presence of chromatin (Andersen *et al.*, 1997). This suggested the occurrence of a gradient of phosphorylation-inactivated stathmin around mitotic chromosomes. A striking consequence of the observed stathmin-tubulin interaction gradients can be envisaged; They seem to produce a cytoplasmic environment with graduated MT-stabilizing activity that could provide intracellular guidance for MTs before they actually reach a potential capture site in the cell cortex or at the chromosomes. This would result in preferential MT growth along these gradients (Stukenberg, 2003). Indeed, a subset of pioneering MTs in the leading edge (Waterman-Storer and Salmon, 1998) seems to be stabilized selectively compared with those in the center of the cell. Recent reports (Wittmann *et al.*, 2004) propose Rac1-Pak1–mediated inactivation of stathmin to be at least in part responsible for this localized stabilization. In mitotic cells, it was shown that a stathmin phosphorylation gradient is necessary for correct spindle formation (Niethammer *et al.*, 2004)**.** Thus, stathmin is critically important not only for the formation of the mitotic spindle when cells enter mitosis but also for the regulation of post-metaphase events and proper exit from mitosis.

Stathmin is over expressed in cancer cells

Stathmin is an oncoprotein and a mitotic regulator that functions via its ability to modulate MT stability. High levels of expression of stathmin have been observed in a wide variety of human malignancies, including leukemia/lymphoma, prostate carcinoma, ovarian carcinoma, and breast carcinoma. Stathmin expression is associated with cellular proliferation (Hosoya *et al.*, 1996). The stathmin gene is highly expressed in breast cancers (Curmi *et al.*, 2000), leukemia (Roos *et al.*, 1993), prostate cancer (Friedrich *et al.*, 1995), and lung cancer (Chen *et al.*, 2003), and is thought to be a useful marker for neoplastic transformation. In addition, antisense inhibition of stathmin expression and taxol synergistically inhibit the growth and clonogenic potential of K562 cells, suggesting that stathmin expression may represent an important molecular target for development of novel anticancer therapies (Iancu *et al.*, 2000). Further, antisense inhibition of stathmin expression is required to maintain the transformed

phenotype of K562 cells. These findings suggest that high levels of stathmin expression are necessary to maintain the transformed phenotype of leukemic cells. Inhibition of stathmin expression in malignant cells interferes with their progression through the cell cycle and abrogates their transformed phenotype. Thus, stathmin provides an attractive molecular target for disrupting the mitotic apparatus and arresting the growth of malignant cells.

2.1.2 Microtubule depolymerising Kinesins

2.1.2.1 Kin I

The kinesins of the Kin I/ MCAK family are MT destabilising proteins. They are unusual motor proteins (Kim and Endow, 2000), since they do not move along the surface of MT filaments. Instead, they use energy from ATP hydrolysis to bind to the ends of MTs, remove tubulin subunits and thus trigger depolymerisation. Removal of the *Xenopus* MCAK (XKCM1) from egg extracts dramatically increases the size of the MT arrays (Walczak, 2000) by suppressing catastrophes (Tournebize *et al.*, 2000). Overexpressing MCAK in tissue culture cells leads to an almost complete loss of MTs, perhaps by increasing catastrophes. The localization of MCAK at kinetochores suggests that they could trigger depolymerization during mitosis (Maney *et al.*, 1998). The combination of XKCM1 and a MAP (XMAP215) has been shown to reconstitute the physiological properties of dynamic instability *in vitro* (Kinoshita *et al.*, 2001). Thus it seems that, by increasing the catastrophe rate, MCAKs are central to the generation of dynamic MTs inside cells.

In the presence of non-hydrolysable ATP analogues, MCAK-family proteins bind to the ends of MTs and form curled protofilaments—the rams' horns (Desai *et al.*, 1999). These observations suggest that MCAK proteins bind preferentially to the bent form of the tubulin dimer. Even growing MTs are expected to have a small flair at their ends owing to internal strain of the GTP subunits and MCAK may discriminate between the ends of a MT and the lattice (that is, the lateral surface) by recognizing these slightly bent subunits in the flared region. Rather than moving along the surface of microtubules like other motor proteins, these unusual kinesins (Kim *et al.*, 2000) use energy from ATP hydrolysis to bind to the ends of microtubules, remove tubulin subunits and thus trigger depolymerization (Desai *et al.*, 1999).

2.1.2.2 Kar3p

Kar3p is the founding member of a conserved family of kinesin-related proteins. This family is characterized by a carboxyl-terminal motor domain as well as MT minus end-directed motility (Endow *et al.*, 1994). The crystal structures of the Kar3p and NCD motor domains have been solved and compared to that of kinesin (Kull *et al.*, 1996). All three show a strong conservation of secondary structural elements with a few minor differences, mainly in the protein surface loops. Therefore, the motor domains of Kar3p and its relatives probably bind MTs and hydrolyze ATP using the same general mechanism as other kinesins.

Kar3p is a minus-end-directed yeast kinesin that can depolymerize taxol-stabilized MTs from their minus ends *in vitro* (Endow *et al.*, 1994). In *S. cerevisiae*, deletion of *KAR3* resulted in increased numbers and lengths of cytoplasmic MTs (Saunders *et al.*, 1997). Kar3p is localized to spindle pole bodies from the beginning until the late anaphase. The observations are consistent with Kar3p acting at spindle pole bodies to stimulate MT minus-end depolymerization. This activity may contribute to the poleward MT flux measured in other cell types.

Several proteins are capable of cutting MTs. These include katanin (McNally and Thomas, 1998), p56 (Shiina *et al.*, 1992) and elongation factor α (Shiina *et al.*, 1994).

2.1.3 Mechanistic differences of Microtubule-Depolymerizing factors

The structural and functional characteristics of stathmin are very distinct from those of XKCM1/XKIF2 and katanin, suggesting that these molecules destabilize MTs by a different mechanism. Stathmin is monomeric and exhibits a labile, predominantly α-helical structure, whereas XKCM1/XKIF2 are most probably homodimeric molecules with a kinesin-like fold, and katanin is a heterodimer organized into an enzymatic ring-like subunit and a centrosome-targeting subunit. XKCM1/XKIF2 and katanin bind to and release from tubulin in an ATP-dependent manner, whereas the binding activity of stathmin is tightly regulated by specific phosphorylation events. Both stathmin and XKCM1/XKIF2 were found to destabilize MTs by targeting directly MT ends. However, stathmin most likely interacts predominantly at the extremity of the plus end of the MT, and activation of the GTPase of β-tubulin is a

prerequisite for its catastrophe-promoting activity. In contrast, XKCM1/XKIF2 can promote catastrophes at both the plus and minus end of the MT without the need to induce GTP hydrolysis. Katanin, on the other hand, promotes disassembly of MTs by generating internal breaks within an MT.

2.2 Microtubule Stabilising Factors

2.2.1 The XMAP215/Dis1 Family of MAPs

The XMAP215/Dis1 MT-associated proteins are long, thin monomers that may span up to eight tubulin dimers along a protofilament (Cassimeris *et al.*, 2001). At the N-terminus, these proteins have several TOG (hepatic tumor over-expressed protein) domains that are thought to mediate protein-protein interactions. The C-terminal part of several members of the family contains coiled-coil regions that are required for MT and MTOC localisation. XMAP215 is one of the key regulators of MTs dynamics in *Xenopus laevis*. In other organisms, too, the respective homologues appear to play essential roles in the organisation of microtubules. XMAP215 proteins affect several different aspects of microtubule organisation by acting both at their plus and minus ends. They act in a different way from classical MAPs, as the proteins do not simply bind along the microtubule lattice, but prefer to bind to microtubule ends.

XMAP215 proteins presumably accumulate at MT plus ends, as shown for homologues in budding yeast (Stu2) and *Dictyostelium discoideum* (DdCP224) (Rehberg and Gräf, 2002). The most prominent effects of the proteins can indeed be observed at plus ends. *In vitro*, XMAP215 can bind directly to MTs; it stimulates growth and shrinkage rates and also reduces the rescue frequency. As a consequence, MTs are more dynamic and have a greater steady-state length. In *Xenopus* egg extract, however, the main function of the protein is to stabilise MTs by reducing the number of catastrophes. It does so by antagonising the activity of the kinesin Xkcm1, a MT destabilising protein (Tournebize *et al.*, 2000). The N-terminal part of XMAP215 alone is sufficient to suppress catastrophes presumably by interacting directly with Xkcm1 (Popov *et al.*, 2001). Together, the two proteins appear to constitute a

basic system that controls MT dynamics in frog extract. In other organisms also, XMAP215 and Xkcm1 homologues have been shown to counteract each other. Possibly constituting a conserved basic system to regulate microtubule dynamics, they might interact with other proteins to change dynamics in specific situations. Consistent with this view is the observation that XMAP215 phosphorylation changes in a cell cycle-dependent way. Phosphorylation of XMAP215 *in vitro* by the cyclin-dependent kinase CDK1 reduces its ability to increase the polymerization rate (Vasquez *et al.*, 1999). XMAP215 proteins are usually found at centrosomes, spindle pole bodies or interphase MTOCs. Their localisation as centrosomal resident proteins is probably mediated by the TACC (transforming, acidic coiled-coil containing) proteins (Sato *et al.*, 2004) and MT are not required.

Interestingly, the XMAP215 homologue (Msps) localises to microtubule minus ends at the spindle poles even in *Drosophila* meiotic cells, which form spindles lacking a centrosome. Not so much is known about the function of XMAP215 proteins at the MTOCs, which is obscured by their effect on microtubule dynamics at the plus ends. Msps is needed to ensure the integrity of the bipolar spindle by stabilising or bundling microtubules at the spindle poles. In *Xenopus* egg extracts and pure tubulin, XMAP215 can nucleate microtubules from centrosomes and anchor the minus ends of nascent microtubules(Popov *et al.*, 2001).

The role of the XMAP215 homologue in budding yeast, Stu2, is unclear. Studies show that Stu2 destabilises microtubules *in vitro* by reducing the growth rate, which produces more catastrophes and a shorter steady state length of the microtubules (van *et al.*, 2003). Accordingly, depletion of Stu2 reduces microtubule dynamics *in vivo*, implying fewer catastrophes or rescues (Kosco *et al.*, 2001). These effects oppose those of XMAP215. However, in the absence of Stu2 the anaphase spindle undergoes a defect in elongation and eventually breaks, suggesting that Stu2 is required in the spindle to increase microtubule length. It is also unclear whether the protein reduces the average length of cytoplasmic MT as different mutants of Stu2 yield conflicting results.

2.2.2 Microtubule Plus End-Tracking (+TIPs) Proteins

An important function of microtubules is to transport cellular structures such as chromosomes, mitotic spindles and other organelles inside cells. By attaching the ends of

microtubules to cellular structures, the structures are pushed or pulled around the cell as the microtubules grow and shrink. A microtubule end exhibits at least three properties: it has alternate structures; it undergoes a biochemical transition defined by GTP hydrolysis; and it forms a distinct target for the binding of specific proteins. These properties characterise the microtubule as a molecular machine, which switches between growing and shrinking modes. Each mode is associated with a specific end structure on which end-binding proteins can assemble to modulate dynamics and couple the dynamic properties of microtubules to the movement of cellular structures.

A number of MT-associated proteins were shown to specifically accumulate at growing MT plus ends (Carvalho *et al.*, 2003;Galjart and Perez, 2003). They have been termed "+TIPs", for *plus* end-*t*rack*i*ng *p*roteins (Schuyler and Pellman, 2001). Clip-170 was the first +TIP to be described (Rickard and Kreis, 1990). Later, other proteins were also shown to localise to microtubule tips. They include EB1, tea1p, dynactin, APC/Kar9, Lis1 or the CLASPs. APC and CLASPs, however, only localise to a subset of microtubule tips extending toward cellular growth sites, which might be selectively stabilized thereby.

Table 1. Main groups of +TIPs from different organisms and their structure.

Vertebrate protein	**Homologues**	**Structure**
CLIP-170/CLIP-115	D-CLIP-190 (Dm); Bik1p (Sc); Tip1p (Sp)	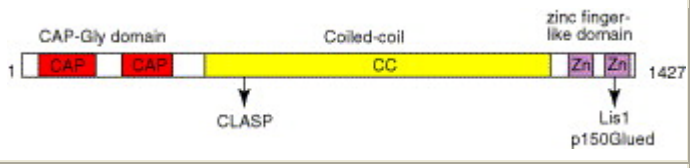
Dynactin[a] (p150Glued)	Glued (Dm); Dnc-1 (Ce); Nip100p (Sc); Ssm4p (Sp); NudM (An)	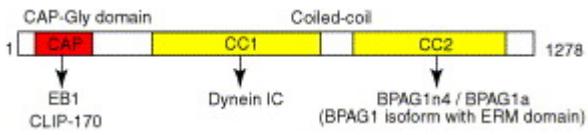
EB1,2,3	EB1 (Dm); DdEB1 (Dd); Bim1p (Sc); Mal3p (Sp)	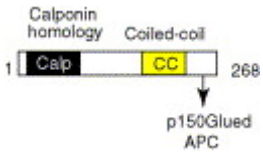
CLASP1,2	MAST/orbit (Dm); Cls-2/R107.6 (Ce); Stu1p (Sc)	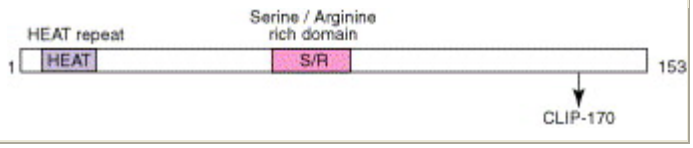

Vertebrate protein	Homologues	Structure
LIS1	Lis1 (Dm); Lis-1 (Ce); Pac1p (Sc); NudF (An)	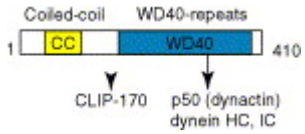
Dynein[a] (Dynein HC) (several isoforms)	Dhc64C (Dm); Dhc-1 (Ce); DHC (Dd); Dyn1 (Sc); Dhc1 (Sp); NudA (An)	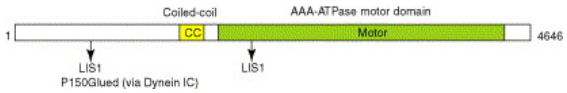
APC, APC2/APCL	dAPC1, E-APC/dAPC2 (Dm); apr-1(Ce); Kar9 (Sc)[b]	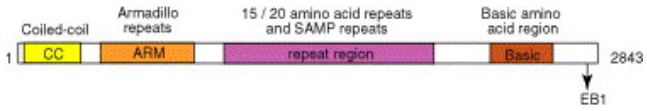
ACF7, BPAG1	Shot/Kakapo (Dm); vab10 (Ce)	
XMAP215/ChTOG[c]	Msps (Dm); ZYG-9 (Ce); DdCP224 (Dd); Stu2p (Sc); Dis1p, Alp14p (Sp)	

The main groups of vertebrate +TIPs are listed. The structural motifs for each protein are illustrated in the diagram (proteins are not drawn to scale because of the large differences in size). The arrows indicate protein partners that bind directly to specific domains. When the binding domain is unknown, an arrowhead is used. An: *Aspergillus nidulans*; Ce: *Caenorhabditis elegans*; Dd: *Dictyostelium discoideum*; Dm: *Drosophila melanogaster*; Sc: *Saccharomyces cerevisiae*; Sp: *Schizosaccharomyces pombe* (adapted from Akhmanova and Hoogenraad, 2005).

2.2.2.1 The Clip-170 Protein Family

Clip-170 was first isolated as a microtubule-associated protein in HeLa cells where it accumulated at microtubule tips and also localised to the mitotic spindle (Rickard *et al.*, 1990). Clip-170 is able to directly bind taxol-stabilised MTs. Clip-170 is able to bind directly taxol-stabilised microtubules. It contains two CAP-Gly domains in its N-terminus, each followed by a short serine-rich stretch. These domains have redundant function and are responsible for microtubule binding *in vitro* as well as *in vivo*. They are followed by heptad repeats forming a long coiled-coil domain that constitutes most of the protein and by two short metal binding motifs at the C-terminus (Pierre *et al.*, 1994). EM studies have shown that the protein has a highly elongated form. The central coiled-coil region mediates homodimerisation (Scheel *et al.*, 1999).

Clip-170 specifically localises to growing microtubule plus ends. Like EB1, it forms comet-like structures that move through the cell together with the growing microtubule end. If a microtubule slows down, the comet becomes shorter and a shrinking microtubule filament newly acquires a comet at its tip by undergoing rescue. *In vitro*, however, an N-terminal fragment of Clip-170 including the CAP-Gly and part of the coiled-coil domain does not accumulate at microtubule tips, but is found all along microtubules. It preferentially localises to microtubules that polymerised after addition of the protein, rather than to those that were assembled before. The fragment did not show preference for microtubule filaments polymerized with GMPCPP, a slowly hydrolysable GTP analogue, compared to others containing GDP-tubulin. It could be crosslinked with α- and β-tubulin *in vitro*, and in sedimentation velocity experiments, showed interaction with unpolymerised tubulin and promoted the formation of tubulin oligomers (Diamantopoulos *et al.*, 1999).

2.2.2.2 The EB1 Protein Family

The MAPRE (Microtubule-associated protein RP/EB family member 1) protein family constitutes a highly conserved group of proteins that localize preferentially to the plus end of microtubules in both the nucleus and cytoplasm. In addition, MAPRE family members are characterized by their capability to bind to the C-terminus of the APC protein and to tubulin to stabilize microtubules. MAPRE proteins have been characterised recently as a new family of microtubule-associated proteins with up to 7 homologues, consisting to date of EB1, EB2, EB3, and EBF3, and the highly related RP1, RP2, and RP3 proteins (Su *et al.*, 1995;Juwana *et al.*, 1999). EB3 was shown to be expressed in neurons and to interact with a neuron-specific homologue of APC, APCL (Nakagawa *et al.*, 2000). RP1 was identified by its induction upon T lymphocyte activation; it shares APC binding and subcellular localization with EB1 (Juwana *et al.*, 1999). Mitotic defects observed in yeast where EB1/RP1 homologues have been characterized, demonstrate a critical role for EB/RP proteins in mitosis.

The EB1 family of microtubule-associated proteins is conserved in eukaryotes. In general, they stabilise microtubules. Members of the EB1 family have a conserved domain structure composed of a single N-terminal calponin homology domain (CH domain), followed by a less

conserved, unstructured region, a short coiled-coil region, and the EB1-like domain. CH domains are found in many cytoskeletal and signalling proteins (Korenbaum and Rivero, 2002). Proteins with more than one CH domain were shown capable of binding actin. The CH domain of EB1, however, binds to microtubules *in vitro*, probably through electrostatic interactions (Bu and Su, 2003;Hayashi and Ikura, 2003). The C-terminus of EB1, including the coiled-coil and EB1-like domains, is responsible for the binding of several interacting proteins, for example APC or p150glued, a component of the dynactin complex (Bu *et al.*, 2003). Full-length EB1 was shown to bind directly to polymerised tubulin in microtubule co-pelleting assays (Berrueta *et al.*, 1998;Tirnauer *et al.*, 2002b).

EB1 localises to Microtubule Plus Ends

EB1 is concentrated at microtubule plus ends of almost every cellular system in which the protein was studied so far (Tirnauer and Bierer, 2000). It does so during interphase or when astral microtubules and spindles appear. EB1 is also present along the microtubule lattice, but less frequently than at plus ends. In purified tubulin, only the lattice-binding was seen *in vitro*. Increasing the expression of EB1 mainly enhances EB1 binding along the lattice (Schwartz *et al.*, 1997;Tirnauer *et al.*, 1999). One exception was observed in *Xenopus* interphase extract, where EB1 localises uniformly along the MT lattice even at low expression levels (Tirnauer *et al.*, 2002b). EB1 forms a comet-shaped structure at plus ends, since the amount of protein gradually decreases with the distance from the plus end. In live imaging studies of EB1 tagged with GFP, the protein accumulates at growing microtubule plus ends and moves together with them; it disappears from microtubule tips that undergo catastrophe and begin to shorten (Mimori-Kiyosue *et al.*, 2000;Tirnauer *et al.*, 2002b).

The rapid recovery along the microtubule lattice of *Xenopus* egg extract evidenced by EB1-GFP following photo bleaching (FRAP) indicates that EB1 binds transiently along microtubules. Individual EB1-GFP speckles in the comets remained static during their lifetime, contradicting transport of EB1 toward the plus ends. These findings suggest that EB1 binds to microtubules through two different mechanisms: direct association with low affinity to the microtubule lattice, and enhanced binding to the microtubule plus ends. The plus-end binding might be due to copolymerisation with tubulin or to recognition of the structural or chemical properties of the plus-end (Tirnauer *et al.*, 2002b).

EB1 proteins also localise to MTOCs, centrosomes and spindle pole bodies. This localisation does not appear to involve microtubules, since depolymerisation of microtubules using drugs does not abolish it. Some studies show that centrosome localisation is not mediated by the CH domain in human cells, but by the C-terminal part of the protein (Askham *et al.*, 2000;Rehberg *et al.*, 2002;Louie *et al.*, 2004).

EB1 Promotes Microtubule Stability

EB1 proteins stabilise microtubules and increase their steady-state length in most organisms studied till date. This is not seen *in vitro* if using only purified EB1 and tubulin (Nakamura *et al.*, 2001;Tirnauer *et al.*, 2002a) but if MT seeds are added EB1 induces microtubule elongation and bundling. This implies that EB1 can promote the growth of microtubules but cannot nucleate them (Ligon *et al.*, 2003). Studies of several organisms indicate that EB1 increases the steady-state length of MTs.

In *Xenopus* extract, depletion of EB1 from cytostatic factor (mitotic) extract causes dramatic shortening of microtubules in asters nucleated from centrosomes, although no change in microtubule length was seen in interphase extract. Addition of human EB1 to both types of extract reduces the pausing time in which microtubules neither grow nor shrink; it also increases the rescue frequency and decreases both the catastrophe frequency and the depolymerisation rate. The combined effects cause microtubules to be longer and more stable (Tirnauer *et al.*, 2002b).

The EB1 homologue, Bim1, was found in budding yeast through a two-hybrid screen designed to identify α-tubulin interactors. Deletion of *bim1* results in impaired cell growth at extreme temperatures and confers hypersensitivity to microtubule destabilising drugs. Overexpression of the protein is lethal, yielding cells that arrest with undivided nuclei, impairment of nuclear migration to the bud neck, and short and misoriented spindles (Schwartz *et al.*, 1997). These effects of Bim1 on microtubule dynamics are particularly prominent in G1 phase; the protein increases the shrinkage rate as well as the catastrophe and rescue frequencies and strongly reduces microtubule pausing (Tirnauer *et al.*, 1999;Adames and Cooper, 2000). Thus, in the deletion mutant, microtubules are shorter and less dynamic. The astral microtubules are consequently less likely to capture the bud neck with their plus

ends, which is essential for pulling the dividing nuclei toward the bud. The increase in catastrophe frequency caused by Bim1 is opposite to the effect of EB1 in *Xenopus* extract.

Knockdown of *Drosophila* EB1 inhibited microtubule dynamics in interphase. The catastrophe and rescue rates decreased, whereas pausing time increased. However, the overall organisation or length of microtubules did not change, similar to the effect of EB1 depletion in *Xenopus* interphase extract. This stability might be explained by the fact that only one of several EB1 proteins was knocked down in this study. More dramatic effects were seen in mitosis: astral microtubules were short or completely absent, the spindle smaller and more compact, the spindle microtubules detached from the centrosomes, and spindle poles were less focussed. Misalignment of the spindle and defects in spindle elongation and chromosome segregation (Rogers *et al.*, 2002) were also observed.

EB1 also localises to MTOCs, but little is known about its related functions. Knockdown of EB1 using RNAi caused in one study a reduction of microtubules minus-end anchoring at centrosomes, resulting in a less focussed array of microtubules. Also, microtubule regrowth from the centrosome was delayed after treatment with a microtubule-destabilizing drug (Louie *et al.*, 2004). In conclusion, EB1 plays a crucial role in maintaining the stable MT.

EB1-mediated Interaction Networks

Evidence indicates that the distribution of individual +TIPs is often determined by interactions with other +TIPs. For example, the *Schizosaccharomyces pombe* homologue of CLIP-170, Tip1p, is transported to the plus end by Tea2p kinesin, but its accumulation at the MT end also involves
the EB1 homologue Mal3p (Busch and Brunner, 2004). Similarly APC, in addition to being transported by kinesin II, can also associate with MT tips through binding to EB1 (Su *et al.*, 1995). Analysis of interactions between +TIPs reveals a complex network (figure 7). The mutual affinity of the +TIPs for each other is likely to contribute to their concentration at MT ends. Since most +TIPs can associate with MTs directly, interactions between them may take place mainly in the context of MT binding. +TIP distribution is probably influenced also by competition for MT binding sites.

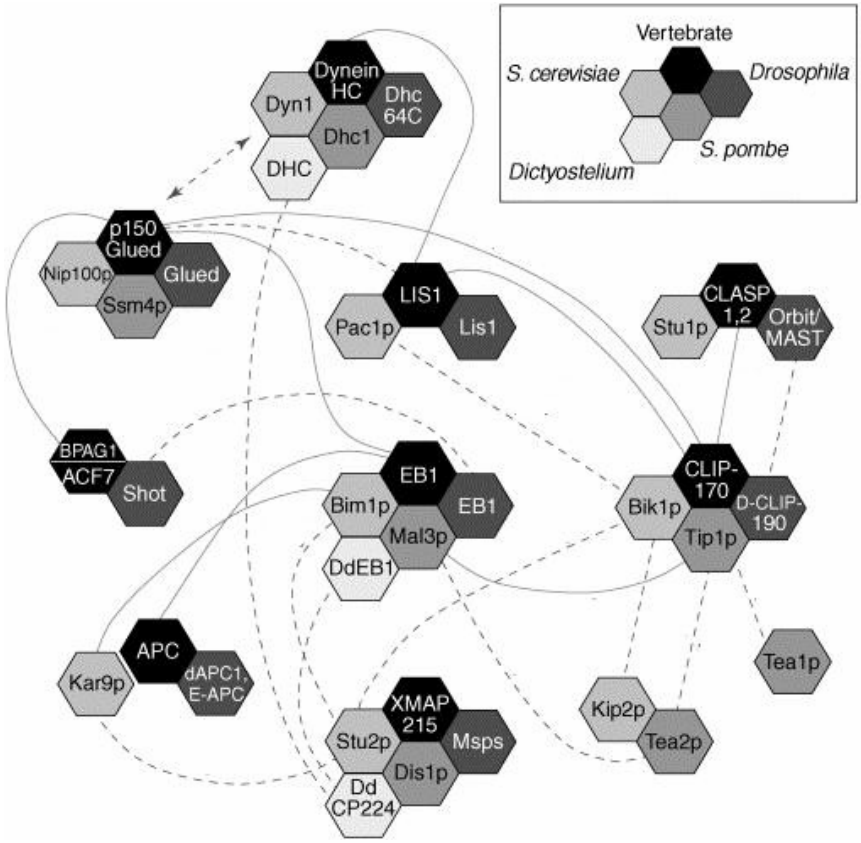

Vertebrate, *Drosophila, S. cerevisiae, S. pombe* and *Dictyostelium* +TIP homologues are indicated by boxes. Interactions, demonstrated to be direct, are shown by solid lines, and interactions, demonstrated only by yeast-two hybrid assays and/or co-immunoprecipitations from crude cell lysates, are shown by broken lines. The double-headed arrow indicates the interaction between dynein and dynactin complexes . (Akhmanova and Hoogenraad, 2005)

For example, CLIP-115 and CLIP-170 have very similar MT-binding domains (Table 1), and in CLIP-115-knockout cells the binding of CLIP-170 to the MT ends is enhanced (Hoogenraad *et al.*, 2002).

EB1 Interaction with Tumour Suppressor APC

EB1 was identified originally in a two-hybrid screen as a binding partner of the human tumour suppressor protein adenomatous polyposis coli (APC) (Su *et al.*, 1995). APC is a large multidomain protein (300 kDa) with a variety of functions including cellular signalling and organisation of the cytoskeleton. A major role of APC in the cytoplasm is the degradation, in cooperation with Axin and the kinase GSK3β, of β-catenin when Wnt signaling is not activated. In differentiated or confluent cells, APC mainly localises to the plasma membrane, especially at the sites of cell-cell contact; the localisation depends on the presence of actin

(Rosin-Arbesfeld *et al.*, 2001). There it may influence the genesis or maintenance of cell adhesion junctions or the regulation of the Wnt signalling pathway.

In addition, APC affects an apparently separate function in the regulation of the cytoskeleton. In subconfluent or migrating cells, it clusters on a subset of MTs close to the cortex. These are oriented toward lamellipodia or other cellular extensions. GFP-tagged APC moves specifically along these MTs and accumulates at their growing plus ends (Mimori-Kiyosue *et al.*, 2000). This accumulation depends on the interaction with the plus-end-directed kinesin KIF3A-KIF3B, which presumably transports the protein along MTs (Jimbo *et al.*, 2002). Another function of APC related to the cytoskeleton has been observed upon induction of migration in cultured cells (rat astrocytes), where APC is involved in the repositioning of the MTOC, downstream of Cdc42. A recent study speculated that repositioning occurs as a result of local capture of microtubules at the leading edge via APC, followed by dynein microtubule motor-dependent pulling on the microtubules (Etienne-Manneville and Hall, 2003).

The EB1-APC interaction was confirmed both *in vivo* and *in vitro* in pull-down assays. The EB1 binding site in APC is located at the C-terminal end of the protein. APC always colocalises with EB1 on the subset of microtubules with which it is associated. Whereas EB1 localisation to microtubule plus ends is independent of APC, APC probably relies on EB1 for its accumulation at microtubule tips. This proposal is based on the finding that the complex composed of the C-terminal part of APC and the EB1 binding domain colocalises with EB1 on growing microtubule ends all over the cell. APC has another C-terminal domain that is capable of binding microtubules on its own. However, a protein fragment containing only this domain does not accumulate at microtubule tips, but rather disperses over the entire microtubule(Askham *et al.*, 2000).

A recent study characterized a repeat domain in APC that is rich in Ser, Pro and basic residues and binds EB1 (Slep *et al.*, 2005). A similar domain has been found in microtubule–actin crosslinking factor-2 (MACF2), a mouse spectraplakin that resembles ACF7. The EB1-binding domain in CLASPs also contains repeat motifs rich in Ser, Pro and basic residues (Mimori-Kiyosue *et al.*, 2005). Alignment of the EB1-binding domains of APC, MACF2 and CLASP2 reveals homology.

Two studies have shown that full-length APC and the C-terminal part of APC containing the EB1 binding site are able to stabilise microtubules *in vitro* and *in vivo*, and observed a correlation between the dissociation of APC from a microtubule end and the occurrence of catastrophes (Nakamura *et al.*, 2001). One of these studies showed that the C-terminal part of APC only stabilises microtubules *in vitro* in the presence of EB1. Interestingly, replacing EB1 by its fission yeast homologue mal3p maintained the stabilising effect even though no homologue of APC is known in yeast (Nakamura *et al.*, 2001). This suggests that EB1 proteins are highly conserved with respect to their function. The interaction with EB1 might allow accumulation of APC at microtubule tips, while APC would facilitate interaction with specific membrane sites. APC could be involved in microtubule search and capture mechanisms at cellular protrusions, where it might selectively stabilize microtubules extending into the protrusions. The APC-EB1 interaction might therefore play a role in cell migration or adhesion.

A similar role for APC was predicted in the targeting of microtubules to kinetochores in mitosis. APC and EB1 function together in mitosis to regulate spindle dynamics and chromosome alignment (Green *et al.*, 2005). APC mutant cells are defective in spindle formation and chromosome segregation, yielding many short spindle microtubules that are unable to connect to kinetochores. Indeed APC localises to the ends of microtubules that are embedded in kinetochores (Fodde *et al.*, 2001;Kaplan *et al.*, 2001). Remarkably, APC is mutated in most cases of sporadic colorectal tumours and in familial colon cancer, which occurs in families with an inherited predisposition to develop this disease. These mutations truncate the C-terminal part of APC containing the EB1 binding domain. The deletion of the EB1 binding site in APC alone appears insufficient to induce tumours in mice (Smith *et al.*, 2003). However, the loss of the APC-EB1 interaction may lead to predisposition to cancer and could influence later stages of tumour progression, for example, due to resulting chromosome instability (Green and Kaplan, 2003).

There is no homologue of APC in budding yeast. However, budding yeast EB1 (Bim1) binds with its C-terminus to Kar9, a protein that might have functions similar to APC in relation to microtubules. Bim1 is required for the localisation of Kar9 along microtubules and at their plus ends; *in vitro,* Kar9 co-pellets with microtubules only in the presence of Bim1 (Lee *et al.*, 2000). Kar9 localises to the old spindle pole body and transfers in the G1 phase to the tips of cytoplasmic microtubules. It then binds the myosin Myo2, which translocates Kar9 and the

associated microtubule along actin cables to the bud neck. The capture of the microtubule tip at the bud neck is also thought to involve Kar9. The microtubule starts to shrink while remaining attached to the bud neck, so that the nucleus is pulled toward the bud. This process implicates Kar9 in the search and capture of the bud neck by cytoplasmic microtubules.(Kusch *et al.*, 2002; Liakopoulos *et al.*, 2003). Thus, Bim1 has at least two important functions in budding yeast cells: to stabilise microtubules so that they can grow long enough to reach their target sites, and to localise another factor - Kar9 - to the microtubule tip, which allows it to interact with the target site at the bud neck.

EB1-Dynactin Interaction

In addition to MT and APC binding, EB1 also associates with $p150^{Glued}$, a component of the dynein/dynactin motor complex (Berrueta *et al.*, 1999;Tirnauer *et al.*, 2002a). A recent report indicates that EB1 and $p150^{Glued}$ may form a ternary complex with MTs to promote MT polymerization (Ligon *et al.*, 2003).

EB1 has been shown to co-immunoprecipitate the dynactin components $p150^{glued}$, p50/dynamitin, and the intermediate chain of dynein, from lymphocytes and epithelial cells (Berrueta *et al.*, 1999). The interaction of EB1 proteins with components of the dynein/dynactin complex is well established (Berrueta *et al.*, 1999;Askham *et al.*, 2002;Bu *et al.*, 2003;Ligon *et al.*, 2003). It has been shown recently that EB1 interacts with the CAP-Gly domain of $p150^{glued}$ (Bu *et al.*, 2003;Hayashi *et al.*, 2005). Dynein is a minus-end directed MT motor, and dynactin is a complex of proteins that binds to dynein as well as to cargo proteins and activates transport of these cargoes by dynein. The dynactin component $p150^{glued}$ was shown to colocalise with EB1 at microtubule plus ends and to punctuate staining in the cytoplasm, along microtubules and at the centrosome.

The role of the EB1-$p150^{glued}$ interaction at microtubule tips is currently not clear. Overexpression of a C-terminal fragment of EB1 disrupts $p150^{glued}$ localisation to centrosomes and causes defects in microtubule minus-end focusing and anchoring at the centrosomes. This indicates that the interaction of EB1 and dynactin may serve to anchor minus ends to the centrosome (Askham *et al.*, 2002). Dynactin localizes to cortical sites and is required for spindle rotations. EB1 may regulate dynactin localization as with APC or,

reciprocally, dynactin may help to load EB1 onto the microtubules. In motile cells, dynein, like APC, is required for the Cdc42-dependent repositioning of the centrosome in the direction of migration. Whether interaction with EB1 influences this function, however, is not known (Palazzo *et al.*, 2001).

EB1 Interaction with other MAPs

A Rho family GTPase, Rho, was found to promote the formation of stable, de-tyrosinated, non-dynamic MT plus ends through its effector mDia, a formin that normally stimulates actin nucleation (Palazzo *et al.*, 2001;Li and Higgs, 2003). These stable microtubules extend preferentially in polarised, cultured cells from the MTOC at the nucleus toward the leading edge. Like the reorientation of the MTOC, they possibly help to bias microtubule-dependent vesicle transport towards the leading edge. mDia interacts directly with APC and the N-terminus of EB1, suggesting that Rho and mDia act by stabilising the microtubule tip complex (Wen *et al.*, 2004).

Increasing evidence indicates that the XMAP215/Dis1 family of MAPs also interacts with EB1. So far, very little is known about the role of this interaction. A two-hybrid screen of *Saccharomyces cerevisiae* identified Bim1 as an interactor of the XMAP215 homologue Stu2 (Chen *et al.*, 1998). Studies of *Dictyostelium discoideum* have shown that the two proteins co-immunoprecipitate and co-localise at the centrosome, the kinetochore and especially on the tips of interphase and spindle microtubules. Notably, this is the case despite the fact that *Dictyostelium* interphase microtubules do not show dynamic instability. However, the functions of the proteins do not seem to overlap much in *Dictyostelium*, because the XMAP215 homologue DdCP224 specifically affects interphase microtubule length and microtubule interaction with the cell cortex, while DdEB1 is involved in spindle formation (Hestermann and Graf, 2004).

III. Results

1. Thermodynamics of the Op18/stathmin-tubulin interaction

Srinivas Honnappa, Brian Cutting, Wolfgang Jahnke, Joachim Seelig and Michel O. Steinmetz

Journal of Biological Chemistry**,** (2003), 278(40):38926-34

This publication describes the findings of the first project carried out during my thesis. The aim of this research was to address a number of open issues on the tubulin-stathmin system. Originally, stathmin was identified as a protein that sequesters tubulin dimers and promotes catastrophes of microtubules. However, the exact mechanism of stathmin acting on microtubules was not fully understood. Moreover, other *in vivo* and *in vitro* studies concluded that stathmin acts as a pH-sensitive bifunctional protein. The paper aimed at providing a structural basis for understanding the tubulin-stathmin interation.

In this paper we employed ITC, electron microscopy, CD-spectroscopy, and NMR to investigate the biophysical and structural properties of the tubulin-stathmin interaction. The paper analyses the thermodynamics of tubulin-stathmin system, yielding quantitative interaction parameters. In addition, this publication addresses the question of whether small changes in pH have a significant effect on the conformation of free and tubulin-bound stathmin at the single residue level. Attempts to solve the structure of stathmin bound to tubulin by TROSY NMR were not successful.

My contribution to this publication was to purify stathmin in milligram amounts. Subsequently, I carried out all the biophysical characterization of tubulin-stathmin using ITC and CD and wrote the corresponding sections in experimental procedures. B. Cutting and W. Jahnke performed the NMR experiments, and J. Seelig the analysis of ITC.

THE JOURNAL OF BIOLOGICAL CHEMISTRY
Vol. 278, No. 40, Issue of October 3, pp. 38926–38934, 2003
Printed in U.S.A.

Thermodynamics of the Op18/Stathmin-Tubulin Interaction*

Received for publication, May 27, 2003, and in revised form, June 26, 2003
Published, JBC Papers in Press, July 14, 2003, DOI 10.1074/jbc.M305546200

Srinivas Honnappa‡, Brian Cutting§, Wolfgang Jahnke§, Joachim Seelig¶, and Michel O. Steinmetz‡‖

From the ‡Structural Biology, Paul Scherrer Institut, CH-5232 Villigen PSI, §Central Technologies, Novartis Pharma AG, CH-4002 Basel, and the ¶Department of Biophysical Chemistry, Biozentrum, University of Basel, CH-4056 Basel, Switzerland

Op18/stathmin (stathmin) is an intrinsically disordered protein involved in the regulation of the microtubule filament system. One function of stathmin is to sequester tubulin dimers into assembly incompetent complexes, and recent studies revealed two tubulin binding sites per stathmin molecule. Using high sensitivity isothermal titration calorimetry, we document that at 10 °C and under the conditions of 80 mM PIPES, pH 6.8, 1 mM EGTA, 1 mM $MgCl_2$, 1 mM GTP these two binding sites are of equal affinity with an equilibrium binding constant of $K_0 = 6.0 \times 10^6$ M^{-1}. The obtained large negative molar heat capacity change of $\Delta C_p^0 = -860$ cal mol^{-1} K^{-1} (referring to tubulin) for the tubulin-stathmin binding equilibrium suggests that the hydrophobic effect is the major driving force of the binding reaction. Replacing GTP by GDP on β-tubulin had no significant effect on the thermodynamic parameters of the tubulin-stathmin binding equilibrium. The proposed pH-sensitive dual function of stathmin was further evaluated by circular dichroism spectroscopy and nuclear magnetic resonance. At low temperatures, stathmin was found to be extensively helical but devoid of any stable tertiary structure. However, in complex with two tubulin subunits stathmin adopts a stable conformation. Both the stability and conformation of the individual proteins and complexes were not significantly affected by small changes in pH. A 4-fold decrease in affinity of stathmin for tubulin was revealed at pH 7.5 compared with pH 6.8. This decrease could be attributed to a weaker binding of the C terminus of stathmin. These findings do not support the view that stathmin works as a pH-sensitive protein.

Microtubule (MT)[1] filaments are dynamic polymers made of α/β-tubulin heterodimers that are essential for a wide variety of central cellular functions in all eucaryotes, including cell transport, cell motility, and mitosis. One of the key properties of MTs is that of "dynamic instability" (1). Dynamic instability comprises the continuous switching between catastrophes (depolymerization or shrinkage phase) and rescues (polymerization or growing phase) of individual MTs and is central to MT function. In recent years, it has become clear that the balance between MT-stabilizing and -destabilizing factors is responsible for the observed switching between growth and shrinkage of MTs *in vivo* (2). Therefore, obtaining molecular insights into the mechanisms of action of MT regulatory factors is essential to understand how they contribute to the dynamic state of MTs during the cell cycle.

The members of the phylogenetically well conserved Op18/stathmin family are phosphorylation-controlled MT-destabilizing proteins (reviewed in Refs. 3–8). They are important for proper cell cycle progression in many types of proliferating eucaryotic cells (3, 4, 8), were found to be crucial for the development of the nervous system in *Drosophila* (9), promote neurite outgrowth through regulation of MT dynamics in growth cones (10), and are implicated in a wide variety of cancers (11, 12). Human Op18/stathmin (referred to as stathmin (3)) is an evolutionary well conserved 17-kDa cytoplasmic phosphoprotein. The monomeric protein consists of a N-terminal capping domain (13, 14) and a C-terminal helical interaction domain (13, 15–19). Originally, stathmin was described as a protein that binds to tubulin dimers and increases the catastrophe frequency of MT *in vitro* (20). Subsequent studies have identified two putative mechanisms for stathmin: (i) Tubulin dimer sequestration that slows MT growth rate (21, 22) and (ii) direct stimulation of MT plus-end catastrophes (23–29). The sequestering mechanism is largely supported by recent structural and biophysical studies (13, 14, 16–18, 30–32). As illustrated in Fig. 1, the C-terminal helical domain of the stathmin-like domain (SLD) of the neural isoform RB3 can bind two head-to-tail aligned α/β-tubulin heterodimers. The tubulin subunits in the ternary complex are tilted with respect to each other by ~25°. The N-terminal part of stathmin was found to cap one α-tubulin monomer to prevent further longitudinal tubulin assembly. Hence, binding of stathmin to tubulin makes these sequestered tubulin subunits efficiently assembly incompetent.

However, other *in vivo* and *in vitro* studies converged to the hypothesis that stathmin works as a pH-sensitive bifunctional protein: At pH 6.8 stathmin is supposed to act as a sequestering protein, whereas at pH 7.5 it primarily stimulates MT plus-end catastrophes without significantly interacting with tubulin subunits (24, 28). This view is supported by deletion mapping, which indicated that the N terminus of stathmin is required for plus-end catastrophe promotion, whereas the function of the C-terminal helical domain is to bind tubulin dimers (24, 29). In contrast to the well characterized sequestering mechanism, the molecular details of how stathmin interacts with MT ends and triggers catastrophes are not clear.

Here we have combined isothermal titration calorimetry (ITC), transmission electron microscopy (TEM), circular dichroism (CD) spectroscopy, and nuclear magnetic resonance

* This work was supported by the Swiss National Science Foundation (Grant 31-58800.99 to J. S. and Grant 31-64978.01 to M. O. S.). The costs of publication of this article were defrayed in part by the payment of page charges. This article must therefore be hereby marked "*advertisement*" in accordance with 18 U.S.C. Section 1734 solely to indicate this fact.

‖ To whom correspondence should be addressed. Tel.: 41-56-310-4754; Fax: 41-56-310-2080; E-mail: michel.steinmetz@psi.ch.

[1] The abbreviations used are: MT, microtubule; CD, circular dichroism; SLD, stathmin-like domain; HSQC, heteronuclear single quantum coherence; ITC, isothermal titration calorimetry; PIPES, 1,4-piperazinediethanesulfonic acid; TEM, transmission electron microscopy; TROSY, transverse-relaxation optimized spectroscopy.

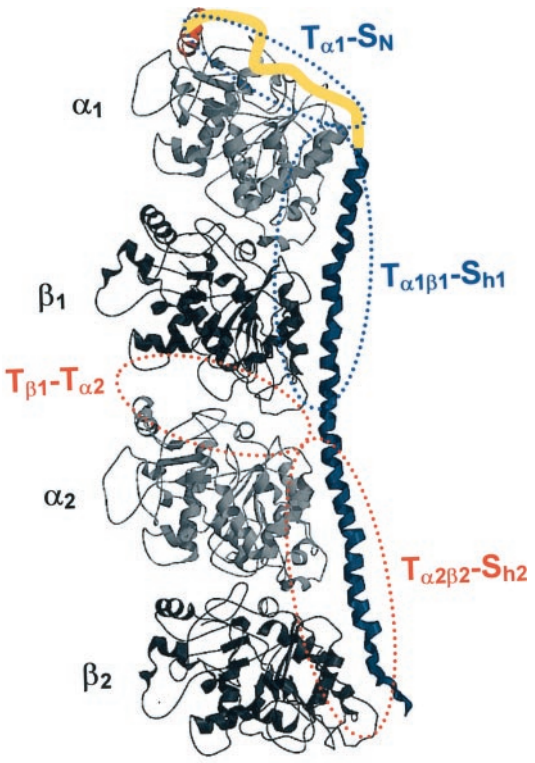

FIG. 1. **Current structural view of the ternary tubulin-stathmin complex.** The structure of the complex has been investigated by electron microscopy (13), by a 4-Å resolution x-ray structure of the tubulin-RB3-SLD complex (note that RB3-SLD exhibits 72% identity with stathmin (17)), and by chemical cross-linking (14). The tubulin-stathmin complex consists of two head-to-tail aligned α/β-tubulin heterodimers (represented as *light* and *dark gray ribbons*) that are tilted with respect to each other by ~25°. The 4-Å x-ray structure shows the C-terminal domain of stathmin folded into an extended 91-residue helix (represented as a *blue ribbon*) that interacts in a regular fashion along the two longitudinally aligned tubulin dimers. Because of the lack of resolution, the interaction face of the helix with tubulin could not be defined. The N-terminal domain (schematically represented as *yellow slip knot*), which was not resolved in the x-ray electron density map, was found to bind close to helix 10 (red helix at the tip of the α1-tubulin monomer) and to the loop connecting helix 10 with beta strand 9 of the α1-tubulin monomer (14). These represent critical secondary structural elements that are involved in establishing both longitudinal as well as lateral protofilament contacts of tubulin subunits within the MT wall (48). Four contact points (denoted $T_{\alpha1}$-S_N, $T_{\alpha1\beta1}$-S_{h1}, $T_{\beta1}$-$T_{\alpha2}$, and $T_{\alpha2\beta2}$-S_{h2}; see also "Discussion") between the two tubulin subunits and stathmin are indicated by *dotted blue* (for the first tubulin subunit) and *red* (for the second tubulin subunit) *circles*.

(NMR) spectroscopy to investigate the biophysical and structural characteristics of the interaction of stathmin with tubulin. We report that stathmin binds two tubulin subunits with equal affinities under all conditions investigated. The thermodynamic data suggest that the hydrophobic effect represents the major driving force governing the tubulin-stathmin binding reaction. The affinity of stathmin for tubulin as well as the stabilities and conformations of the individual proteins are not significantly affected by small changes in pH. Nevertheless, the small affinity change that was observed between pH 6.8 and 7.5 can be attributed to the weaker binding of the C terminus of stathmin. The results presented are discussed in the context of current functional and structural data on the tubulin-stathmin system.

EXPERIMENTAL PROCEDURES

Protein Preparations—The cloning of the human full-length stathmin cDNA into the bacterial expression vector pET-16b (Novagen) is outlined in Ref. 13. Recombinant stathmin was expressed in LB medium using the *Escherichia coli* host strain JM109(DE3) (Promega), affinity-purified as His_6-tagged fusion protein by immobilized metal affinity chromatography on Ni^{2+}-Sepharose (Amersham Biosciences), and separated from the N-terminal His_6 tag by proteolytic cleavage with an immobilized snake venom prothrombin activator (for details, see Ref. 13). After dialysis in 20 mM Tris-HCl, pH 8.0, a RESOURCE Q (Amersham Biosciences) anion exchange chromatography step using a NaCl gradient from 0 to 500 mM was performed.

For the preparation of $^2H/^{13}C/^{15}N$ uniformly labeled stathmin, cells were grown in modified new minimal medium (33, 34): 55 mM KH_2PO_4, 100 mM K_2HPO_4, 10 mM Na_2SO_4, 1 mM $MgSO_4$, 1 mg/liter Ca^{2+}, 1 mg/liter Fe^{2+}, 1 μg/liter Cu^{2+}, 1 μg/liter Mn^{2+}, 1 μg/liter Zn^{2+}, 1 μg/liter MnO_4^{2-}, 10 mg/liter thiamine, 10 mg/liter biotin, 3 g/liter d_7-$^{13}C_6$-D-glucose, and 1 g/liter $^{15}NH_4Cl$. Transformed bacteria were stepwise adapted to 99.9% D_2O in new minimal medium supplemented with 100 μg/ml ampicillin prior to expression. A 1-liter cell culture was induced with 1 mM isopropyl-1-thio-β-D-galactopyranoside after growth at 37 °C to an A_{600} of 0.6. Affinity purification and processing of the recombinant triple-labeled stathmin was the same as for the unlabeled protein. The homogeneities (~99%), identities, and labeling efficiencies of protein samples were confirmed by matrix-assisted laser desorption ionization-mass spectrometry.

Highly pure bovine brain GTP-tubulin was obtained from Cytoskeleton Inc. GDP-tubulin was prepared by incubating 1 mg/ml GTP-tubulin in G buffer, pH 6.8 (80 mM PIPES-KOH, 1 mM $MgCl_2$, 1 mM EGTA) supplemented with 2 mM GDP on ice for 40 min (35).

All protein samples were centrifuged at 4 °C and at full speed for 10 min in a tabletop Eppendorf centrifuge prior to the experiments. Concentrations of protein samples were determined by the Advanced Protein Assay (Cytoskeleton Inc.).

High Sensitivity ITC—ITC experiments were performed using a VP-ITC calorimeter (Microcal Inc., Northampton, MA). For each experiment, the sample cell (volume 1.4 ml) was filled with a ~10 μM tubulin solution in G buffer pH 6.8 or 7.5 supplemented with either 1 mM GTP or 2 mM GDP. A 300-μl syringe was filled with a solution of ~100 μM stathmin (present in the same buffer as tubulin). The reference cell contained buffer only. Typically, 5-μl stathmin aliquots from the stirred syringe (305 rpm) were injected 40 times into the sample cell. At each injection, tubulin was bound to stathmin, leading to a characteristic heat signal. Integration of the individual calorimeter traces yielded the heat of binding, h_i, of each injection step. The heats of dilution of stathmin were subtracted from the titration data. During the course of the titration the total tubulin concentration is slightly diluted due to the addition of stathmin. This effect is small but nevertheless was taken into account in the evaluation. The binding isotherms were fitted via a non-linear least squares minimization method to determine the binding stoichiometry, n, the equilibrium binding constant, K_0, and the change in enthalpy, ΔH^0 (see "Results"). For all titrations, the experimental conditions warranted that tubulin remained in the soluble heterodimeric state.

Glycerol Spraying/Low-angle Rotary Metal Shadowing and TEM—Protein samples (0.5 mg/ml) in G buffer, pH 6.8, supplemented with 1 mM GTP were incubated for 1 h at room temperature after which glycerol was added to a final concentration of 30%. The samples were immediately sprayed onto freshly cleaved mica and rotary shadowed in a BA 511M freeze-etch apparatus (Balzers) with platinum/carbon at an elevation angle of 3–5° (36). Electron micrographs were taken in a Philips Morgagni TEM operated at 80 kV equipped with a Megaview III charge-coupled device camera. Approximately 400 particles were counted from single micrographs and visually classified into globular and elongated specimens, 8–10 nm and 8–10 × 16–20 nm, respectively.

CD Spectroscopy—Protein samples were in 8 mM PIPES-KOH, pH 6.8 or 7.5, 1 mM $MgCl_2$, 1 mM EGTA, and 1 mM GTP. Far-UV CD spectra and thermal unfolding profiles were recorded on a Jasco J-810 spectropolarimeter (Jasco Inc.) equipped with a temperature-controlled quartz cell of 0.1-cm path length. The spectra shown are the averages of five accumulations and were evaluated with the Jasco and Sigma Plot (Jandel Scientific) software. A ramping rate of 1 °C·min^{-1} was used to record the thermal unfolding profiles. The apparent midpoints of the transitions, values of T_m, were taken as the maximum of the derivative, $d[\Theta]_{222}/dT$.

NMR Spectroscopy—NMR experiments were carried out at 23 °C on a Varian UnityPlus spectrometer operating at a ^1H frequency of 600 MHz. Samples of $^2H/^{13}C/^{15}N$-labeled stathmin and unlabeled tubulin were in G buffer at pH 6.8 or 7.5. Both ^{15}N-^1H HSQC and ^{15}N-^1H TROSY experiments were recorded. However, the TROSY spectra were not superior to the HSQC spectra, probably due to the high proton density in non-deuterated tubulin. The data were analyzed with the VNMR software.

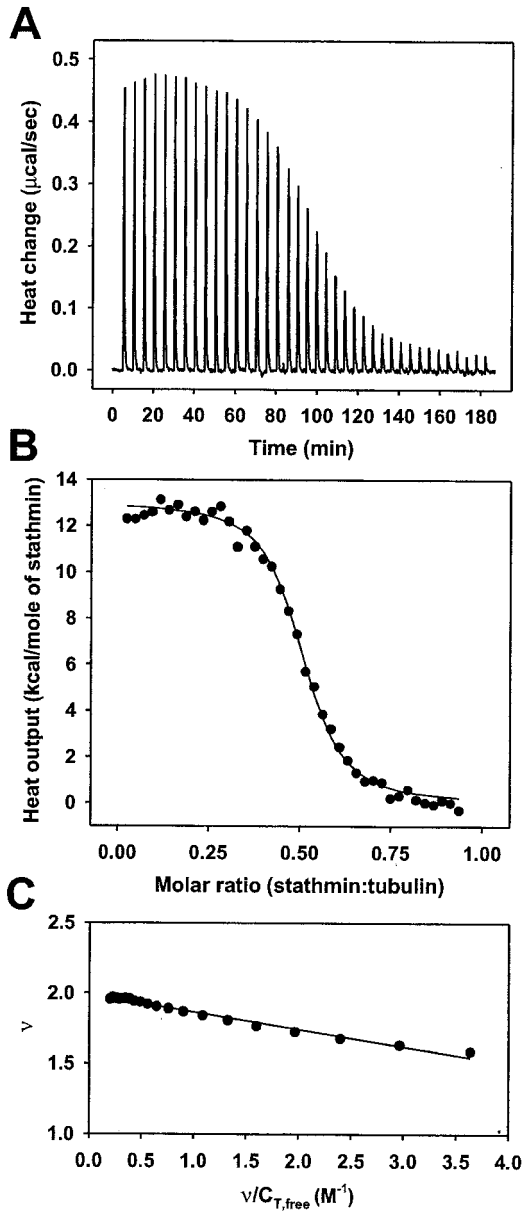

FIG. 2. **ITC analysis of the tubulin-stathmin binding equilibrium.** *A*, raw data obtained for 40 injections, each of 5 μl, of stathmin (84.0 μM) into the sample cell containing 12.8 μM GTP-tubulin. *B*, integrated heats of reaction (*closed circles*) with the best fit to the data (*line*). The fit was calculated with $n = 2$ by a non-linear least squares minimization to Equation 2 and yielded $\Delta H^0_{\text{GTP-tubulin}} = 15.0 \pm 0.14$ kcal mol^{-1} GTP-tubulin and $K_0 = 6.0 \times 10^6 \pm 0.61 \times 10^6$ M^{-1}. *C*, Scatchard plot (Equation 6) of the binding data (*closed circles*). The *straight line* is obtained with $n = 1.99$ and $K_0 = 8.2 \times 10^6$ M^{-1}. The measurement was carried out at 10 °C in 80 mM PIPES-KOH, pH 6.8, 1 mM $MgCl_2$, 1 mM EGTA, 1 mM GTP.

RESULTS

Analysis of the Tubulin-Stathmin Binding Equilibrium by ITC—To assess the thermodynamic binding parameters of the tubulin-stathmin binding equilibrium, ITC studies were performed. Fig. 2*A* shows a typical titration profile in which 12.8 μM GTP-tubulin (referred to as the α/β-tubulin heterodimer with GTP occupying the exchangeable E-site on β-tubulin (2)) is titrated with stathmin. Each titration peak corresponds to the injection of 5-μl aliquots of a 84.0 μM stathmin solution. At 10 °C, the reaction is endothermic, and the reaction heats decrease with increasing injection numbers as less and less free tubulin is available for stathmin binding. The total stathmin concentration in the calorimeter cell varies during the course of the titration and increases from 0.3 μM after the first injection to 10.5 μM after 40 injections. After ~30 injections, all tubulin is bound to stathmin, and no further heat is produced. Fig. 2*B* shows the integrated heats of reaction as a function of the stathmin:tubulin molar ratio.

The analysis of the binding isotherm is based on a model that assumes n independent and equal binding sites on stathmin for tubulin. If C^0_S, $C_{T,bound}$, and $C_{T,free}$ denote the concentration of total stathmin in the calorimeter cell, and the concentration of bound and free tubulin, respectively, then the binding isotherm can be described as (37),

$$\frac{C_{T,bound}}{C^0_S} = n\,\frac{K_0 C_{T,free}}{1 + K_0 C_{T,free}} \qquad \text{(Eq. 1)}$$

where K_0 is the intrinsic equilibrium binding constant for a single binding site. Equation 1 can be solved for $C_{T,bound}$ via,

$$C_{T,bound} = \frac{1}{2}\left(\frac{1}{K_0} + C^0_T + nC^0_S\right) - \frac{1}{2}\sqrt{\left(\frac{1}{K_0} + C^0_T + nC^0_S\right)^2 - 4nC^0_S C^0_T} \qquad \text{(Eq. 2)}$$

where C^0_T is the total concentration of tubulin in the calorimeter cell. If we denote with h_i the measured heat of the ith injection step and by $r^{(k)}$ the fraction of bound tubulin after a total of k injections, then Equation 3 results.

$$r^{(k)} = \frac{\sum_1^k h_i}{\sum_1^m h_i} \qquad \text{(Eq. 3)}$$

The numerator gives the cumulative heat of the first k injections, the denominator is the total heat produced when the supply of the tubulin is exhausted after a total of m injections. The concentrations of bound and free tubulin are then given by Equations 4 and 5.

$$C^{(k)}_{T,bound} = C^0_T \cdot r^{(k)} \qquad \text{(Eq. 4)}$$

$$C^{(k)}_{T,free} = C^0_T(1 - r^{(k)}) \qquad \text{(Eq. 5)}$$

$C_{T,bound}$ and $C_{T,free}$ can thus be determined without any assumptions about the binding mechanism. Because $C_{T,bound}$ is directly accessible via the heats of titration, it is possible to calculate unambiguously the stoichiometry, n, the apparent molar heat of reaction, ΔH^0, and the equilibrium binding constant, K_0, via a non-linear least squares fit to Equation 2 (38, 39). The *solid line* in Fig. 2*B* calculated with $n = 2$ represents the best fit to the experimental data and yielded $\Delta H^0_{\text{GTP-tubulin}} = 15.0 \pm 0.14$ kcal mol^{-1} GTP-tubulin, and $K_0 = 6.0 \times 10^6 \pm 0.61 \times 10^6$ M^{-1}.

The classic way of representing biochemical binding data is by using the Scatchard plot, which plots,

$$\nu = n - K_D\frac{\nu}{C_{T,free}} \qquad \text{(Eq. 6)}$$

where $K_D = 1/K_0$ denotes the dissociation constant, $\nu = C_{T,bound}/C^0_S$, and $C_{T,free}$ can be determined according to Equations 3–5. Fig. 2*C* shows the corresponding plot. A straight line is obtained with $n = 1.99$ and $K_0 = 8.2 \times 10^6$ M^{-1}, which agrees with the non-linear least squares fit shown in Fig. 2*B*. All titration experiments performed were also analyzed by Scatchard plots (not shown). It should be noted, however, that the evaluation of the measured h_i via a non-linear least squares fit to Equation 2 is more accurate.

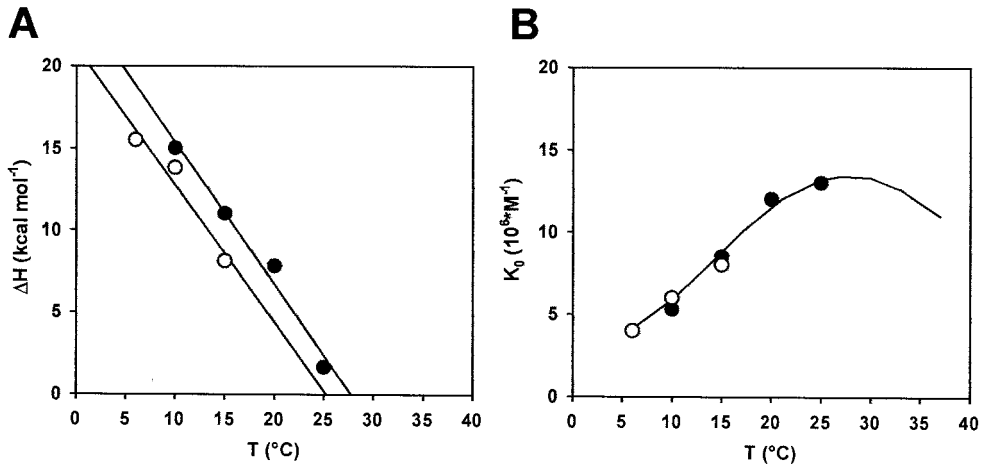

FIG. 3. **Monitoring the tubulin-stathmin binding equilibrium as a function of temperature.** *A*, reaction enthalpies ΔH^0 of GTP-tubulin- (*closed circles*) and GDP-tubulin-stathmin (*opened circles*). The reaction enthalpies decrease linearly with temperature according to $\Delta H^0_{\text{GTP-tubulin}}$ (kcal mol^{-1} GTP-tubulin) = $-0.86\ T(°C) + 24.0$ and $\Delta H^0_{\text{GTP-tubulin}}$ (kcal mol^{-1} GDP-tubulin) = $-0.85\ T(°C) + 21.2$. *B*, equilibrium binding constants K_0 for the GTP-tubulin- (*closed circles*) and GDP-tubulin-stathmin (*opened circles*) interaction as a function of temperature. The *solid line* is the theoretical prediction calculated with the van't Hoff equation (Equation 7).

Next, the GTP-tubulin-stathmin binding reaction was monitored as a function of temperature. Fig. 3 (*A* and *B*) illustrates the variation of the reaction enthalpy and the binding constant with temperature. The reaction enthalpy was found to be endothermic at low temperatures and decreased linearly with temperature according to $\Delta H^0_{\text{GTP-tubulin}}$ (kcal mol^{-1} GTP-tubulin) = $-0.86\ T(°C) + 24.0$ (Fig. 3*A*). Extrapolation to higher temperatures predicts $\Delta H^0_{\text{GTP-tubulin}} = 0$ kcal mol^{-1} at 28 °C and exothermic $\Delta H^0_{\text{GTP-tubulin}}$ values above this temperature. Hence, below 28 °C the interaction between GTP-tubulin and stathmin is completely entropy-driven, above this temperature both enthalpy and entropy contribute favorably to the binding reaction. The slope of the *straight line* in Fig. 3*A* corresponds to the molar heat capacity change of the binding reaction $\Delta C^0_p = -860$ cal mol^{-1} K^{-1} (referring to tubulin). This is a very large negative change in heat capacity indicative of a hydrophobic reaction. Considering the temperature dependence of the binding reaction, K_0 reaches a maximum value of $K_0 = 1.3 \times 10^7$ M^{-1} at 28 °C when $\Delta H^0_{\text{GTP-tubulin}} = 0$ kcal mol^{-1} and decreases again thereafter. The *solid line* in Fig. 3*B* is the theoretical prediction of the temperature dependence of K_0 calculated with the van't Hoff equation taking ΔC^0_p into account in Equation 7.

$$\frac{d \ln K_0}{dT} = \frac{\Delta H^0 + \Delta C^0_p (T - T_0)}{RT^2} \qquad \text{(Eq. 7)}$$

The free energy can then be calculated according to $\Delta G^0 = -RT \ln K$, and the entropy term is $T\Delta S^0 = \Delta H^0 - \Delta G^0$. The corresponding evaluations are summarized in Table I.

It has been reported that stathmin only modestly enhances the slow basal GTPase activity of tubulin (26, 28, 29, 40–42). To ensure that GTP hydrolysis does not influence the binding isotherm within the time scale of the experiment, ITC measurements with GDP-tubulin (referred to as the α/β-tubulin heterodimer with GDP occupying the exchangeable E-site on β-tubulin (2)) were carried out. As summarized in Table I, the thermodynamic parameters remained almost constant at pH 6.8. The reaction enthalpy varied linearly with $\Delta H^0_{\text{GTP-tubulin}}$ (kcal mol^{-1} GDP-tubulin) = $-0.85\ T(°C) + 21.2$ and extrapolation to higher temperatures predicts $\Delta H^0_{\text{GTP-tubulin}} = 0$ kcal mol^{-1} at 26 °C (Fig. 3). Hence, within the accuracy of the measurements, the binding constants are identical for both GTP- and GDP-tubulin. Consistent with previous reports (30, 31), changing the pH from 6.8 to 7.5 had little influence on the thermodynamic parameters (Table I). At 10 °C and pH 7.5 the equilibrium binding constant was $K_0 = 1.4 \times 10^6$ M^{-1}, four times smaller than the one measured at pH 6.8.

TABLE I
Thermodynamic binding parameters derived from the titration of tubulin with stathmin

ITC measurements were carried out in 80 mM PIPES, 1 mM EGTA, 1 mM $MgCl_2$ supplemented with either 1 mM GTP (for tubulin-GTP) or 2 mM GDP (for tubulin-GDP) at the indicated temperature (*T*) and pH value.

T	pH	ΔH^a	$K_0{}^b$	ΔG^c	$T\Delta S^d$
°C		*kcal mol^{-1}*	*10^1 M^{-1}*	*kcal mol^{-1}*	*kcal mol^{-1} K^{-1}*
Tubulin-GTP					
10	6.8	15.0	6.0	−8.7	23.7
15	6.8	11.0	8.5	−9.1	20.1
20	6.8	7.8	12.0	−9.5	17.3
25	6.8	1.7	13.0	−9.7	11.3
10	7.5	14.4	1.4	−7.9	22.3
Tubulin-GDP					
6	6.8	15.6	4.0	−8.4	24.0
10	6.8	13.8	6.0	−8.7	22.5
15	6.8	8.1	8.0	−9.1	17.2

[a] Reaction enthalpy per mol of tubulin. The fitting error for each value was ≤2%.
[b] Equilibrium binding constant. The fitting error for each value was ≤15%.
[c] Reaction free energy.
[d] Reaction entropy term.

In summary, the ITC results revealed that under all conditions investigated stathmin binds two tubulin subunits with equal intrinsic affinities. They further suggest that at physiological temperatures, the hydrophobic effect is the major driving force governing the tubulin-stathmin binding reaction.

Visualization of Tubulin-Stathmin Complexes by TEM—Complex formation at different stathmin to tubulin molar ratios was visualized directly by TEM (Fig. 4). In the absence of stathmin, GTP-tubulin molecules, after glycerol spraying and subsequent rotary metal-shadowing, yielded >95% uniformly distributed globular particles, 8–10 nm in diameter (Fig. 4*A*). In the presence of stathmin at a 0.5:1 molar ratio, ~20% of the particles were still 8–10 nm in diameter, however, ~80% of them were distinctly elongated with dimensions of 8–10 × 16–20 nm (Fig. 4*B*). The elongated particles have been previously identified as ternary tubulin-stathmin complexes (13). In the presence of stathmin at a 1.25:1 molar ratio, ~70% of the particles were 8–10 nm in diameter and only ~30% revealed the elongated shape of 8–10 × 16–20 nm (Fig. 4*C*). Note that

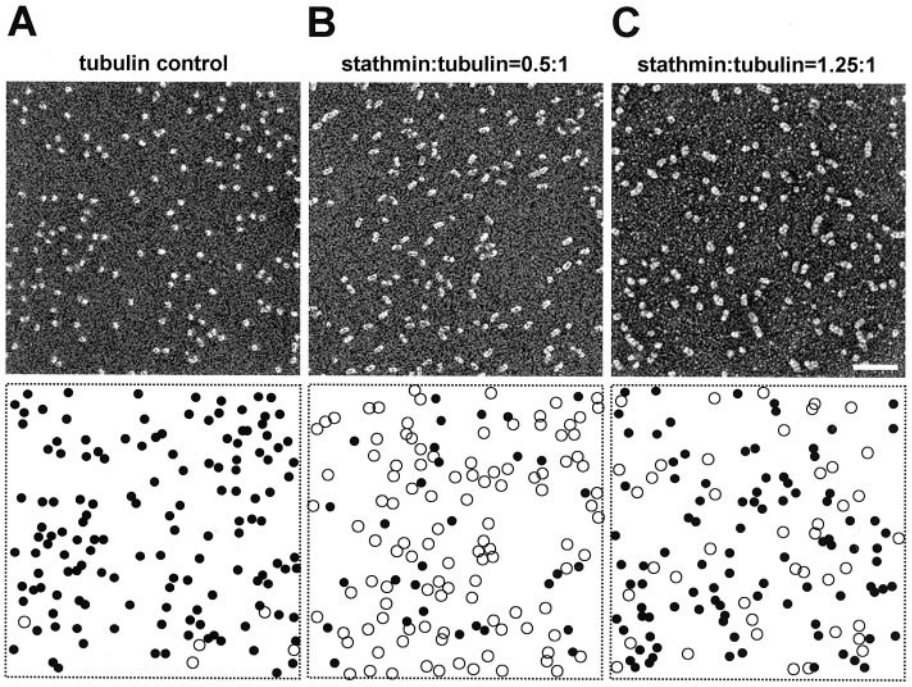

FIG. 4. **Visualizing tubulin-stathmin complexes by TEM.** *A*, glycerol-sprayed/rotary metal shadowed tubulin subunits in the absence of stathmin. *B*, mixture of stathmin and GTP-tubulin at a 0.5:1 molar ratio. *C*, mixture of stathmin and GTP-tubulin at a 1.25:1 molar ratio. *Scale bar*, 100 nm. Beneath each electron micrograph the assignment of the globular 8–10 nm (*black dots*) and elongated 8–10 × 16–20 nm (*circles*) particles is shown.

because of its elongated and thin structure (1 nm in diameter (13)) the excess of unbound stathmin does not affect the evaluation. Together, these findings suggest that the 8- to 10-nm particles seen in the presence of equimolar amounts of stathmin correspond predominantly to binary tubulin-stathmin complexes.

CD and NMR Measurements on the Tubulin-Stathmin System—It has been proposed that a shift in pH from 6.8 to 7.5 switches the function of stathmin from tubulin sequestration to specific stimulation of MT catastrophes (8, 24, 28). To probe for conformational differences of the tubulin-stathmin system at these two pH values, far-UV CD and NMR measurements were carried out. As shown in Fig. 5*A*, CD spectra recorded at 5 °C from stathmin and pH 6.8 or 7.5 revealed two minima centered at 207 and 222 nm characteristic of proteins with ~60% helical content for both pH values. The differences in the mean molar ellipticities [Θ] between the two spectra were less than 4% throughout the wavelength range. Similar, fully reversible non-cooperative thermal unfolding transitions were obtained for both pH values (Fig. 5*B*). The profiles indicate that stathmin unfolds rapidly with increasing temperature. Spectra recorded at different temperatures revealed a constant shift in the wavelength of the first minimum from 207 at 5 °C to 200 nm at 70 °C, consistent with a shift in the equilibrium from helix to random coil (not shown). Throughout the temperature range from 5 to 70 °C, the conformational difference of stathmin between pH 6.8 and 7.5 is marginal. Similar experiments were carried out with tubulin in the absence and presence of stathmin. CD spectra recorded from GTP-tubulin at 5 °C and pH 6.8 or 7.5 revealed minima centered at 208 and 222 nm characteristic for the presence of ~40% helical structure (Fig. 5*C*). The differences in the mean molar ellipticities [Θ] between the two spectra were less than 5% throughout the wavelength range. Similar cooperative thermal unfolding profiles with single midpoint of transitions T_m centered at 59.0 and 58.4 °C for pH 6.8 and pH 7.5, respectively, were obtained (Fig. 5*D*). The profiles were not reversible upon cooling. As for stathmin, the conformational difference of GTP-tubulin between pH 6.8 and 7.5 is marginal throughout the temperature range from 5 to 50 °C. In the presence of a 0.5:1 molar ratio of stathmin to GTP-tubulin, a slight increase of 10% in the helical signal at 15 °C compared with free GTP-tubulin was apparent (Fig. 5*D*). This finding suggests that, at low temperatures, extensive helix formation in stathmin is not induced upon binding to tubulin. The change in helical conformation can be estimated by the $[\Theta]_{222}$ value according to $-\Delta[\Theta]_h = (\frac{1}{3} \times [\Theta_S] + \frac{2}{3} \times [\Theta_T]) - [\Theta_{complex}]$, where $[\Theta_S]$, $[\Theta_T]$, and $[\Theta_{complex}]$ are the mean residue ellipticities measured at 222 nm of stathmin, tubulin, and tubulin-stathmin, respectively. A calculation at 10 and 35 °C yields $\Delta[\Theta]_h$ values of approximately −1000 and −2500 deg cm^2 dmol^{-1}, respectively. This corresponds to a 3–7% increase in the helical structure of stathmin upon binding to tubulin within this temperature range if it is assumed that the tubulin subunits do not contribute to $\Delta[\Theta]_h$. The thermal unfolding profiles obtained in the presence of a 0.5:1 molar ratio of stathmin to GTP-tubulin at pH 6.8 and 7.5 revealed single transitions centered at T_m = 61.2 and 59.6 °C, respectively (Fig. 5*D*). The progressions and corresponding T_m values of the profiles were very similar to their counterparts recorded from pure GTP-tubulin, suggesting that the bound stathmin melts in parallel with the tubulin subunits and does not significantly increase their thermal stabilities.

NMR of uniformly $^{2}H/^{13}C/^{15}N$-labeled stathmin and unlabeled GTP-tubulin was used to assess possible pH-induced conformational differences of stathmin when bound to tubulin at the single residue level. At pH 6.8, the two-dimensional $^{15}N,^{1}H$ correlation spectrum (HSQC or TROSY) of unbound stathmin revealed ~50 sharp and ~90 broader backbone N-H resonances (Fig. 6*A*; see also Ref. 13). The sharp resonances are characteristic of unstructured and flexible residues. The broader resonances with limited chemical shift dispersion indicate that these residues are in rapid exchange between random coil and helical conformations. In the presence of a 1:0.4 molar ratio of GTP-tubulin to stathmin, the $^{13}C/^{15}N$ labels allowed the selective monitoring of stathmin residues in the predominantly formed ternary tubulin-stathmin complex. As expected for a large 200-kDa complex, at pH 6.8 most resonances disappeared in the HSQC spectrum indicating that most stathmin residues adopt a stable conformation upon binding to tubulin (Fig. 6*B*). Eight stathmin backbone N-H resonances remained visible in the HSQC spectrum characteristic of flexible residues. Additional signals are not seen in TROSY

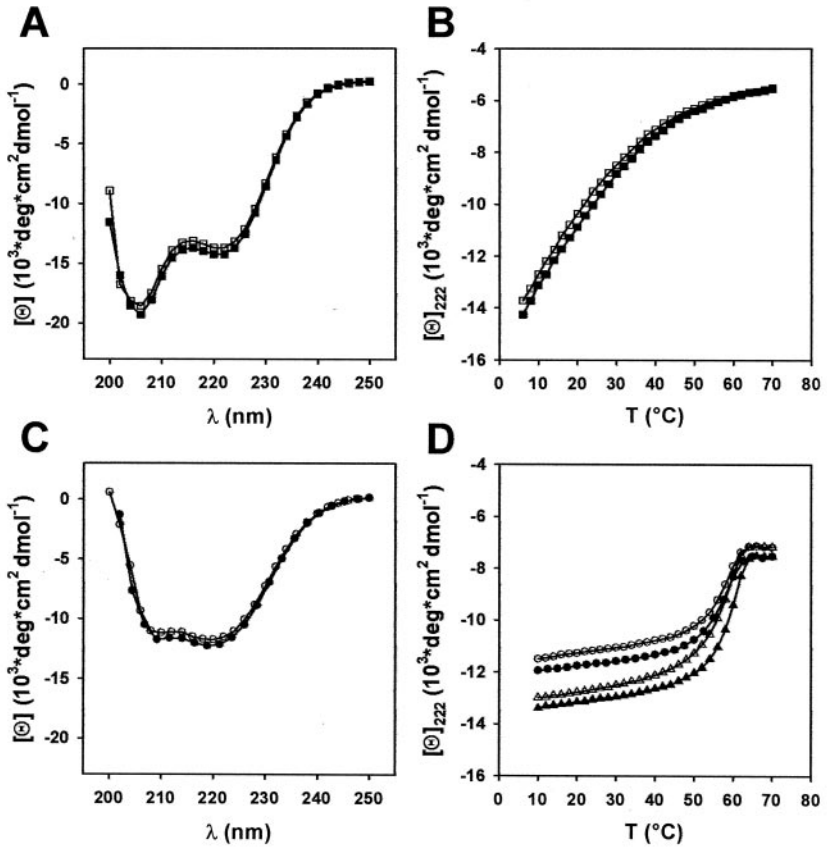

FIG. 5. **CD analysis of the tubulin-stathmin system.** *A*, far-UV CD spectra of 20 μM stathmin recorded at 5 °C and pH 6.8 (*closed squares*) or pH 7.5 (*opened squares*). *B*, thermal unfolding profiles of 20 μM stathmin recorded at 222 nm. *Symbols* are the same as for *A*. *C*, far-UV CD spectra of 10 μM GTP-tubulin recorded at 5 °C and pH 6.8 (*closed circles*) or pH 7.5 (*opened circles*). *D*, thermal unfolding profiles of 10 μM GTP-tubulin (*closed circles*) and a mixture of 10 μM GTP-tubulin and 5 μM stathmin (*closed triangles*) recorded at 222 nm and at pH 6.8 (*closed symbols*) or pH 7.5 (*opened symbols*).

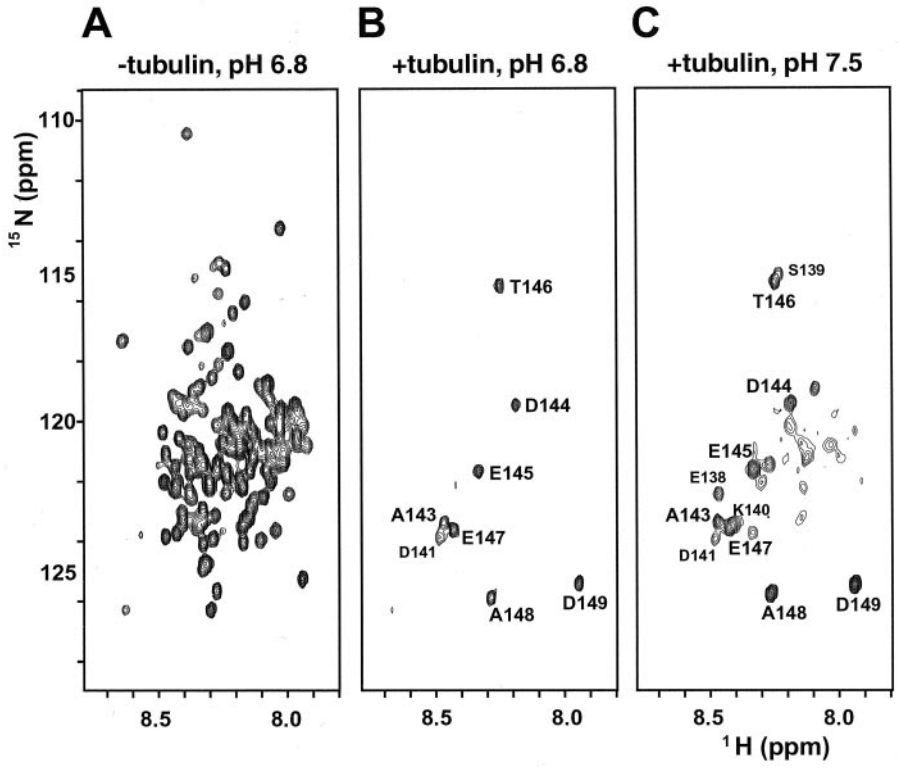

FIG. 6. **NMR analysis of the tubulin-stathmin system.** *A*, ^{15}N,^{1}H HSQC spectra of 50 μM unbound ^{2}H/^{13}C/^{15}N-labeled stathmin recorded at 23 °C. *B* and *C*, ^{15}N,^{1}H HSQC spectra of a 200 μM GTP-tubulin-stathmin solution (1:0.4 molar ratio of GTP-tubulin to stathmin) recorded at 23 °C and pH 6.8 (*B*) or pH 7.5 (*C*). Assignments are indicated for stathmin residues that are flexible in the ternary tubulin-stathmin complex.

spectra, probably due to the high proton density in non-deuterated tubulin. Heteronuclear three-dimensional NMR experiments identified these eight resonances as the C-terminal stathmin sequence Asp^{141}–Asp^{149} (note that Pro^{142} has no amide proton and therefore no HSQC peak). At pH 7.5 (Fig. 6*C*), five intense and five to ten weaker N-H resonances in addition to Asp^{141}–Asp^{149} were observed in the HSQC spectrum. Three out of the five intense resonances were identified as residues Glu^{138}–Lys^{140}. It is reasonable to speculate that the remaining two intense and the five to ten weaker resonances also stem from the C terminus. No N-terminal stathmin residues were observed in the HSQC spectrum indicating that these residues

adopted a stable conformation in the tubulin-stathmin complex at pH 7.5. The observed 4-fold decrease in affinity upon changing the pH from 6.8 to 7.5 (Table I) can thus be structurally explained on a per-residue basis and attributed to a weaker interaction of the C terminus of stathmin to tubulin.

In summary, the CD and NMR results demonstrate that stathmin, although extensively helical at lower temperatures, is devoid of any stable tertiary structure in aqueous solutions. However, in complex with two tubulin subunits all except its last eight to fifteen C-terminal residues adopt a stable conformation. This conformational behavior classifies stathmin into the growing family of the so-called "intrinsically disordered proteins" (43). The results further suggest that the conformations, thermal stabilities, and dynamics of the tubulin-stathmin system are only modestly sensitive to small changes in pH.

DISCUSSION

Mechanism of Tubulin-Stathmin Complex Formation—The binding equilibrium between tubulin and stathmin has been investigated by surface plasmon resonance (17, 19, 22, 32), by pull-down experiments (26, 28, 41), and most recently by a non-equilibrium-perturbing sequestration assay (31). All these studies indicated that stathmin interacts with two α/β-tubulin heterodimers in the low micromolar range. In analytical ultracentrifugation (21, 30) and gel filtration (18, 22, 32) studies only ternary (denoted T_2S) but not binary (denoted TS) complexes were isolated. Consistent with this observation, pull-down assays using agarose bead-coupled antibodies against glutathione *S*-transferase- and FLAG-tagged stathmin variants suggested that the binding of tubulin to stathmin is highly cooperative and that binary TS complexes are labile intermediates (26, 28, 41). However, only dissociation constants but no other thermodynamic data have been reported in these studies.

The advantage of the ITC equilibrium method is its high sensitivity and precision. As illustrated by Fig. 2*A*, the binding of tubulin to stathmin is fast and occurs within the response time of the calorimeter. Analysis of the binding isotherms either by a non-linear least squares fitting method or by Scatchard plots revealed a simple two-site binding mechanism. Surprisingly, the two sites appeared to be independent and identical with respect to binding affinity, which implicates that, at a molar excess of stathmin over tubulin, formation of binary TS complexes should occur. This prediction is supported by the TEM analysis shown in Fig. 4, which revealed that, at a 1.25:1 molar ratio of stathmin relative to tubulin, significant amounts of TS complexes are formed indeed in addition to T_2S. The current structural view of the asymmetric T_2S complex (Fig. 1) suggests that, besides tubulin-stathmin interactions, tubulin-tubulin interactions between the β1- and α2-tubulin monomers may also contribute to the overall stability of the ternary complex. Hence, the two tubulin binding sites on stathmin are probably not fully independent. Nevertheless, the present ITC analysis clearly revealed that both sites are characterized by the same intrinsic equilibrium binding constant K_0. The structure of T_2S shows that site 1 (denoted s1) comprises contact points between the N-terminal capping domain of stathmin and regions of α1-tubulin (denoted $T_{\alpha1}$-S_N) and contact points between the first half of the C-terminal helical domain of stathmin and parts of the $\alpha1\beta1$-tubulin heterodimer (denoted $T_{\alpha1\beta1}$-S_{h1}). Site 2 (denoted s2) comprises contact points between parts of the β1- and α2-tubulin monomers (denoted $T_{\beta1}$-$T_{\alpha2}$) and contact points between the second half of the helical domain of stathmin and regions of the $\alpha2\beta2$-tubulin heterodimer (denoted $T_{\alpha2\beta2}$-S_{h2}). The finding that both tubulin binding sites on stathmin are characterized by the same binding constant implies that the binding energetic of s1 = $T_{\alpha1}$-S_N + $T_{\alpha1\beta1}$-S_{h1} is equal to s2 = $T_{\beta1}$-$T_{\alpha2}$ + $T_{\alpha2\beta2}$-S_{h2} (Fig. 1). If it is assumed that the contribution of $T_{\alpha1\beta1}$-S_{h1} = $T_{\alpha2\beta2}$-S_{h2}, it follows that the asymmetry caused by the N-terminal domain of stathmin (contact point $T_{\alpha1}$-S_N) is compensated by the β1- and α2-tubulin monomer interaction $T_{\beta1}$-$T_{\alpha2}$ within the T_2S complex.

The finding that stathmin possesses two similar binding sites for tubulin under all conditions investigated (Table I) contrasts with earlier studies suggesting that the second tubulin subunit is bound distinctly tighter than the first (26, 28, 30, 31, 41). Notably, such a highly cooperative binding mechanism would explain why only the ternary T_2S and no binary TS complexes were found so far. At present, we can only speculate on the origin of this discrepancy. Earlier binding assays used different physical and chemical solution conditions and required tagging, immobilization, and separation of the different species. These manipulations might have entailed additional interactions, conformational changes, and perturbations in the equilibrium leading to a stabilization of the T_2S complex.

Consistent with the present analysis, the tubulin-stathmin binding equilibrium can be described as,

$$2T + S \rightleftarrows T + TS \rightleftarrows T_2S$$

REACTION 1

with $K_1 = K_2 = K_0$ as outlined above. The overall binding constant is $K_{S\rightarrow T_2S} = K_1 \times K_2 = K_0^2$, and the corresponding dissociation constant is $K_{T_2S\rightarrow S} = 1/K_0^2$. The most recent data on the tubulin-stathmin binding equilibrium are those reported in Ref. 31. Using a non-equilibrium-perturbing sequestration assay these authors found $K_{T_2S\rightarrow S} = 0.1\ \mu M^2$ at 37 °C and pH 6.8 leading to $K_0 = K_{S\rightarrow T_2S}^{-1/2} = 3.2 \times 10^6\ M^{-1}$. Extrapolation of the present data (Table I) to 37 °C yields $K_0 = 1 \times 10^7\ M^{-1}$, in reasonable agreement with the earlier result.

As illustrated in Fig. 3, the interaction of stathmin with tubulin is highly temperature-dependent. Around 28 °C the reaction enthalpy is zero and decreases from positive values at low temperatures to negative values at high temperatures. The temperature dependence of the binding constant is coupled to ΔH^0 through van't Hoff's law. Consequently, K_0 reaches a maximum where $\Delta H_0 = 0$ kcal mol^{-1}. The large negative heat capacity change of $\Delta C_p^0 = -860$ cal mol^{-1} K^{-1} (referring to tubulin) is typical of a hydrophobic reaction. When two hydrophobic surfaces come into close contact, they release their hydration water resulting in a reduction of the heat capacity of the complex. Empirical studies on proteins have shown that the transfer of an apolar surface area of 1 nm^2 in size from a polar to a non-polar environment makes a contribution to $\Delta C_{p,app}^0$ of -45 cal mol^{-1} (44). Accordingly, the ΔC_p^0 value for the tubulin-stathmin binding reaction could be interpreted as a hydrophobic surface area of about 19 nm^2, which is brought from a polar to a non-polar environment. Because both stathmin and tubulin must contribute equally to the process, the estimated hydrophobic contact area of the two molecules is ~9.5 nm^2. The total buried surface area between tubulin-RB3-SLD (note that the N-terminal domain of RB3-SLD was not resolved in the 4-Å x-ray structure of the complex) and β1-tubulin-α2-tubulin was estimated to be ~32 nm^2, *i.e.* ~16 nm^2 per binding site (17). Hence, a rough guess is that ~50% of the total buried surface area per binding site might be hydrophobic, which is a reasonable value. Another factor that could contribute to ΔC_p^0 is a change in the hydration state of stathmin upon folding. The CD measurements (Fig. 5) indicated that between 10 and 35 °C, stathmin, although not assuming a stable tertiary fold by itself, experiences moderate structure formation upon binding to tubulin. Accordingly, this effect is not expected to largely influence ΔC_p^0 at physiological temperatures. However, the present data do not rule out whether additional factors also contribute

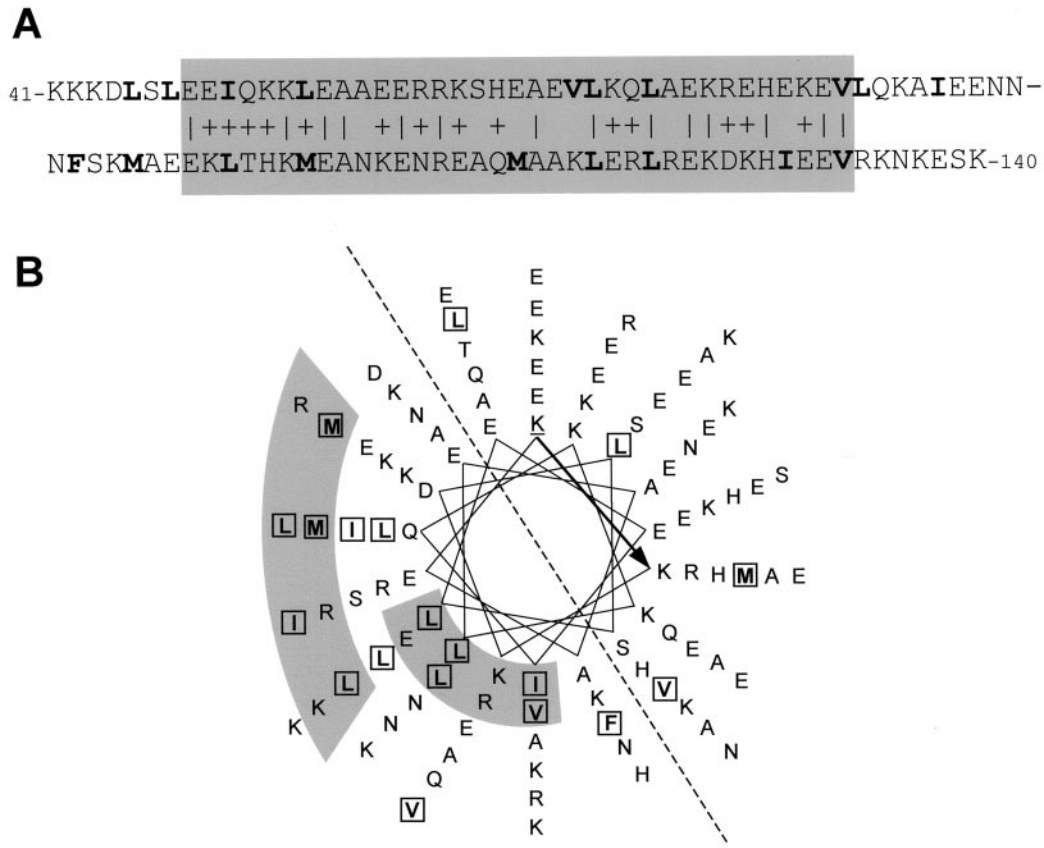

FIG. 7. **The C-terminal stathmin helix contains a sequence duplication and is amphipathic.** *A*, primary amino acid sequence of Lys^{41}–Lys^{140} of stathmin with the 35-residue sequence duplication (40% identity and 80% similarity (17, 45)) aligned and *highlighted* in *gray*. Identical (*perpendicular lines*) and similar (*plus signs*) residues are indicated between the two sequence stretches. Bulky hydrophobic residues (*i.e.* Ala excluded) are in *boldface*. *B*, helical wheel representation of the sequence shown in *A*. The starting residue, Lys^{41}, is *underlined*. Bulky hydrophobic residues are marked by *boxes*. The *dashed line* divides the idealized and continuous helix in two equal parts highlighting the amphipathic character of the sequence stretch. Bulky hydrophobic residues participating in the hydrophobic seam of the helix (*left part*) and located within the two homologous sequence sites are *highlighted* in *gray*.

to the large negative heat capacity change of the tubulin-stathmin binding equilibrium.

The current structural view of T_2S (Fig. 1) together with deletion mapping (13, 18, 19, 26, 29, 41) and mutational studies (40, 42) indicate that the helical domain of stathmin accounts predominantly for the binding free energy. Interestingly, the interaction sites of the two α/β-tubulin heterodimers with the RB3-SLD helix ($T_{\alpha1\beta1}$-S_{h1} and $T_{\alpha2\beta2}$-S_{h2}; Fig. 1) appear conserved in the 4-Å structure of the complex (17). This finding indicates that two homologous sequence sites on the helical domain of stathmin may mediate the interactions with the two α/β-tubulin heterodimers. Indeed, a 35-residue duplication, Glu^{48}–Val^{82} and Glu^{99}–Val^{133}, with 40 and 80% identity and similarity, respectively, is found in the sequence spanning residues Lys^{41}–Lys^{140} of stathmin (Fig. 7*A* (17, 45)). Notably, the continuous helix formed by Lys^{41}–Lys^{140} is amphipathic with most of the bulky hydrophobic residues of Glu^{48}–Val^{82} and Glu^{99}–Val^{133} clustering on one side of the helix (Fig. 7*B*). Due to a lack of resolution, the interacting residues of RB3-SLD in the ternary complex could not be identified. However, considering the large negative ΔC_p^0 value for the tubulin-stathmin equilibrium (see discussion above), it appears reasonable to speculate that binding of the helical domain of stathmin to the tubulin subunits is established by apolar residues present in its hydrophobic seam and on the surface of the two α/β-tubulin heterodimers. The sixteen stathmin residues that separate the two duplicated tubulin binding sites may allow for correct positioning of these hydrophobic sites with respect to the interacting tubulin target residues. The importance of amphipathic helix-mediated interactions between an intrinsically disordered protein and its binding target is a frequently encountered mechanism in other disordered protein systems (43).

Does Stathmin Work as a pH-sensitive Bifunctional Protein?—In vitro studies have proposed that a small change in pH from 6.8 to 7.5 switches the function of stathmin from tubulin sequestration to direct stimulation of MT catastrophes (8, 24, 28). This change in function implies that at the lower pH value stathmin binds preferentially to tubulin subunits, whereas at the higher pH value specific structural determinants present at MT ends are predominantly targeted. In principle, the structural features of stathmin suggest that the molecule, besides sequestering tubulin subunits, might be able to specifically recognize MT ends (13, 17, 46). To further clarify this important issue we have systematically addressed the question whether the affinities, stabilities, and conformations of the tubulin-stathmin system assessed at pH 6.8 and 7.5 supports the proposed pH-sensitive dual function of stathmin.

The physicochemical consequences on the stathmin and tubulin polypeptide chains expected in lowering the pH from 7.5 to 6.8 is a change in protonation state of acidic residues. The only residue side chain titrating in a polypeptide near physiological pH is the imidazole group of histidine (pK_a value of ~6.5–7.0 (47)). The principle effects anticipated by a shift in the protonation state of His are (i) a change in protein conformation and/or stability and (ii) a change in the binding energetics of His side chains engaged at a specific binding site. Both, the long and the short range mechanisms can influence

the affinity of a protein-complex system. Several lines of evidence clearly indicate that the protonation state of His residues only modestly alters the biophysical characteristics of the tubulin-stathmin system. Analytical ultracentrifugation studies (21, 30), binding experiments (31), and CD measurements (Fig. 5) conducted at pH 6.8 and 7.5 revealed only small differences in conformation and stability of stathmin, tubulin, and tubulin-stathmin complexes at these two pH values. NMR shows that at both pH values most of the stathmin residues, including the N-terminal domain that is proposed to be necessary for catastrophe promotion (24, 29), are stably bound to tubulin with a few C-terminal residues remaining disordered and flexible (Fig. 6). Consistent with the structural data, ITC revealed a mere -0.8 kcal mol^{-1} difference in the free binding energies between pH 6.8 and pH 7.5 (Table I). Therefore, together with the observation that stathmin is highly expressed *in vivo* (note that catastrophe promotion is a substoichiometric process), these findings suggest that within the living cell non-phosphorylated stathmin primarily sequesters tubulin subunits and by doing so destabilizes the MT network regardless of small changes in pH. In this context, it is important to note that there have been no reports so far that directly assess MT-end binding activity or enhanced MT turnover and accompanying steady-state GTPase activity, features that would be essential for stathmin representing an authentic MT catastrophe-promoting factor (30, 31).

Acknowledgments—We are indebted to Dr. F. Winkler for insightful discussions and support. We thank P. Ganz for assistance with the ITC measurements, Dr. U. Grauschopf for help with the CD spectropolarimeter, Dr. B. Maco for assistance with the rotary metal-shadowing experiments, and Dr. J. Missimer for careful reading of the manuscript. We are grateful to the Interdisciplinary Center for Microscopy of the University of Basel and to the Institute for Molecular Biology and Biophysics of Eidgenössische Technische Hochschule Zürich for access to the TEM and CD spectropolarimeter, respectively.

REFERENCES

1. Mitchison, T., and Kirschner, M. (1984) *Nature* **312,** 237–242
2. Desai, A., and Mitchison, T. J. (1997) *Annu. Rev. Cell Dev. Biol.* **13,** 83–117
3. Sobel, A. (1991) *Trends Biol. Sci.* **16,** 301–305
4. Gavet, O., Ozon, S., Manceau, V., Lawler, S., Curmi, P., and Sobel, A. (1998) *J. Cell Sci.* **111,** 3333–3346
5. Lawler, S. (1998) *Curr. Biol.* **8,** R212–R214
6. Andersen, S. S. (2000) *Trends Cell Biol.* **10,** 261–267
7. Walczak, C. E. (2000) *Curr. Opin. Cell Biol.* **12,** 52–56
8. Cassimeris, L. (2002) *Curr. Opin. Cell Biol.* **14,** 18–24
9. Ozon, S., Guichet, A., Gavet, O., Roth, S., and Sobel A. (2002) *Mol. Biol. Cell* **13,** 698–710
10. Riederer, B. M., Pellier, V., Antonsson, B., Di Paolo, G., Stimpson, S. A., Lutjens, R., Catsicas, S., and Grenningloh, G. (1997) *Proc. Natl. Acad. Sci. U. S. A.* **94,** 741–745
11. Melhem, R., Hailat, N., Kuick, R., and Hanash, S. M. (1997) *Leukemia* **11,** 1690–1695
12. Bièche, I., Lachkar, S., Becette, V., Cifuentes-Diaz, C., Sobel, A., Lidereau, R., and Curmi, P. A. (1998) *Br. J. Cancer* **78,** 701–709
13. Steinmetz, M. O., Kammerer, R. A., Jahnke, W., Goldie, K. N., Lustig, A., and van Oostrum, J. (2000) *EMBO J.* **19,** 572–580
14. Müller, D. R., Schindler, P., Towbin, H., Wirth, U., Voshol, H., Hoving, S., and Steinmetz, M. O. (2001) *Anal. Chem.* **73,** 1927–1934
15. Doye, V., Boutterin, M. C., and Sobel, A. (1990) *J. Biol. Chem.* **265,** 11650–11655
16. Wallon, G., Rappsilber, J., Mann, M., and Serrano, L. (2000) *EMBO J.* **19,** 213–222
17. Gigant, B., Curmi, P. A., Martin-Barbey, C., Charbaut, E., Lachkar, S., Lebeau, L., Siavoshian, S., Sobel, A., and Knossow, M. (2000) *Cell* **102,** 809–816
18. Redeker, V., Lachkar, S., Siavoshian, S., Charbaut, E., Rossier, J., Sobel, A., and Curmi, P. A. (2000) J. *Biol. Chem.* **275,** 6841–6849
19. Steinmetz, M. O., Jahnke, W., Towbin, H., Garcia-Echeverria, C., Voshol, H., Müller, D., and van Oostrum, J. (2001) *EMBO Rep.* **2,** 505–510
20. Belmont, L. D., and Mitchison, T. J. (1996) *Cell* **84,** 623–631
21. Jourdain, L., Curmi, P., Sobel, A., Pantaloni, D., and Carlier, M.-F. (1997) *Biochemistry* **36,** 10817–10821
22. Curmi, P. A., Andersen, S. S., Lachkar, S., Gavet, O., Karsenti, E., Knossow, M., and Sobel, A. (1997) *J. Biol. Chem.* **272,** 25029–25036
23. Tournebize, R., Andersen, S. S., Verde, F., Doree, M., Karsenti, E., and Hyman, A. A. (1997) *EMBO J.* **16,** 5537–5549
24. Howell, B., Larsson, N., Gullberg, M., and Cassimeris, L. (1999) *Mol. Biol. Cell* **10,** 105–118
25. Howell, B., Deacon, H., and Cassimeris, L. (1999) *J. Cell Sci.* **112,** 3713–3722
26. Larsson, N., Segerman, B., Howell, B., Fridell, K., Cassimeris, L., and Gullberg, M. (1999) *J. Cell Biol.* **146,** 1289–1302
27. Arnal, I., Karsenti, E., and Hyman, A. A. (2000) *J. Cell Biol.* **149,** 767–774
28. Holmfeldt, P., Larsson, N., Segerman, B., Howell, B., Morabito, J., Cassimeris, L., and Gullberg, M. (2001) *Mol. Biol. Cell* **12,** 73–83
29. Segerman, B., Holmfeldt, P., Morabito, J., Cassimeris, L., and Gullberg, M. (2003) *J. Cell Sci.* **116,** 197–205
30. Amayed, P., Carlier, M. F., and Pantaloni, D. (2000) *Biochemistry* **39,** 12295–12302
31. Amayed, P., Pantaloni, D., and Carlier, M. F. (2002) *J. Biol. Chem.* **277,** 22718–22724
32. Charbaut, E., Curmi, P. A., Ozon, S., Lachkar, S., Redeker, V., and Sobel, A. (2001) *J. Biol. Chem.* **276,** 16146–16154
33. Budisa, N., Steipe, B., Demange, P., Eckerskorn, C., Kellermann, J., and Huber, R. (1995) *Eur. J. Biochem.* **230,** 788–796
34. Wiltscheck, R., Kammerer, R. A., Dames, S. A., Schulthess, T., Blommers, M. J., Engel, J., and Alexandrescu, A. T. (1997) *Protein Sci.* **6,** 1734–1745
35. Howard, W. D., and Timasheff, S. N. (1986) *Biochemistry* **25,** 8292–8300
36. Fowler, W. E., and Aebi, U. (1983) *J. Ultrastruct. Res.* **83,** 319–334
37. van Holde, K. E., Johnson, W. C., and Ho, S. P. (1998) *Principles of Physical Biochemistry*, Prentice Hall, Upper Saddle River, New Jersey
38. Wiseman, T., Williston, S., Brandts, J. F., and Lin, L. N. (1989) *Anal. Biochem.* **179,** 131–137
39. Seelig, J. (1997) *Biochim. Biophys. Acta* **1331,** 103–116
40. Larsson, N., Segerman, B., Melander Gradin, H., Wandzioch, E., Cassimeris, L., and Gullberg, M. (1999) *Mol. Cell. Biol.* **19,** 2242–2250
41. Segerman, B., Larsson, N., Holmfeldt, P., and Gullberg, M. (2000) *J. Biol. Chem.* **275,** 35759–35766
42. Brännström, K., Segerman, B., and Gullberg, M. (2003) *J. Biol. Chem.* **278,** 16651–16657
43. Wright, P. E., and Dyson, H. J. (1999) *J. Mol. Biol.* **293,** 321–331
44. Baker, B. M., and Murphy, K. P. (1998) *Methods Enzymol.* **295,** 294–315
45. Maucuer, A., Doye, V., and Sobel, A. (1990) *FEBS Lett.* **264,** 275–278
46. Meurer-Grob, P., Kasparian, J., and Wade, R. H. (2001) *Biochemistry* **40,** 8000–8008
47. Cantor, C. R., and Schimmel, P. R. (1980) *Biophysical Chemistry Part I: The Conformation of Biological Macromolecules*, pp. 41–53, W. H. Freeman and Co., New York
48. Nogales, E., Whittaker, M., Milligan, R. A., and Downing, K. H. (1999) *Cell* **96,** 79–88

2. Control of intrinsically disordered stathmin function by multisite phosphorylation

Srinivas Honnappa, Wolfgang Jahnke, Joachim Seelig and Michel O. Steinmetz

Submitted (2005)

Our previous results revealed that stathmin is an intrinsically disordered protein providing an excellent model system to explore the fundamentals of multi-site protein phosphorylation. The structural consequences of reversible multiple protein phosphorylation, a mechanism frequently used by living cells for the regulation of numerous cellular signaling pathways and metabolic functions, are poorly understood. Although it is well known that sequential cell-cycle-dependent phosphorylation of four serine residues (Ser16, 25, 38, and 63), abolishes the microtubule destabilizing activity of stathmin, we still have limited knowledge on the molecular basis of this regulatory effect.

The paper explains the strategy to construct several selected Ala mutants of Ser in order to phosphorylate stathmin at specific sites *in vitro*. In addition, the paper explains the protocol to phosphorylate and purify different mutants *in vitro* and analyse them using native-PAGE. ITC was used to assess systematically the tubulin-binding properties of wild-type and phosphorylated stathmin. CD and NMR were used to investigate the structural properties of stathmin upon phosphorylation. The publication clarifies the structural basis of multisite phosphorylation in regulating the activity of intrinsically disordered protein.

My contribution to this paper was to purify all stathmin mutants and prepare the phosphoisoforms, including the ^{15}N-labeled stathmin phosphoisoform. In addition, I performed all the biochemical assays and biophysical characterizations using ITC and CD, and wrote the corresponding sections in experimental procedures. W. Janke performed the NMR analysis and J. Seelig helped us to interpret the ITC data.

Manuscript

Classification: Biological Sciences, Biophysics

Control of intrinsically disordered stathmin by multisite phosphorylation

Srinivas Honnappa[1], Wolfgang Jahnke[2], Joachim Seelig[3] and Michel O. Steinmetz[1]

[1]Biomolecular Research, Structural Biology, Paul Scherrer Insititut, CH-5232 Villigen PSI, Switzerland

[2]Central Technologies, Novartis Pharma AG, CH-4002 Basel, Switzerland

[3]Department of Biophysical Chemistry, Biozentrum, University of Basel, CH-4056 Basel, Switzerland

*Corresponding author: Michel O. Steinmetz

Biomolecular Research

Structural Biology

Paul Scherrer Institut

CH-5232 Villigen PSI, Switzerland

Phone: +41-56-310-4754

Fax: +41-56-310-5288

E-mail: michel.steinmetz@psi.ch

Manuscript information:	Nr. of text pages: 19
	Nr. of figures: 5
Word and character count:	Total words in the abstract: 133
	Total characters in the paper: 37'535
Supporting Information	2 tables and 4 figures

Abbreviations: CD, circular dichroism; EGTA; ethylene glycol-bis(2-aminoethylether)-N,N,N,N-tetra acetic acid; HSQC, heteronuclear single quantum correlation; ITC, isothermal titration calorimetry; NMR, nuclear magmetic resonance; NOE, nuclear Overhauser effect; PAGE, polyacrylamide gel electrophoresis; PBS, phosphate buffered saline; PCR, polymerase chain reaction; PDB, Protein Data Bank; PIPES, piperazine-1,4-bis(2-ethanesulfonic acid); SLD, stathmin-like domain

ABSTRACT

Stathmin is an intrinsically disordered protein implicated in the regulation of microtubule dynamics and in the development of cancer. The activity of stathmin is down-regulated by phosphorylation of four serine residues, a mechanism allowing local stathmin activity gradients essential for mitotic spindle assembly to be established. Here we have analyzed the properties of seven stathmin phosphoisoforms to bind tubulin and inhibit microtubule formation. Using calorimetric and spectroscopic methods, we found that phosphorylation of Ser16 and Ser63 disrupts the formation of a tubulin-interacting β-hairpin and a helical segment, respectively, explaining the dominant role of these residues in regulating cell cycle progression. The new insight into the tubulin-stathmin interaction provides a molecular basis for understanding the factors that control intrinsically disordered protein systems implicated in a wide range of biological processes and in human diseases.

INTRODUCTION

Intrinsically disordered proteins have enormously gained in interest not only because they are ever more recognized to play key roles in many central cellular processes including cell cycle control, signal transduction, and transcriptional regulation but also because of their particular importance for cancer development and protein deposition diseases (1-4). Strikingly, recent genome database searches indicated that >30% of all eukaryotic proteins may be completely or partially disordered (5). This high frequency of occurrence has provoked a change of the paradigm that stable tertiary structure is necessary for protein function.

Intrinsically disordered polypeptide chain segments are primarily involved in molecular recognition and posttranslational modification including phosphorylation (6). Little is known, however, regarding the nature and mechanism of control of protein-protein interactions involving intrinsically disordered proteins. Stathmin is a entirely disordered protein (7, 8) implicated in the regulation of microtubule dynamics (reviewed by (9-13)). The soluble cytoplasmic molecule destabilizes microtubules by binding tubulin dimers (7, 14-16) and stimulating catastrophes (referred to as the transition of microtubule growth to shortening) (17, 18), playing a central role for cell proliferation, cell migration, and mitotic spindle formation. Interestingly, stathmin is expressed in high amounts in a wide variety of human malignancies (9-13) and its overexpression correlates with increased cell motility and invasion of human sarcomas *in vivo* (19).

Characteristic of intrinsically disordered proteins, stathmin is devoid of stable tertiary structure in isolation (7, 8, 20, 21); while its N-terminal moiety adopts little regular secondary structure the C-terminal domain populates an ensemble of transient helical conformations (Figure 1A). Upon binding of stathmin to two head-to-tail aligned α/β-tubulin heterodimers, the amino terminus folds into a β-hairpin and the carboxy terminal helical domain becomes strongly stabilized (15, 16). The curved and capped structure of the ternary tubulin-stathmin

complex (denoted T_2S; Figure 1B) provides a structural basis for understanding how stathmin family proteins destabilize microtubules.

In vivo, the activity of stathmin is down-regulated by posttranslational phosphorylation in response to a number of signals on four serine residues, Ser16, Ser25, Ser38, and Ser63 (22-25). In mitotic cells, for example, phosphorylation by an unknown kinase-phophatase system allows creating local stathmin activity gradients, a process essential for regulating microtubule dynamics and spindle formation (26-29). Phosphorylation of all four serine residues at the G2/M transition occurs sequentially; Ser25 and Ser38 are first phosphorylated by Cdk1, with subsequent phosphorylation of Ser16 and Ser63 by unknown kinase systems (22). Phosphorylation of Ser16 and Ser63 strongly down regulates the microtubule destabilizing activity of stathmin (22-25, 30). In contrast, phosphorylation of Ser25 and Ser38 has only moderate down regulating effect but is a prerequisite for allowing phosphorylation of Ser16 and Ser63 *in vivo* (22).

The current knowledge of the tubulin-stathmin interaction provides a unique basis to gain detailed insight into factors regulating intrinsically disordered protein systems. To define how multiple phosphorylation sites control stathmin function we here have explored seven stathmin phosphoisoforms by combining energetic and structural information.

MATERIALS AND METHODS

Cloning and polypeptide chain preparations

For the production of high amounts of pure stathmin phosphoisoforms, seven specific serine-to-alanine mutants were constructed: Ser25,38,63Ala (for p16); Ser 16,25,38Ala (for p63); Ser25,38Ala (for p16,63); Ser16,63Ala (for p25,38); Ser63Ala (for p16,25,38); Ser16Ala (for p25,38,63); Ser16,25,38,63Ala (4A). Importantly, the microtubule-polymerization inhibition and tubulin-binding activities, the secondary structure content, and the thermal stability of the quadruple mutant 4A were indistinguishable from the wild-type, justifying the validity of the approach (supplementary Figures 1 and 2). To produce the mutant molecules, two silent nucleotide mutations, G66C and G141C, were introduced by PCR into the human pET-16b (Novagen) stathmin clone (7) generating *Sac*I and *Xho*I recognition sites between the codons for Ser16 and Ser25, and Ser38 and Ser63, respectively. This new plasmid was used for the subsequent cloning of all mutants via synthetic oligonucleotide adapter primers at either *Nde*I/*Sac*I, *Sac*I/*Xho*I, or *Xho*I/*Bbv*CI recognition sites. The production of the ΔN mutant (stathmin residues 41-149) is described in (20).

Recombinant unlabelled and ^{15}N uniformly labeled stathmin proteins were bacterially expressed, purified, and processed as described (7, 8). Specific phosphorylation by PKA (for phosphorylation of Ser16 and Ser63) and a mixture of MAPK and CdC_2 (for phosphorylation of Ser25 and Ser38) was achieved by incubating the proteins with the respective kinases (2.8, 2.0, and 0.5 U PKA, MAPK, and/or CdC_2, repectively, per μg of stathmin) in 50 mM Tris-HCl, pH 7.5, 10 mM $MgCl_2$, 5 mM EGTA, 2 mM DTT, 500 mM ATP for 6-8 hours at 30 °C. Product formation was assessed by native-PAGE. Kinases were heat inactivated at 75°C for 10 min. Phosphoisoforms were purified to high homogeneity (>93%) by anion exchange chromatography. Highly pure bovine brain GTP-tubulin was obtained from Cytoskeleton Inc. N-acetylated and C-amidated peptides were assembled on an automated continuous-flow synthesizer employing standard methods.

The identities of stathmin proteins were assessed by mass spectral analyses. Concentrations of protein samples were determined by the Advanced Protein Assay (Cytoskeleton Inc.).

Tubulin-polymerization assay

In vitro polymerization of tubulin was performed according to (22). Briefly, 4 μM tubulin in G buffer (80 mM PIPES-KOH, pH 6.8, 1 mM $MgCl_2$, 1 mM EGTA, 1 mM GTP) supplemented with 4 mM $MgCl_2$ was preincubated with 4 μM of stathmin (in the same buffer) for 30 min at room-temperature in a total reaction volume of 100 μl. Polymerization was initiated by adding 1 μl of a 400 μM taxol stock solution and incubating at 37 °C for 1.5 hours. Microtubules were separated from tubulin-stathmin oligomers by sedimentation at 300‘000 g for 15 min at 37 °C in an Optima TLX ultracentrifuge (Beckman Instruments). The protein contents of supernatants and pellets were analyzed with the bicinchoninic acid protein assay reagent (Pierce).

Biophysical analysis

High-sensitivity ITC experiments were carried out on a VP-ITC calorimeter (Microcal Inc., Northampton, MA). For each experiment, the temperature controlled sample cell (volume 1.4 ml) was filled with either ~10 μM (for wt, 4A, p25,38, S16E, and S63E) or ~20 μM (for p16, p63, p16,63, p16,25,38, p25,38,63, p16,25,38,63) GTP-tubulin in G buffer (80 mM PIPES-KOH, pH 6.8, 1 mM $MgCl_2$, 1 mM EGTA, 1 mM GTP). Either 5 μl (for stathmin-wt, -4A, -p25,38, -S16E, and S63E) or 10 μl (for p16, p63, p16,63, p16,25,38, p25,38,63, p16,25,38,63) ~100 μM stathmin aliquots (present in the same buffer as tubulin) were injected into the sample cell. Binding isotherms were fitted via a nonlinear least squares minimization method assuming two independent and equal binding sites on stathmin for tubulin.

Protein samples (0.35 mg/ml) for CD were in PBS (10 mM sodium phosphate, pH 7.4, 150 mM NaCl). Far-ultra violet CD spectra and thermal unfolding profiles were recorded on a Jasco J-810 spectropolarimeter (Jasco Inc.) equipped with a temperature controlled quartz cell of 0.1 cm path length. A ramping rate of $1°C*min^{-1}$ was used to record the thermal unfolding profiles.

$^{15}N,^{1}H$ HSQC NMR experiments of 19 mg/ml protein samples in G buffer were carried out at 25 °C on a Varian UnityPlus 600 spectrometer operating at 600 MHz proton frequency. For resonance assignment, 3D ^{15}N-edited TOCSY-HSQC using a clean DIPSI-2 mixing sequence, and 3D ^{15}N-HSQC-TOCSY-NOESY-HSQC were recorded.

Modeling

The 3.5 Å resolution X-ray crystal structure of the tubulin-RB3 stathmin-like domain (SLD) complex (PDB entry 1SA0), and the PyMol (http://www.pymol.org) and MOLOC (http://www.moloc.ch/) software packages were used for the modeling studies. Accuracy of the conformations of key residue side chains was verified by inspecting the electron density map for PDB entry 1SA0. Solvent accessible area calculations were carried out with the program NACCESS (http://wolf.bms.umist.ac.uk/naccess/). The stathmin residues 29-45 in Figure 1B were taken from PDB entry 1SA1. In Figure 4C, Tyr63 of RB3-SLD was replaced by a serine to reflect the human stathmin sequence. Stathmin and RB3-SLD share 72% sequence identity and 82 and 92% of all tubulin-contacting RB3-SLD residues are invariant or similar in stathmin.

RESULTS AND DISCUSSION

To define how phosphorylation of Ser16, Ser25, Ser38, and Ser63 controls the function of stathmin, milligram amounts of pure single (p16 and p63), double (p25,38 and p16,63), triple (p16,25,38 and p25,38,63), and quadruple (p16,25,38,63) stathmin phosphoisoforms were produced (Figure 2). The activities of the proteins were assessed *in vitro* by a microtubule polymerization assay. Under the experimental conditions applied the efficiency to inhibit microtubule formation decreased from 90 to 0 % with increasing degree of phosphorylation (supplementary Figure 1A). These findings are consistent with stathmin sequestering tubulin dimers into assembly incompetent complexes (14), a process controlled by phosphorylation. In agreement with the microtubule-polymerization data obtained *in vivo* (22-25), phosphorylation of Ser16 and Ser63 contributes most to stathmin inactivation.

The energetics of the tubulin-stathmin interaction was assessed by isothermal titration calorimetry (ITC; supplementary Figure 2). Between 6 and 25 °C, stathmin binds two tubulin subunits and all thermodynamic parameters are thus referred to the ternary tubulin-stathmin T_2S complex (supplementary Table 1). As shown in Figure 3A, the binding reaction is predicted to be driven by both enthalpy and entropy at physiological temperatures. The large negative heat capacity change of $\Delta C^0_{p,T_2S,obs}$ =-1504 cal mol^{-1} K^{-1} suggests that the hydrophobic effect (removal of non-polar surface from water) promotes T_2S complex formation (31). As a consequence, the apparent entropic and enthalpic contributions to the free energy change of complex formation vary with temperature in a linear and nearly parallel manner, changing sign at ~28 and ~44 °C, respectively.

Empirical studies on proteins showed that the removal of hydrophobic and polar surface from water contribute -45 and 26 cal mol^{-1} per 100 Å^2, respectively, to ΔC^0_p (32). We have calculated the total buried hydrophobic and polar surface areas from the 3.5 Å resolution X-ray crystal structure of the ternary complex formed between the stathmin homologue RB3 and tubulin (denoted T_2R; (15)) as 5316 and 3074 Å^2, respectively.

Accordingly, the estimated heat capacity change $\Delta C^0_{p,T_2S,cal}$ amounts -1593 cal mol^{-1} K^{-1} , in good agreement with the experimentally obtained value for the tubulin-stathmin complex (see above). These findings are consistent with a mechanism in which dehydration of the protein-protein interface is the major driving force of T_2S complex formation.

ITC showed that each stathmin phosphoisoform bound two tubulin dimers as observed for unmodified stathmin (supplementary Figure 2; supplementary Table 2). The equilibrium dissociation constant, K_{D,T_2S}, of T_2S for unmodified stathmin is 0.53 μM^2 under the conditions applied (Figure 3B). This relatively high value underscores the dynamic nature of the tubulin-stathmin equilibrium observed in cellular systems. Single phosphorylation of Ser16 or Ser63 increases K_{D,T_2S} 17- and 113-fold, respectively. A strong effect was found with p16,63 which displays a 233-fold reduced binding affinity (Figure 3B). Dual phosphorylation of Ser25 and Ser38 reduced K_{D,T_2S} only 4-fold and the down regulating effect of the single phosphoisoforms was only marginally enhanced (on average 1.4-fold) by additional phosphorylation of Ser25 and Ser38. The ITC data of p16,25,38,63 could not be evaluated because binding was too weak. For all measured stathmin phosphoisoforms, a reduced binding entropy that is partially offset by an increased binding enthalpy is observed (Figure 3C).

The finding that phosphorylation of Ser16 and Ser63 contributes most to the reduced binding of stathmin explains the dominant role of these residues for *in vivo* inactivation (22-25). The moderate effect obtained with phosphorylation of Ser25 and Ser38 correlates with their location in the proline/serine-rich loop segment of stathmin (Figure 1) which is poorly ordered in the T_2R complex (15, 16). The local perturbation caused by phosphorylated Ser25 and Ser38, however, is expected to facilitate phosphorylation of the adjacent Ser16 and Ser63 residues as suggested from *in vivo* data (22).

Remarkably, a linear correlation between the free energy change of T_2S complex formation and the tubulin polymerization inhibition activities of stathmin phosphoisoforms is observed (Figure 3D). In agreement with cell biological data (22-25), this correlation

suggests that already moderate changes in the tubulin-stathmin equilibrium significantly influence microtubule dynamics and as a consequence microtubule function in a particular *in vivo* situation. This conclusion provides an energetic basis for understanding how spatial gradients of differentially inactive stathmin molecules promote localized microtubule growth, a process essential for, e.g., mitotic spindle assembly (26-29).

The secondary structures and thermal stabilities of stathmin phosphoisoforms were probed by circular dichroism (CD) spectroscopy. CD recorded at low temperature from unmodified stathmin revealed a spectrum with ~45% helical content (Figure 4A). Characteristic of proteins lacking stable tertiary structure, a fully reversible, broad unfolding transition to a random coil structure was observed upon thermal denaturation (Figure 4B). Phosphorylation of Ser63 reduces both the helical content (20-30 % in the 5-30 °C temperature range) and the thermal stability of stathmin. In contrast, phosphorylation of Ser16, Ser25, and Ser38 affects only moderately its secondary structure throughout the 5-80 °C temperature range.

Our biophysical and biochemical studies in combination with structural information on the ternary T_2R complex provide a strong basis for understanding the mechanism underlying Ser63 and Ser16 phosphorylation. A correlation between secondary structure and markedly reduced tubulin-binding affinity is apparent with stathmin isoforms phosphorylated at Ser63. Remarkably, in T_2S Ser63 (tyrosine in T_2R) projects into the solvent and is not involved at the protein-protein interface (Figure 4C). However, the residue is embedded within stathmin's major helix nucleation site, Glu55-Ala73, which drives helix formation of the helical domain in isolation (Figure 1). Nuclear magnetic resonance (NMR) experiments of peptides encompassing Glu55-Ala73 demonstrated that the presence of the phosphoryl group on Ser63 introduces a kink in the helical backbone leading to the dispersion of the peptide sequence Glu55-Arg61 (20). The driving force of this distortion can be explained by the strong propensity of phosphoserine to interact with the main chain (33). Mutating Ser63 to glutamic acid (S63E) only moderately affects the secondary structure, thermal stability, and tubulin binding affinity of stathmin (supplementary Table 2; supplementary Figure 4),

underscoring the unique properties of the bulky dianionic phosphoryl group to disrupt the helical conformation of the helix nucleation site. This local effect explains the reduced tubulin-binding activities of stathmin isoforms phosphorylated at Ser63. The phosphoryl group hinders the alignment of residues Lys53, Leu54, Ala57, Arg60, and Arg61 which tightly interact with the α1-tubulin monomer (Figure 4C).

As shown in Figure 5A, in T_2R Ser16 is located within the tight turn connecting the two β-strands of the β-hairpin. The residue is stabilized by an intermolecular hydrogen bond formed between its main chain oxygen atom and the side chain of α1Asn356. As a consequence, Ser16 is oriented towards the α1-tubulin surface and introduction of a phosphoryl group is expected to result in a steric clash of its bulky phosphorylated side chain. This prediction was tested by NMR experiments. The ^{15}N,^{1}H heteronuclear single quantum correlation (HSQC) measurements of ^{15}N-labelled stathmin and p16 proteins revealed spectra with limited chemical shift dispersion (supplementary Figure 3), characteristic for intrinsically disordered proteins populating an ensemble of helical secondary structures. Comparison of these two spectra, however, reveals three prominent differences. One new peak (at 7.55/118.2 ppm), which originates from an arginine side chain forming a hydrogen bond (most probably Arg14), and two prominent N-H backbone resonance shifts were found in the ^{15}N-p16 HSQC spectrum. The first peak shift (from 8.18/115.1 to 8.79/117.5 ppm) is in a spectral region typical for serine residues and is likely to originate from Ser16. The second peak shift (from 8.25/127.5 to 8.45/127.1 ppm) most probably stems from a residue close in sequence to Ser16.

Upon addition of unlabeled tubulin to ^{15}N-stathmin all except the last eight C-terminal stathmin residues broaden beyond distinction in the HSQC spectrum due to the large ~200 kDa size of the T_2S complex, demonstrating that most stathmin residues become tightly bound (Figure 5B, black). In contrast, ~40 strong and several weaker resonances are visible in the spectrum of the complex formed with ^{15}N-p16 (Figure 5B, red). Most of these resonances are broad showing limited chemical shift dispersion, characteristic for residues

that are in rapid exchange between weakly bound and unbound random coil states. Some peaks originate from the N-terminal domain of stathmin. First, both resonances shifting upon phosphorylation of unbound stathmin and which most likely stem from Ser16 and Arg14 (see above) are visible in the HSQC spectrum of the complex formed with ^{15}N-p16, indicating that they are not tightly bound to tubulin. Second, a stathmin fragment lacking the first 40 N-terminal residues (ΔN) showed similar tubulin-binding properties as p16 (supplementary Table S2). Third, substituting glutamic acid for Ser16 (S16E) partially mimics the effect of phosphorylation on T_2S complex formation (supplementary Table 2; supplementary Figure 4) consistent with the hypothesis that steric clash with α1-tubulin and intramolecular interaction of the bulky phosphoryl group with the backbone (33) and/or Arg14 side chain is the underlying mechanism. These findings demonstrate that phosphorylation of Ser16 strongly impairs binding of the β-hairpin to α1-tubulin and explain the reduced tubulin-binding activities of stathmin isoforms phosphorylated at Ser16. As Ser16 is conserved throughout stathmin family proteins (9), this mechanism is expected to apply to all stathmin homologues.

From an energetic point of view the down-regulating effect of stathmin phosphorylation can be explained by the substantial loss in hydration entropy upon T_2S complex formation which is larger in magnitude than the gain in enthalpy of the system. Consistent with this conclusion, phosphorylation of Ser16 and Ser63 disrupts the formation of the β-hairpin and the helix nucleation site, respectively, impairing binding of these two key secondary structure elements to α1-tubulin and leading to the exposure of non-polar surface to water. This important finding opens an avenue to design strategies to interfere with abnormal microtubule dynamics observed in many human malignancies displaying high levels of stathmin expression (9). Targeting the β-hairpin and/or helix nucleation site of stathmin is expected to perturb the dynamic equilibrium of the microtubule filament system possibly inhibiting tumor invasion *in vivo* (19) or even inducing apoptosis of transformed cells (34).

Taken together, our findings provide new mechanistic insight into the control of stathmin function by multisite phosphorylation. They further offer a molecular basis for understanding the nature and regulation of intrinsically disordered protein systems in general. The ability to combine energetic and structural data thus represents a powerful means to extend our knowledge on factors determining dynamic protein-protein interactions found in a wide variety of fundamental biological processes. The detailed investigation of these factors is expected to be of benefit in the design of therapeutic strategies directed against disorders such as cancer and protein deposition diseases where intrinsically disordered protein segments are frequently implicated.

ACKNOWLEDGMENTS

We are grateful to Dr. M. Knossow for providing electron density maps and to Dr. F. Winkler for insightful discussions and support. We thank the Institute for Molecular Biology and Biophysics of ETH Zürich for access to the CD spectropolarimeter. This work was supported by Grants from the Swiss National Science Foundation #3100AO-107793 (to JS) and #31-64978.01 (to MOS).

REFERENCES

1. Dyson, H. J. & Wright, P. E. (2005) *Nat. Rev. Mol. Cell Biol.* **6**, 197-208.
2. Uversky, V. N., Oldfield, C. J. & Dunker, A. K. (2005) *J Mol. Recognit.* **18**, 343-384.
3. Tompa, P., Szasz, C. & Buday, L. (2005) *Trends Biochem. Sci.* **30**, 484-489.
4. Fink, A. L. (2005) *Curr. Opin. Struct. Biol.* **15**, 35-41.
5. Ward, J. J., Sodhi, J. S., McGuffin, L. J., Buxton, B. F. & Jones, D. T. (2004) *J Mol. Biol.* **337**, 635-645.
6. Iakoucheva, L. M., Radivojac, P., Brown, C. J., O'Connor, T. R., Sikes, J. G., Obradovic, Z. & Dunker, A. K. (2004) *Nucleic Acids Res.* **32**, 1037-1049.
7. Steinmetz, M. O., Kammerer, R. A., Jahnke, W., Goldie, K. N., Lustig, A. & van Oostrum, J. (2000) *EMBO J* **19**, 572-580.
8. Honnappa, S., Cutting, B., Jahnke, W., Seelig, J. & Steinmetz, M. O. (2003) *J Biol. Chem.* **278**, 38926-38934.
9. Curmi, P. A., Gavet, O., Charbaut, E., Ozon, S., Lachkar-Colmerauer, S., Manceau, V., Siavoshian, S., Maucuer, A. & Sobel, A. (1999) *Cell Struct. Funct.* **24**, 345-357.
10. Andersen, S. S. (2000) *Trends Cell Biol.* **10**, 261-267.
11. Walczak, C. E. (2000) *Curr. Opin. Cell Biol.* **12**, 52-56.
12. Cassimeris, L. (2002) *Curr. Opin. Cell Biol.* **14**, 18-24.
13. Rubin, C. I. & Atweh, G. F. (2004) *J Cell Biochem.* **93**, 242-250.
14. Jourdain, L., Curmi, P., Sobel, A., Pantaloni, D. & Carlier, M. F. (1997) *Biochemistry* **36**, 10817-10821.
15. Ravelli, R. B., Gigant, B., Curmi, P. A., Jourdain, I., Lachkar, S., Sobel, A. & Knossow, M. (2004) *Nature* **428**, 198-202.
16. Gigant, B., Wang, C., Ravelli, R. B., Roussi, F., Steinmetz, M. O., Curmi, P. A., Sobel, A. & Knossow, M. (2005) *Nature* **435**, 519-522.
17. Howell, B., Larsson, N., Gullberg, M. & Cassimeris, L. (1999) *Mol. Biol. Cell* **10**, 105-118.
18. Belmont, L. D. & Mitchison, T. J. (1996) *Cell* **84**, 623-631.
19. Baldassarre, G., Belletti, B., Nicoloso, M. S., Schiappacassi, M., Vecchione, A., Spessotto, P., Morrione, A., Canzonieri, V. & Colombatti, A. (2005) *Cancer Cell* **7**, 51-63.
20. Steinmetz, M. O., Jahnke, W., Towbin, H., Garcia-Echeverria, C., Voshol, H., Muller, D. & van Oostrum, J. (2001) *EMBO Rep.* **2**, 505-510.
21. Wallon, G., Rappsilber, J., Mann, M. & Serrano, L. (2000) *EMBO J* **19**, 213-222.

22. Larsson, N., Marklund, U., Gradin, H. M., Brattsand, G. & Gullberg, M. (1997) *Mol. Cell Biol.* **17**, 5530-5539.

23. Horwitz, S. B., Shen, H. J., He, L., Dittmar, P., Neef, R., Chen, J. & Schubart, U. K. (1997) *J Biol. Chem.* **272**, 8129-8132.

24. Kuntziger, T., Gavet, O., Sobel, A. & Bornens, M. (2001) *J Biol. Chem.* **276**, 22979-22984.

25. Wittmann, T., Bokoch, G. M. & Waterman-Storer, C. M. (2004) *J Biol. Chem.* **279**, 6196-6203.

26. Andersen, S. S., Ashford, A. J., Tournebize, R., Gavet, O., Sobel, A., Hyman, A. A. & Karsenti, E. (1997) *Nature* **389**, 640-643.

27. Niethammer, P., Bastiaens, P. & Karsenti, E. (2004) *Science* **303**, 1862-1866.

28. Budde, P. P., Kumagai, A., Dunphy, W. G. & Heald, R. (2001) *J Cell Biol.* **153**, 149-158.

29. Iancu, C., Mistry, S. J., Arkin, S., Wallenstein, S. & Atweh, G. F. (2001) *J Cell Sci.* **114**, 909-916.

30. Di, P. G., Antonsson, B., Kassel, D., Riederer, B. M. & Grenningloh, G. (1997) *FEBS Lett.* **416**, 149-152.

31. Spolar, R. S. & Record, M. T., Jr. (1994) *Science* **263**, 777-784.

32. Luque, I. & Freire, E. (1998) *Methods Enzymol.* **295**, 100-127.

33. Tholey, A., Lindemann, A., Kinzel, V. & Reed, J. (1999) *Biophys. J* **76**, 76-87.

34. Liu, Z., Lu, H., Shi, H., Du, Y., Yu, J., Gu, S., Chen, X., Liu, K. J. & Hu, C. A. (2005) *Cancer Res.* **65**, 1647-1654.

FIGURE LEGENDS

Figure 1. Stathmin is an intrinsically disordered protein that forms ternary complexes with tubulin. (A) In isolation, the C-terminal domain of stathmin (as ribbon representation) populates an ensemble of transient and predominantly extended helical conformations. (B) X-ray crystal structure of the complex formed between the stathmin homologue RB3 (as cartoon representation) and two α/β-tubulin heterodimers (as surface representation). The corresponding stathmin positions for Ser16, Ser25, Ser38, and Ser63 are indicated as yellow spheres. The β-hairpin (residues 2-21), loop region (residues 22-46), helical domain (residues 47-141), and helix nucleation site (residues 55-73) are indicated in red, green, blue, and cyan respectively.

Figure 2. Coomassie-stained native-PAGE of stathmin phosphoisoforms used in the present study. The number of phosphoryl groups incorporated in each stathmin phosphoisoform is given on the left.

Figure 3. Tubulin-binding properties of stathmin and phosphoisoforms. (A) Thermodynamics of T_2S complex formation for unmodified stathmin as a function of temperature. The apparent reaction enthalpies, ΔH^0 (red), and $T\Delta S^0$ (blue), were fitted with a linear regression. The solid line describing the reaction free energy, ΔG^0 (cyan), is the theoretical prediction taking into account $\Delta C^0_{p,T_2S,obs}$. (B) and (C) Equilibrium dissociation constants (B; blue numbers in μM^2) and changes in free energies (B; red numbers in kcal/mol), enthalpies (C, red symbols), and $T\Delta S^0$ (C, blue symbols) of phosphoisoforms relative to unmodified stathmin upon T_2S complex formation. (D) *In vitro* microtubule formation as a function of the free energy of T_2S complex formation in the presence of different stathmin phosphoisoforms.

Figure 4. Structural basis for Ser63 phosphorylation. (A) and (B) Far-UV spectra (A; at 6 °C) and melting profiles (B) recorded by CD for wt (black), p63 (blue), p16,25,38 (green), and p16,25,38,63 (red). (C) Close-up view of T_2R showing the location of stathmin Ser63 and adjacent residue side chains with respect to α1-tubulin. The backbone and residue side chains are shown as yellow line and sticks representations, respectively, and α1-tubulin is shown as surface representation.

Figure 5. Structural basis for Ser16 phosphorylation. (A) Close-up view of T_2R showing the location of the Ser16 side chain with respect to α1-tubulin. Colors and representations are the same as in (Figure 4C). (B) ^{15}N,^{1}H HSQC spectra of tubulin-bound ^{15}N-labeled stathmin (in black with assignments) and p16 (in red). The two resonances which have shifted upon phosphorylation of unbound stathmin (supplementary Figure 4) and most likely originate from Ser16 and an adjacent residue are highlighted by circles.

Figure 1

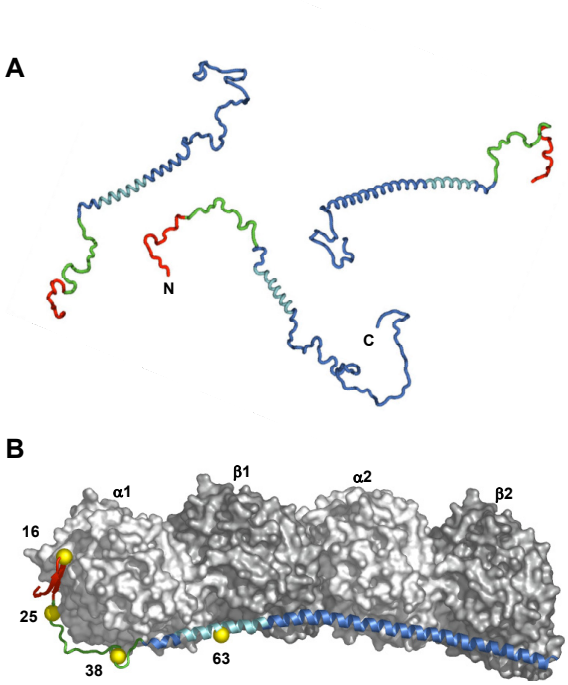

Figure 2

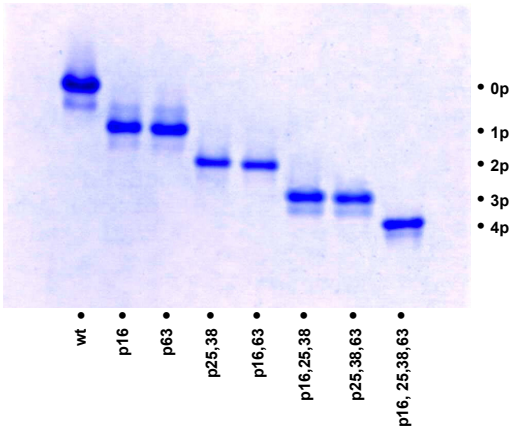
0p
1p
2p
3p
4p
wt
p16
p63
p25,38
p16,63
p16,25,38
p25,38,63
p16, 25,38,63

Figure 3

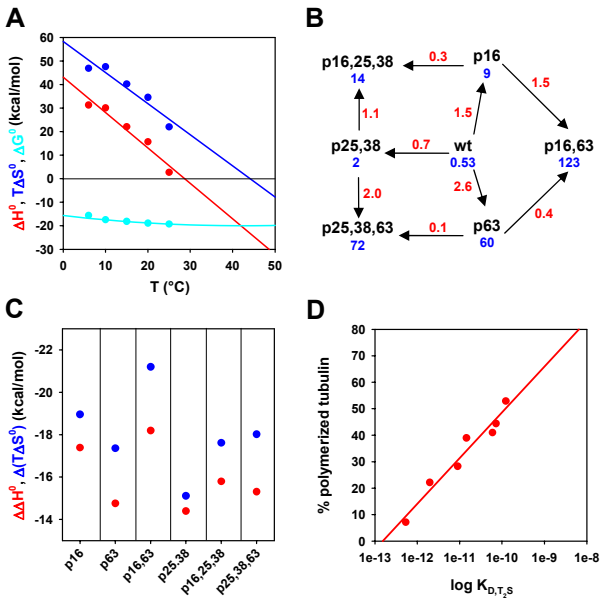
A
B
C
D
ΔH°, TΔS°, ΔG° (kcal/mol)
T (°C)
p16,25,38
14
0.3
p16
9
1.5
1.1
1.5
p25,38
2
0.7
wt
0.53
p16,63
123
2.6
2.0
0.4
p25,38,63
72
0.1
p63
60
ΔΔH°, Δ(TΔS°) (kcal/mol)
p16
p63
p16,63
p25,38
p16,25,38
p25,38,63
% polymerized tubulin
log K D,T,S

Figure 4

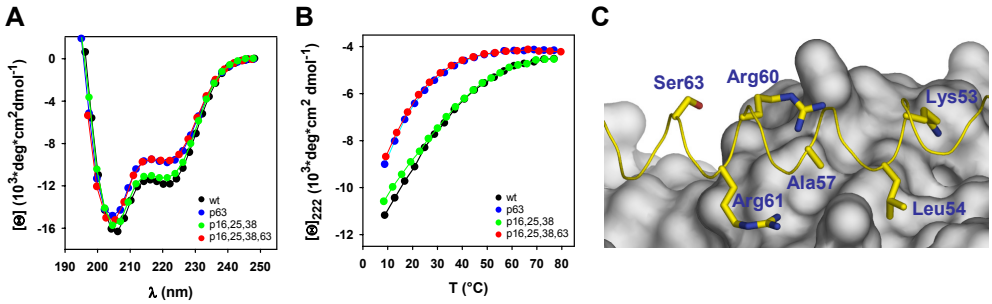
A
B
C
[Θ] (10^3*deg*cm^2dmol^-1)
λ (nm)
wt
p63
p16,25,38
p16,25,38,63
[Θ]222 (10^3*deg*cm^2 dmol^-1)
T (°C)
Ser63
Arg60
Lys53
Ala57
Arg61
Leu54

Figure 5

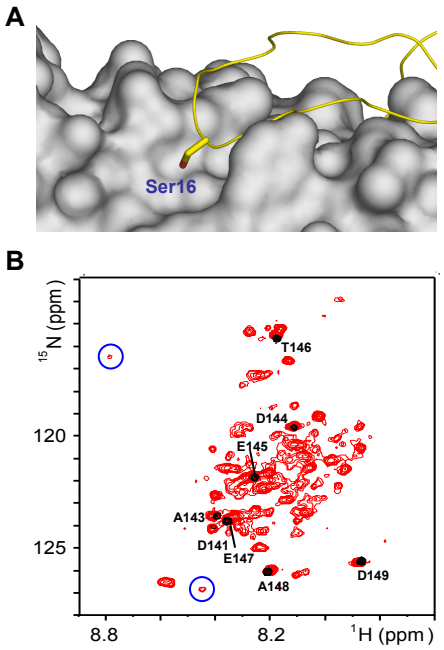
A
Ser16
B
^{15}N (ppm)
120
125
8.8
8.2
^{1}H (ppm)
T146
D144
E145
A143
D141
E147
A148
D149

Supplementary Data

Supplementary Table 1

ITC thermodynamic binding parameters derived from the titration of tubulin with stathmin as a function of temperature. All thermodynamic parameters are referred to the ternary T_2S complex.

T (°C)	ΔH^0 (kcal/mol)	$T\Delta S^0$ (kcal/mol)	ΔG^0 (kcal/mol)
6	31.2	46.8	-15.6
10	30.0	47.5	-17.5
15	22.0	40.2	-18.2
20	15.6	34.5	-18.9
25	2.6	21.9	-19.3

The data at 10, 15, 20, and 25 °C were adapted from (1).

Supplementary Table 2

ITC thermodynamic binding parameters derived from the titration of tubulin with stathmin variants and phosphoisoforms at 6 °C. All thermodynamic parameters are referred to the ternary T_2S complex.

	K_{D,T_2S} (M^2)	ΔH^0 (kcal/mol)	$T\Delta S^0$ (kcal/mol)	ΔG^0 (kcal/mol)
wt	5.3E-13	31.2	46.8	-15.6
4A	4.6E-13	29.8	45.5	-15.7
p16	9.0E-12	13.4	27.5	-14.1
ΔN	1.0E-11	13.6	27.5	-14.0
S16E	3.2E-12	22.2	36.8	-14.6
p63	6.0E-11	16.0	29.0	-13.0
S63E	2.0E-12	33.4	48.3	-14.9
p16,63	1.2E-10	12.6	25.2	-12.6
p25,38	2.0E-12	16.4	31.3	-14.9
p16,25,38	1.4E-11	15.0	28.8	-13.8
p25,38,63	7.2E-11	15.5	28.4	-12.9
p16,25,38,63	n.d.	n.d.	n.d.	n.d.

Supplementary Figure 1

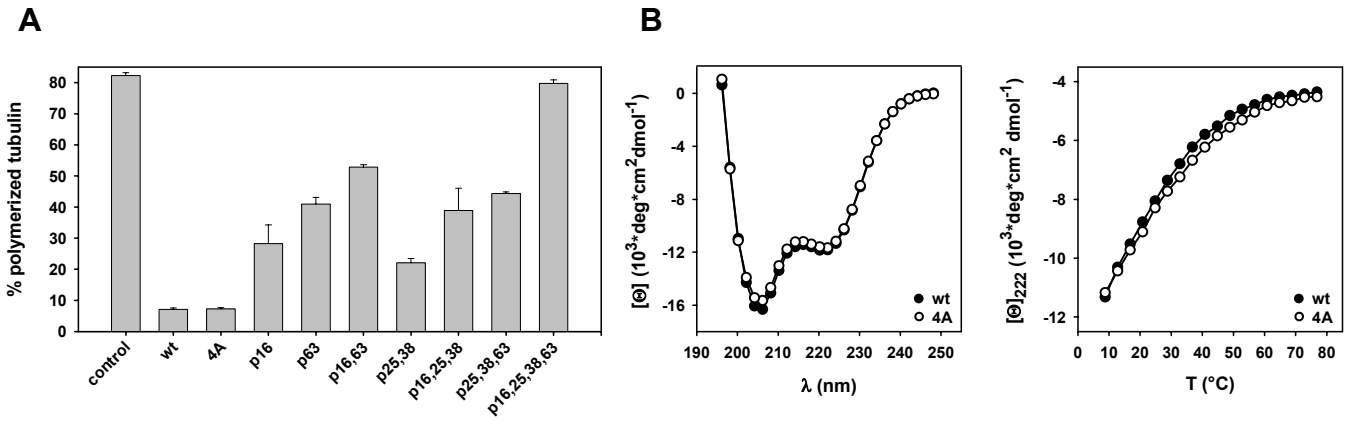

Supplementary Figure 2

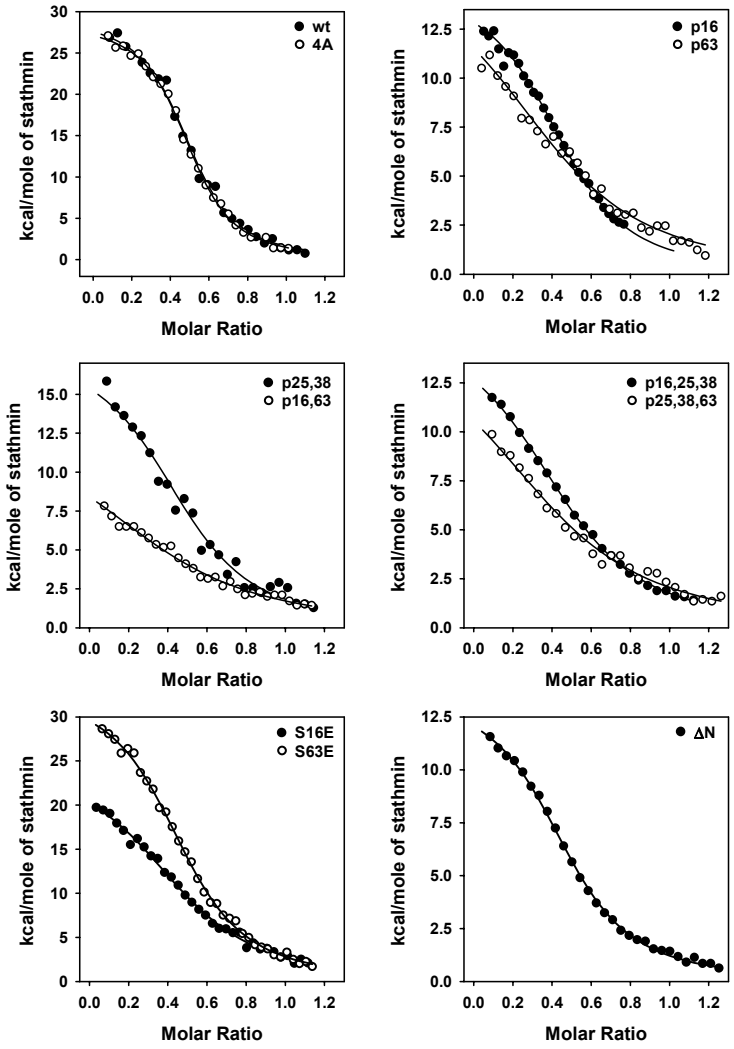

Supplementary Figure 3

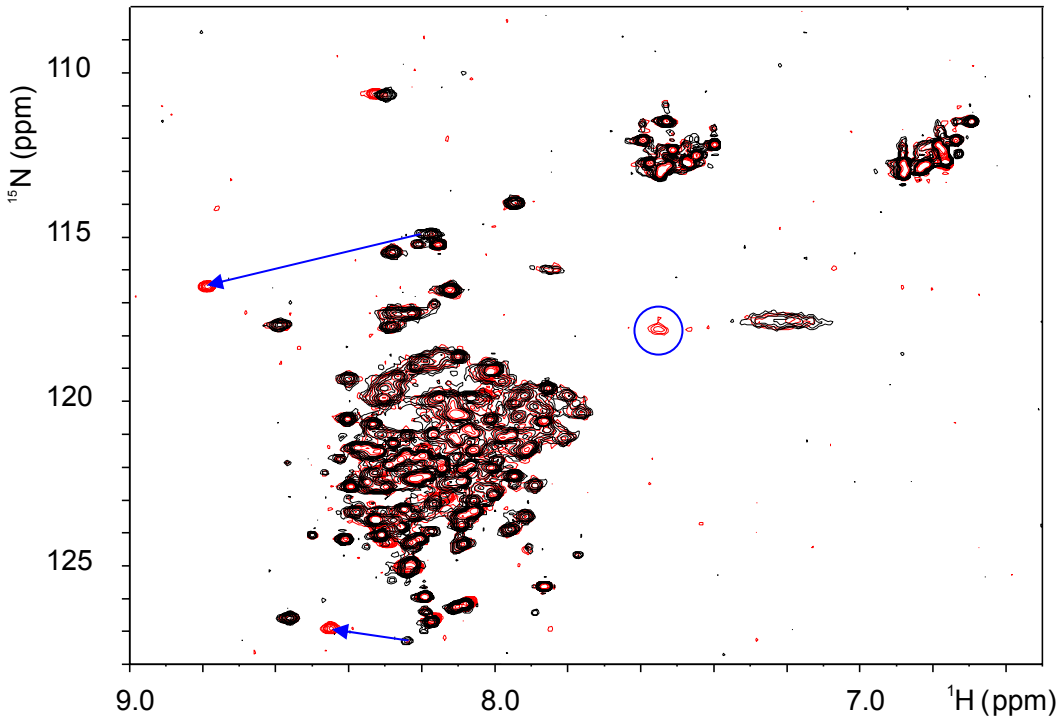

Supplementary Figure 4

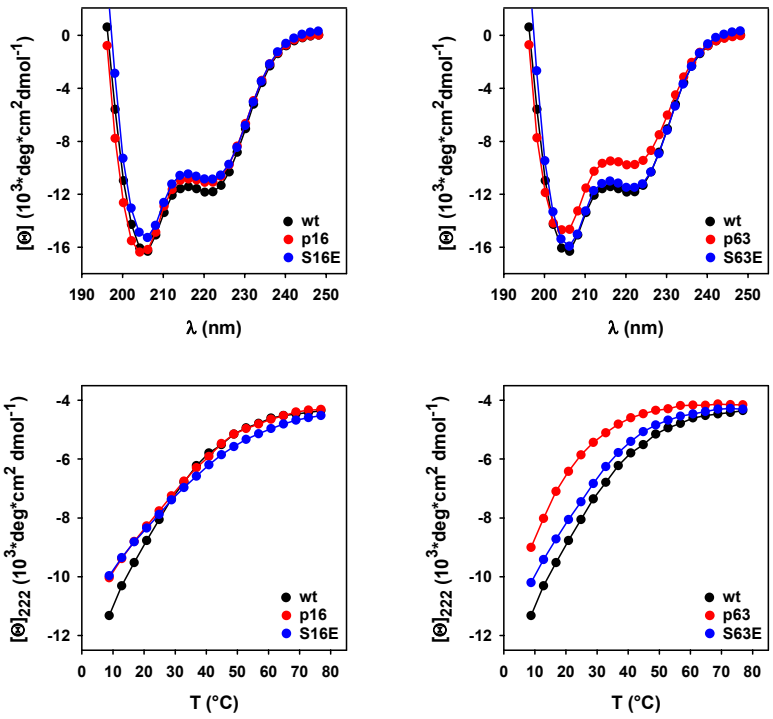

Supplementary Figure Legends

Figure 1. (A) Taxol (4 μM) driven *in vitro* tubulin (4 μM) polymerization in the presence of stathmin variants and phosphoisoforms (4 μM each). (B) CD spectra (left) and thermal unfolding profiles recorded at 222 nm (right) of wt and 4A.

Figure 2. ITC analysis of stathmin phosphoisoforms and mutants. Integrated heats of reaction (symbols) with the best fit to the data (line) are shown for each protein. Binding isotherms were fitted via a nonlinear least squares minimization method assuming two independent and equal binding sites on stathmin for tubulin.

Figure 3. Superposition of $^{15}N,^{1}H$-HSQC spectra of ^{15}N-wt (black) and ^{15}N-pSer16 (red). Spectral changes which most likely originate from Ser16 and adjacent residues are indicated by blue arrows. The new signal at 7.55/118.2 ppm which is due to an arginine side chain forming a hydrogen bond (most likely Arg14) is indicated by a blue circle. The peak is invisible in ^{15}N-wt due to fast solvent exchange, but visible in ^{15}N-pSer16, most likely due to interaction of the arginine side chain with the phosphorylated Ser16 residue which slows down its solvent exchange rate.

Figure 4. CD spectra at 6 °C (left panels) and thermal melts recorded at 222 nm (right panels) for wt, single phosphorylated, and serine-to-glutamate stathmin mutants.

Supplementary References

1. Honnappa, S., Cutting, B., Jahnke, W., Seelig, J. & Steinmetz, M. O. (2003) *J Biol. Chem.* **278**, 38926-38934.

3. Structural insights into the EB1−APC interaction

Srinivas Honnappa, Corinne M John, Dirk Kostrewa, Fritz K Winkler and Michel O Steinmetz

***EMBO Journal* (2005) 24, 261–269**

EB1, a member of a highly conserved protein family binding microtubule ends, was found to target polymerizing microtubule tips *via* its N-terminal domain, where it regulates microtubule dynamics and facilitates molecular recognition of microtubule plus-ends. The C-terminal EB1-like domain interacts with the APC tumor suppressor protein and with $p150^{glued}$, and is thought to be implicated in the recruitment of a macromolecular 'plus-end complex' at microtubule tips. Despite substantial progress made by *in vivo* studies in identifying the interaction networks between +TIP proteins, their detailed nature and mechanisms of regulation are poorly determined.

In order to provide a structural basis for understanding the important role of EB1 proteins, we carried out a biophysical analysis of EB1−APC. We reported the first crystal structure of EB1-C, which contains a unique EB1 sequence motif and is highly conserved from yeast to humans. The publication provides insights into the structural elements involved in EB1-APC interaction.

My contribution to this publication was to carry out the cloning of full length EB1, to purify all the proteins mentioned in the publication, to crystallize and solve the structure of EB1-C, and to perform the biophysical analysis of EB1−APC and its mutants using ITC. C.M. John provided me with clones of EB1-C and its deletion constructs. D. Kostrewa and F.K. Winkler assisted me in solving and interpreting the crystal structure of EB1-C.

The EMBO Journal (2005) 24, 261–269 | © 2005 European Molecular Biology Organization | All Rights Reserved 0261-4189/05
www.embojournal.org

THE EMBO JOURNAL

Structural insights into the EB1–APC interaction

Srinivas Honnappa[1,3], Corinne M John[1,2,3], Dirk Kostrewa[1], Fritz K Winkler[1] and Michel O Steinmetz[1,*]

[1]Biomolecular Research, Structural Biology, Paul Scherrer Institut, Villigen PSI, Switzerland and [2]Institute of Biochemistry, Swiss Federal Institute of Technology (ETH), Zürich, Switzerland

EB1 proteins bind to microtubule ends where they act in concert with other components, including the adenomatous polyposis coli (APC) tumor suppressor, to regulate the microtubule filament system. We find that EB1 is a stable dimer with a parallel coiled coil and show that dimerization is essential for the formation of its C-terminal domain (EB1-C). The crystal structure of EB1-C reveals a highly conserved surface patch with a deep hydrophobic cavity at its center. EB1-C binds two copies of an APC-derived C-terminal peptide (C-APCp1) with equal 5 μM affinity. The conserved APC Ile2805–Pro2806 sequence motif serves as an anchor for the interaction of C-APCp1 with the hydrophobic cavity of EB1-C. Phosphorylation of the conserved Cdc2 site Ser2789–Lys2792 in C-APCp1 reduces binding four-fold, indicating that the interaction APC–EB1 is post-translationally regulated in cells. Our findings provide a basis for understanding the dynamic crosstalk of EB1 proteins with their molecular targets in eukaryotic organisms.

The EMBO Journal (2005) **24,** 261–269. doi:10.1038/sj.emboj.7600529; Published online 23 December 2004
Subject Categories: structural biology; cell cycle
Keywords: coiled coil; microtubule plus-end tracking proteins; phosphorylation; protein–protein interaction; +TIP

Introduction

The intrinsic dynamic properties of microtubules (MTs) are important in establishing and maintaining a specific organization of cellular components during the cell cycle. Diverse factors regulate MT dynamics both spatially and temporally. Among these, a number of proteins and protein complexes have been identified that specifically track growing MT plus ends (referred to as +TIP proteins; Carvalho *et al*, 2003). EB1 (end-binding protein 1) is a member of a highly conserved and ubiquitously expressed family of +TIP proteins that has emerged as a key player in the modulation of MT dynamics in eukaryotic organisms. EB1 proteins are implicated in most if not all MT-based processes including maintenance of cell polarity, regulation of chromosome stability, positioning of the mitotic spindle, and anchoring of MTs to their nucleation sites (Tirnauer and Bierer, 2000; Gundersen, 2002; Carvalho *et al*, 2003; Galjart and Perez, 2003).

The dynamic crosstalk among +TIP proteins together with the observation that EB1 is always localized at growing MT ends suggests that EB1 is involved in the establishment of macromolecular 'plus-end complexes' at MT tips (Schroer, 2001; Galjart and Perez, 2003). In budding yeast, the EB1-mediated interaction network involving Kar9p and the myosin molecule Myo2 is required for MT guidance toward the bud along actin cables to ensure proper spindle alignment (Liakopoulos *et al*, 2003). Thus the role of the EB1 orthologue Bim1p in *Saccharomyces cerevisiae* is to link different functionalities to the MT plus end allowing them to stably capture specialized cellular targets. Similarly, in fission yeast, the EB1 homologue Mal3p transiently tethers the CLIP-170 homologue Tip1p and the kinesin molecule Tea2p into larger particles whose function is to guide MT growing tips to cell ends (Busch *et al*, 2004). In *Drosophila*, the guanine nucleotide exchange factor DRho-GEF2 utilizes EB1-mediated MT dynamics to search for cortical subdomains for directing localized actomyosin contraction (Rogers *et al*, 2004). It appears very likely that similar EB1-dependent MT capture and guided processes are conserved throughout higher eukaryotes (Gundersen, 2002; Kusch *et al*, 2003).

EB1 proteins are comprised of conserved amino- and carboxy-terminal domains (Tirnauer and Bierer, 2000; Bu and Su, 2003). The N-terminal domain is necessary and sufficient for MT binding. Its structure, recently solved by X-ray crystallography, revealed a calponin homology (CH) fold (Hayashi and Ikura, 2003). The C-terminal domain (EB1-C) contains a putative coiled coil, which mediates subunit oligomerization (Rehberg and Gräf, 2002). However, the detailed molecular organization of EB1 proteins is still not known.

EB1-C comprises a unique EB1-like sequence motif that acts as a binding site for other +TIP proteins. It interacts with the carboxy terminus of the adenomatous polyposis coli (APC) tumor suppressor (Su *et al*, 1995; Berrueta *et al*, 1999; Askham *et al*, 2000; Mimori-Kiyosue *et al*, 2000; Nakamura *et al*, 2001; Bu and Su, 2003; Wen *et al*, 2004), a well-conserved 2843-residue +TIP phosphoprotein (Trzepacz *et al*, 1997) with a pivotal function in cell cycle regulation (Dikovskaya *et al*, 2001; Mimori-Kiyosue and Tsukita, 2001). The transient binding of APC to EB1 may play a central role in spindle positioning and fidelity of chromosome segregation (Fodde *et al*, 2001). Together with the fact that APC lacks the EB1-binding site in many malignant human colon tumors, it has been speculated that abrogation of the APC–EB1 interaction may contribute to cancer progression (Su *et al*, 1995; Tirnauer and Bierer, 2000; Fodde *et al*, 2001). Recent data suggest that the interaction between EB1-C and the carboxy terminus of APC (C-APC) is also implicated in the capturing and stabilization of MTs *in vivo* (Wen *et al*, 2004). Interfering with the EB1–APC interaction inhibits fibroblast migration, demonstrating the importance of EB1–APC-mediated stable MT formation in promoting directed cell migration (Wen *et al*,

*Corresponding author. Paul Scherrer Institut, 5232 Villigen PSI, Switzerland. Tel.: +41 56 310 4754; Fax: +41 61 310 5288; E-mail: michel.steinmetz@psi.ch
[3]These authors contributed equally to this work

Received: 22 September 2004; accepted: 30 November 2004; published online: 23 December 2004

2004). Based on the apparent functional conservation, the fact that Kar9p and APC share a sequence site of limited homology (Bienz, 2001), and the finding that the molecules are regulated by post-translational phosphorylation events (Askham *et al*, 2000; Nakamura *et al*, 2001; Liakopoulos *et al*, 2003), it has been proposed that Kar9p may be the functionally related APC molecule in yeast.

Another binding partner of EB1-C is the well-conserved +TIP protein dynactin/p150^{glued}, a component of the large cytoplasmic dynein/dynactin complex (Berrueta *et al*, 1999; Askham *et al*, 2002; Bu and Su, 2003; Goodson *et al*, 2003; Ligon *et al*, 2003). The EB1–p150^{glued}/dynactin interaction is required for the regulation of MT dynamics and for MT anchoring at its nucleation sites during the formation and maintenance of a radial MT array. It should be noted that a growing body of evidence also suggests that EB1, APC, and the dynein/dynactin complex are functional components of centrosomes, which anchor the MT minus end (Berrueta *et al*, 1998; Askham *et al*, 2002; Rehberg and Gräf, 2002; Rogers *et al*, 2002; Louie *et al*, 2004). Thus the dynamic crosstalk between these proteins appears also important for MT nucleation and stabilization at centrosomes.

Despite substantial progress that has been made in identifying the interaction networks between +TIP proteins, their detailed nature and mechanisms of regulation are poorly defined. In order to provide a structural basis for understanding the important role of EB1 proteins, here we have carried out a biophysical analysis of EB1–APC. We conclude that EB1 proteins assemble into dimeric structures, which is mediated by a parallel coiled coil. Using X-ray crystallography and isothermal titration calorimetry (ITC), we propose that a major interaction site between EB1-C and APC involves the APC dipeptide segment Ile2805–Pro2806. We further found that the interaction is regulated by APC phosphorylation of the conserved cyclin-dependent mitotic kinase Cdc2 target residue Ser2789. Our findings are consistent with the APC sequence segment Val2781–Lys2819 being the major interaction site between APC and EB1 and suggest that specific C-APC phosphorylation represents a mechanism for regulating the EB1–APC complex during the cell cycle.

Results

Molecular organization and overall structure of EB1

The EB1 molecule is comprised of three structural domains (Figure 1A): an N-terminal MT-binding domain (residues 1–133; referred to as domain N), a flexible intermediate domain (residues 134–192; referred to as domain I), and a C-terminal +TIP-binding domain (residues 193–268; referred to as domain C). Its amino-terminal segment (residues 193–225; referred to as subdomain Ca) exhibits a high potential for adopting an α-helical coiled-coil structure (Cohen and Parry, 1990; Juwana *et al*, 1999) and the very C-terminal acidic subdomain Cb (residues 226–268) is composed of low-complexity sequence.

The overall structure of EB1 was assessed by analytical ultracentrifugation (AUC), transmission electron microscopy (TEM), and limited proteolysis. Sedimentation velocity and equilibrium AUC experiments yielded an $s_{w,20}$ value of 3.5 S and an average molecular mass of 62 kDa, respectively (monomer mass of recombinant EB1 is 32 kDa). Inspection of EB1 molecules by TEM after glycerol spraying and rotary metal shadowing suggested that two larger globular domains, ~4 nm in diameter, are joined via a smaller domain to form a flexible Y-shaped structure (Figure 1B). The dimension of the larger domains is in agreement with the one deduced from the crystal structure of EB1's N-terminal CH domain (Hayashi and Ikura, 2003). Thrombin digestion of EB1 yielded non-specific cleavage within the sequence Pro145–Pro161 (see Materials and methods), indicating that this segment is flexible. These data establish that EB1 is an elongated dimeric molecule.

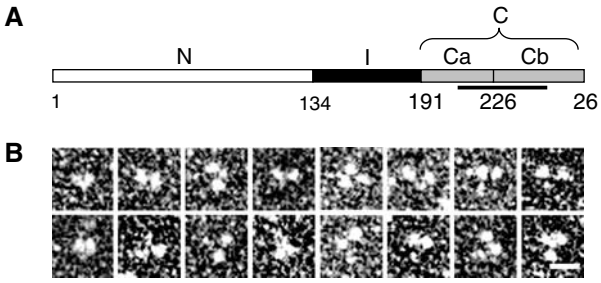

Figure 1 Molecular organization of human EB1. (**A**) Schematic representation of the domain organization of human EB1. Domains N, I, and C (subdivided in Ca and Cb) are depicted in white, black, and gray, respectively. Corresponding domain boundaries are indicated by residue positions. The unique EB1-like sequence motif is highlighted by a line. (**B**) High-magnification TEM gallery of glycerol sprayed/rotary metal shadowed EB1 specimens. Scale bar, 10 nm.

Biophysical solution analysis of EB1-C

To test whether the predicted coiled coil is involved in EB1 dimerization, a fragment corresponding to residues Ala193–Glu225 was prepared. The fragment, referred to as CysEB1-Ca, contained an extra Cys residue to permit disulfide bond formation, and two extra Gly residues for flexibility at its N-terminus to allow determination of the orientation of the helical monomers within the coiled coil (Harbury *et al*, 1993). As shown in Figure 2A, at 5°C and under reducing conditions, CysEB1-Ca displayed a far-ultraviolet (UV) circular dichroism (CD) spectrum characteristic of proteins with a helical content of ~50%. The stability of CysEB1-Ca under the same solution conditions was assessed by a thermal unfolding experiment recorded by CD at 222 nm. The fragment (0.2 mg/ml) revealed a broad transition, indicating that it unfolds readily with increasing temperature and is largely denatured at 55°C (Figure 2B). Consistent with these findings, sedimentation equilibrium experiments at 5°C and under reducing conditions yielded an average molecular mass of 6.2 kDa (monomer mass of CysEB1-Ca is 4.5 kDa), indicating an equilibrium between monomers and dimers of the fragment. An increase of 30% in helical signal and a sigmoidal shaped melting profile with a T_m centered at 43°C was observed for CysEB1-Ca under oxidizing conditions (Figure 2A and B). Both the CD spectrum and the shape of the unfolding profile are characteristic for stable α-helical coiled-coil structures. Reducing and nonreducing SDS–PAGE revealed protein bands migrating at apparent molecular masses consistent with monomers and disulfide bonded dimers, respectively, of CysEB1-Ca (Figure 2A, inset).

These data suggest that subdomain Ca mediates the parallel in-register assembly of two EB1 monomers. However, they

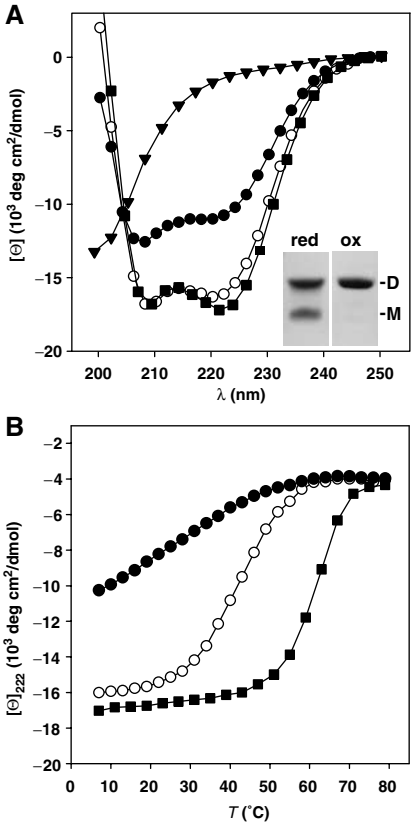

Figure 2 Analysis of EB1-C and fragments. (**A**) Far-UV CD spectra recorded at 5°C of EB1-C (closed squares), CysEB1-Ca under reducing (closed circles) and oxidizing conditions (open circles), and EB1-Cb (closed triangles). Inset: Coomassie blue-stained tricine–SDS–PAGE of CysEB1-Ca under reducing (red) and oxidizing (ox) conditions. The migration positions for monomers (M) and dimers (D) are indicated. (**B**) Thermal unfolding profiles recorded by CD at 222 nm. Symbols are the same as for panel A. The CD measurements were carried out in PBS at a protein concentration of 0.2 mg/ml.

further reveal that the sequence Ala193–Glu225 of EB1 does not form a stable coiled coil in isolation. To assess the effect of the C-terminal flanking subdomain Cb on the stability of the coiled coil, a fragment comprising residues Asp191–Tyr268 of EB1, referred to as EB1-C, was analyzed. The far-UV CD spectrum recorded from EB1-C was characteristic for predominantly (~70%) helical proteins (Figure 2A). The reversible sigmoidal shaped melting profile with a T_m centered at 63°C obtained at a protein concentration of 0.2 mg/ml demonstrates that the EB1-C molecule is very stable (Figure 2B). Sedimentation equilibrium experiments yielded an average molecular mass of 20 kDa consistent with the formation of a dimeric structure (monomer mass of EB1-C is 9.2 kDa). To probe the possibility that the short 43-residue-long subdomain Cb forms a stable structure, the C-terminal EB1 peptide segment Leu226–Tyr268, referred to as EB1-Cb, was analyzed by CD. As shown in Figure 2A, the spectrum is characteristic for peptides with little if any secondary structure.

Together, these findings demonstrate that coiled coil and C-terminus together constitute a stable folding unit.

Crystal structure of EB1-C

The crystal structure of EB1-C was determined by single isomorphous replacement combined with anomalous scattering (SIRAS) using a thiomersal derivative. The asymmetric unit of the crystal contains two largely helical monomers, denoted A and B, which are related by a noncrystallographic two-fold symmetry axis (Figure 3). Each 80-residue monomer starts with a long smoothly curved helix (α1, residues 191–230), which is followed by a hairpin connection leading to a short second helix (α2, residues 237–248) running antiparallel to α1. For the residues C-terminal of α2 (residues 250–268), interpretable density is only observed for segment 250–258 and only in monomer B. In agreement with the CD analysis, this suggests that the C-terminal region is largely disordered in solution. The observed ordering of the nine-residue segment in monomer B is a consequence of the crystal packing (also, see below). The two parallel α1 helices of the EB1-C dimer wrap around each other in a slightly left-handed supercoil up to residue Leu221. With the exception of Arg214 and Tyr217, the residues occupying the core **a** and **d** positions of the four heptad repeats between Ala193 and Leu221 (Figure 4A) pack in the typical 'knobs-into-hole' fashion, consistent with a coiled-coil structure (Harbury *et al*, 1993). Beyond Leu221, the two α1 helices diverge into a fork-like structure. The two α2 helices run antiparallel to helices α1 and form a similar fork in the opposite orientation and rotated by 90°. As a result, two helical segments from each monomer (residues 219–229 and 237–247) form a four-helix bundle (Figure 3). The side chains forming the hydrophobic core of this bundle (equivalent residue pairs are 221/239, 224/242, and 227/245) are highly conserved (Figure 4A). The large hydrophobic surface buried in this bundle is expected to significantly contribute to the observed stability (Figure 2) of the dimeric structure of EB1-C (Supplementary Figure 1).

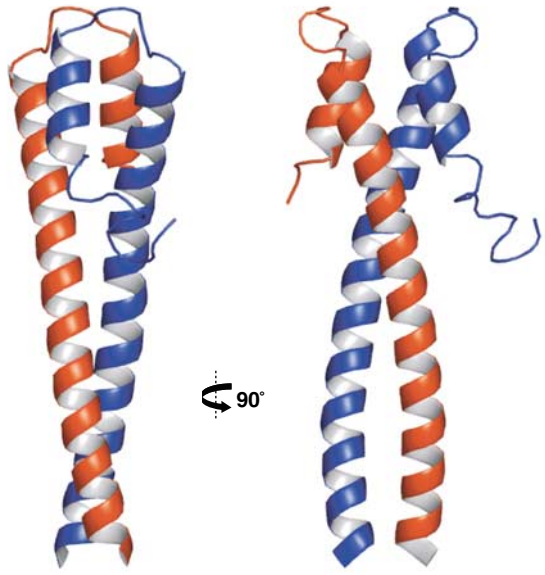

Figure 3 Overall crystal structure of EB1-C in cartoon representation and in two orientations 90° apart. Monomers A and B are colored in red and blue, respectively.

A primary interest of this structure determination was to gain insight into the spatial arrangement of the conserved residues of the unique EB1-like sequence motif (Figure 4A). Remarkably, most of the invariant and highly conserved residues form an extended and contiguous surface patch

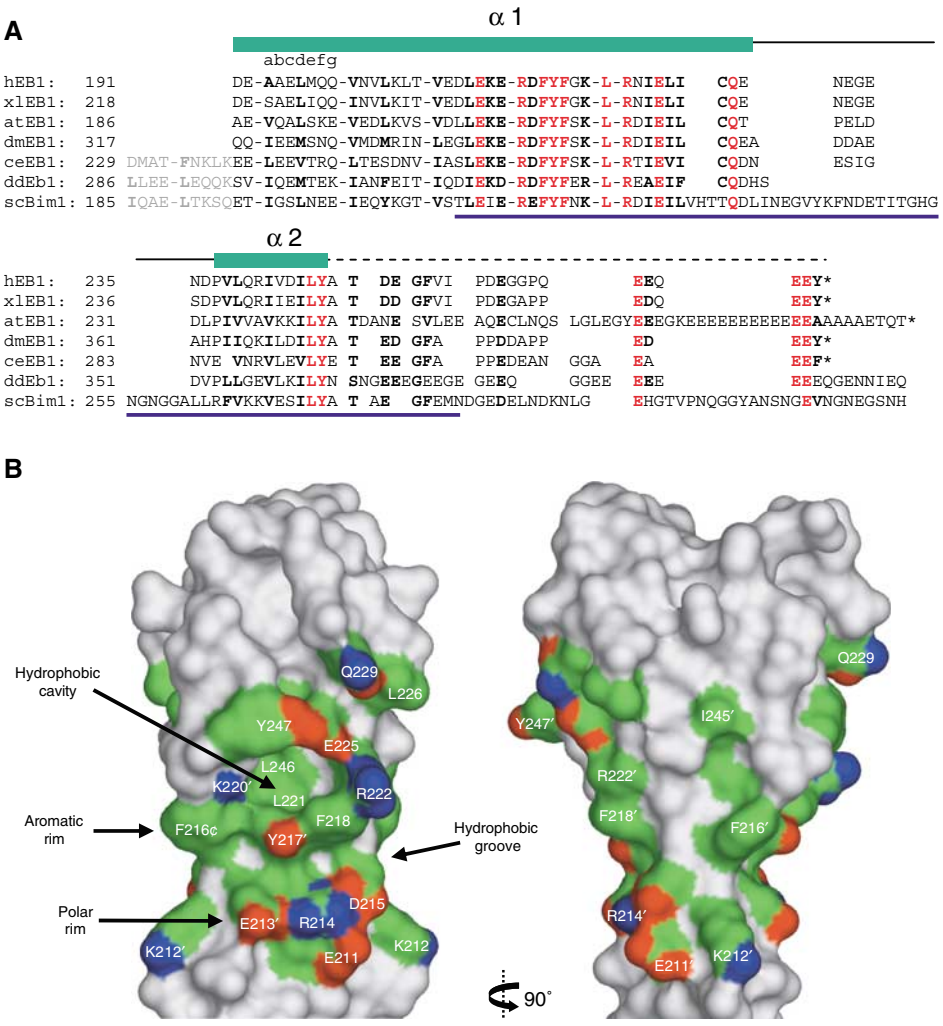

Figure 4 The EB1-like structural motif. (**A**) Structure-based sequence alignment of C-terminal EB1 domains from different species. Sequence identities and accession numbers are as follows: h, *Homo sapiens*, SwissProt: Q15691; xl, *Xenopus laevis*, GenBank: AAH68630; at, *Arabidopsis thaliana*, GenBank: BAB11500; dm, *Drosophila melanogaster*, TrEMBL: Q9V9A6; ce, *Caenorhabditis elegans*, GenBank: NP_507526; dd, *Dictyostelium discoideum*, TrEMBL: Q8WQ86; sc, *Saccharomyces cerevisiae*, SwissProt: P40013. Helices α1 and α2 (green bars), the loop α1–α2 (black line), the carboxy-terminal flexible tail (dashed line), and the EB1-like sequence motif (blue line) are indicated. The N-terminal heptad repeats (abcdefg) are shown as blocks of seven amino-acid residues. Predicted N-terminal heptad repeat sequence extensions in unicellular organisms are shown in gray. Conserved residues are depicted in red (invariant) and bold (highly conserved). (**B**) Surface views of the EB1-like structural motif as seen perpendicular to the coiled-coil axis from two orientations 90° apart (same views as in Figure 3). The flexible peptide segments starting from Thr249 have been removed in both monomers for clarity. Highly conserved and surface accessible amino-acid residue side chains are indicated and colored according to the atom type: blue, nitrogen; red, oxygen; green, carbon. The positions of the polar and aromatic rims and of the hydrophobic cavity are indicated by arrows.

at the interface between the two monomer segments forming the four-helix bundle (Figure 4B). The charged side chains of Glu213′ (a prime is used to discriminate one monomer from the other), Arg214, and Asp215 form a polar rim. Similarly, the side chains of Phe216′, Tyr217′, and Phe218 form an aromatic rim. A wedge-like, predominantly hydrophobic groove is produced between the two rims. In the center of the surface patch, a prominent deep hydrophobic cavity is observed with the Leu221 and Leu246 residues at its floor. One wall is formed by the aromatic rim and the remaining walls are formed by the side chains of the residues Lys220′, Arg222, Glu225, Tyr247, and Ala248. Since the residues involved in the formation of these structural features are highly conserved throughout species and distributed along the entire length of the EB1-like sequence motif, they establish the sequence-to-structure relationship of the Conserved Domain Database sequence motif pfam03271.

For further description, we will refer to cavity A or B depending on whether its floor residues belong to monomer A or B. In the crystal structure, the 19 C-terminal residues are disordered in monomer A but partly ordered in monomer B. The length and sequence of the C-terminal EB1 peptide segment following α2 is less conserved but contains several invariant acidic residues (Figure 4A). Inspection of the structure and interactions of the nine additional residues ordered in monomer B revealed that this peptide segment interacts with both hydrophobic cavities albeit in a distinct manner. It is folded such that it forms an intramolecular interaction by occupying cavity B with its Thr249 side chain and an intermolecular contact by occupying cavity A of a neighboring dimer with its Ile255 side chain. The cavity B/threonine

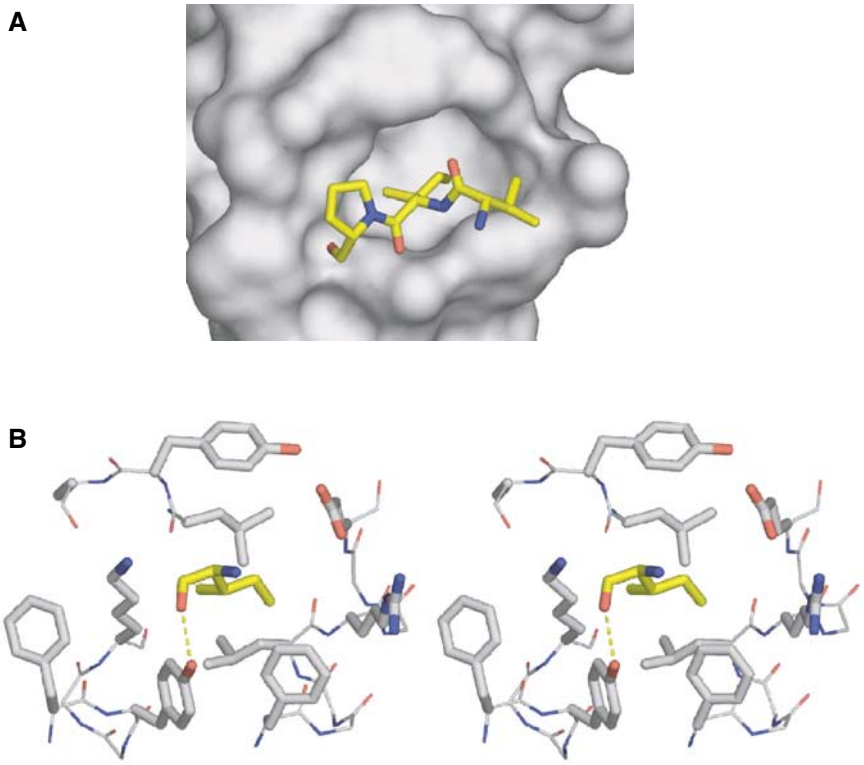

Figure 5 Peptide binding to the hydrophobic cavity of EB1-C. (**A**) Interaction of the tripeptide segment Val254B–Ile255B–Pro256B (in stick representation) originating from a neighboring EB1-C dimer in the crystal with cavity A (in surface representation). (**B**) Stereo view of cavity A with the cavity occupying Ile255 (yellow). All side chains are represented as thick stick models. The cavity-forming residues are as follows: left wall, Lys220′ and Phe216′; right wall, Arg222; lower wall, Phe216, Tyr217′, and Phe218; upper wall, Ala248, Tyr247, and Glu225; floor, Leu221 and Leu246. The intermolecular hydrogen bond formed between the main-chain carbonyl oxygen of Ile255 and the side-chain hydroxyl oxygen of Tyr217 is indicated. Residue side chains are colored according to the atom type: blue, nitrogen; red, oxygen; gray (for cavity-forming residues) or yellow (for Ile255), carbon.

interaction is less attractive as a model for a putative tight interaction. It cannot be energetically very favorable, as it is not observed for monomer A. The cavity A/isoleucine interaction in turn may mimic a similar, biologically relevant interaction (see below). The tripeptide Val254B–Ile255B–Pro256B (from a neighboring dimer in the crystal) packs smoothly to the strictly conserved surface around cavity A (Figure 5A), and the main-chain carbonyl oxygen of Ile255B makes a hydrogen bond to the hydroxyl oxygen of the invariant side chain of Tyr217 (Figure 5B).

Interaction of EB1-C with APC-derived C-terminal peptides

Based on pull-down experiments, the EB1–APC interaction has been mapped to a 40-residue C-terminal segment of APC (Bu and Su, 2003). The characteristic dimeric structure of EB1-C suggests that it may bind two copies of APC simultaneously. To test this hypothesis, a high sensitivity ITC binding study was performed with EB1 fragments and APC-derived C-terminal peptides. Figure 6B (inset of left panel) shows the exothermic ITC profile obtained at 25°C by titrating a 90 μM (monomer concentration) solution of EB1-C with the 39-mer human APC peptide Val2781–Lys2819 (1000 μM; referred to as C-APCp1). Analysis of the data showed that the best fit is obtained with a model that assumes $n = 1$ independent and equal binding sites on the EB1-C monomer for C-APCp1. The fit (Figure 6B, left panel) yielded the equilibrium dissociation constant $K_D = 5.1 \pm 0.2$ μM.

To test whether an intact EB1-like structural motif is required for C-APCp1 binding, a similar ITC experiment was carried out with the stable dimeric CysEB1-Ca fragment under oxidizing conditions. The X-ray structure of EB1-C suggests that in CysEB1-Ca the upper and lower walls of the hydrophobic cavity are compromised, while the aromatic and polar rims are expected to be preserved (Figure 4B). No significant binding was observed by titrating a CysEB1-Ca with C-APCp1 under the same conditions used to assess the interaction between EB1-C and C-APCp1 (not shown). The interaction between the monomeric EB1-Cb fragment with C-APCp1 was probed by CD spectroscopy. The concentration-independent far-UV CD spectrum recorded at 5°C from C-APCp1 was characteristic for peptides with little if any secondary structure. No significant change in secondary structure was observed by incubating equimolar amounts of C-APCp1 with EB1-Cb, indicating that the peptides do not interact (not shown). Together, these findings suggest that an intact and dimeric EB1-like structural motif is important for the EB1–APC binding reaction.

Remarkably, within the C-APCp1 sequence, there is a single isoleucine followed by a proline (Ile2805 and Pro2806; Figure 6A) reminiscent of the tripeptide segment Val254–Ile255–Pro256 bound to the EB1-C cavity A (Figure 5). To test whether the Ile2805–Pro2806 dipeptide is critical for binding, an APC-p1 peptide variant in which these two residues were mutated to serine (referred to as C-APCp1-S) was analyzed by ITC. As shown in Figure 6B (right upper

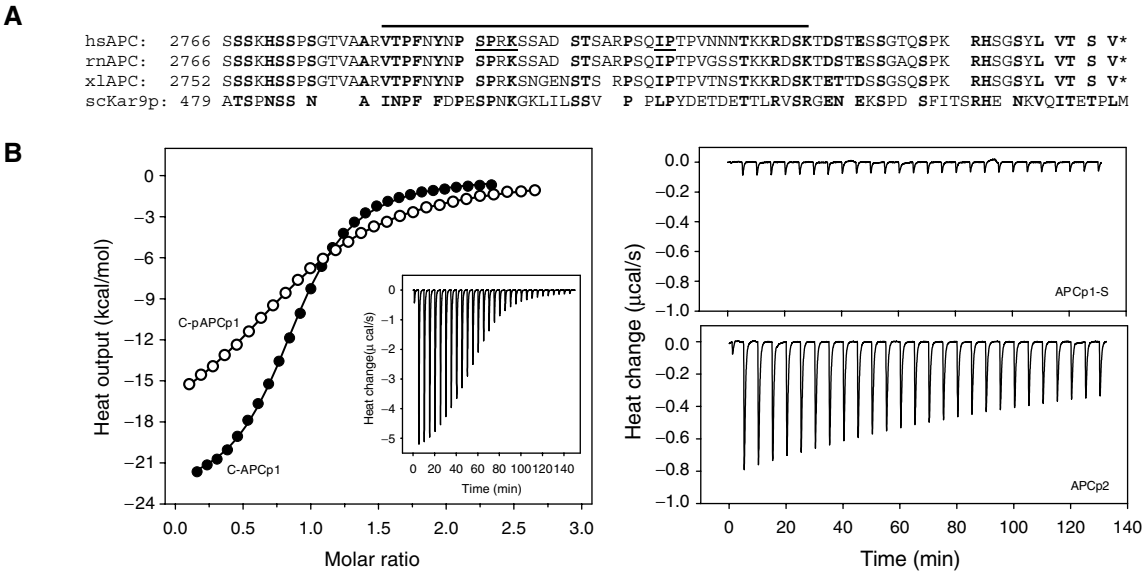

Figure 6 Binding of APC-derived C-terminal peptides to EB1-C. (**A**) Sequence alignment of carboxy-terminal APC segments from different species. Sequence identities and accession numbers are as follows: hs, *Homo sapiens*, SwissProt: P25054; rn, *Rattus norvegicus*, SwissProt: P70478; xl, *Xenopus laevis*, TrEMBL: P70039; sc, *Saccharomyces cerevisiae*, SwissProt: P32526. Conserved residues are depicted in bold. The thick line indicates the C-APCp1 peptide sequence (Val2781–Lys2819). The hsAPC Ile2805–Pro2806 dipeptide segment that was targeted for substitution and the Cdc2 consensus site Ser2789–Lys2792 are underlined. (**B**) ITC binding study. Left panel: Integrated heats of reaction (symbols) with the best fit to the data (lines). The fits were obtained with $n=1$ (referred to the EB1-C monomer) and yielded equilibrium dissociation constants of $K_D=5.1$ ($\Delta H^0_{app}=-21.1$ kcal/mol binding sites) and 17.9 µM ($\Delta H^0_{app}=-19.5$ kcal/mol binding sites) for C-APCp1 (closed symbols) and C-pAPCp1 (phosphorylated at Ser2789; open symbols), respectively. Inset: Raw data obtained for 30 10 µl injections of C-APCp1 (1000 µM) into the sample cell containing 90 µM EB1-C. Right upper panel: Raw data obtained for C-APCp1-S (800 µM) into EB1-C (90 µM). Right lower panel: Raw data obtained for C-APCp2 (970 µM) into EB1-C (90 µM). The measurements were carried out at 25°C in PBS. The concentrations of EB1-C refer to the monomer.

panel), binding of the mutant C-APCp1-S peptide to EB1-C is abolished. In contrast, a truncated 17-residue C-APCp1 variant (Ser2797–Thr2813; referred to as C-APCp2), which contains the isoleucine–proline dipeptide in its center, still specifically interacts with EB1-C although with reduced millimolar affinity (estimated K_D of 300–400 µM; Figure 6B, right lower panel).

These findings demonstrate that the dipeptide segment Ile2805–Pro2806 plays an important role in anchoring C-APCp1 to EB1-C. However, the data obtained on the shorter C-APCp2 peptide suggest that additional C-APCp1 residues besides Ile2805–Pro2806 are necessary to increase the binding affinity. The carboxy terminus of APC is the target of Cdc2 *in vivo* at multiple sites (Trzepacz *et al*, 1997; Askham *et al*, 2000). Notably, the APC sequence segment Ser2789–Lys2792 represents such a Cdc2 consensus site (Figure 6A). To assess whether phosphorylation of Ser2789 affects binding of C-APCp1 to EB1-C, a phosphorylated peptide variant, referred to as C-APCp1-pSer2789, was analyzed by ITC (Figure 6B, left panel). The fit to the data was obtained with $n=1$ independent and equal binding sites on the EB1-C monomer and yielded the equilibrium dissociation constant $K_D=17.9\pm0.2$ µM.

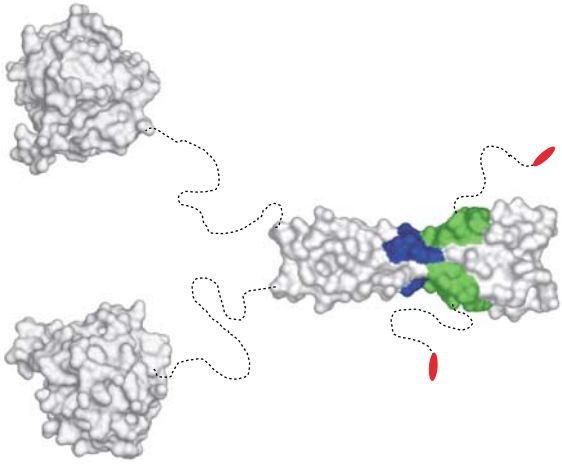

Figure 7 Structural organization of EB1 proteins and mapped +TIP-binding sites. The structures of the globular N-terminal MT-binding (PDB entry 1PA7) and C-terminal EB1 domains are depicted as surface views. Dashed and curved lines schematize flexible peptide segments of the dimeric molecule. The binding sites for APC (hydrophobic cavity and polar rim) and dynactin/p150^{glued} (hydrophobic cavity, polar rim, and C-terminal dipeptide segment) are highlighted by colors: green, hydrophobic groove; blue, polar rim; red, C-terminal dipeptide (see also Figure 4B).

Discussion

Despite the central role of EB1 proteins in many if not all MT-based processes, their detailed molecular organization is still not known. Our biophysical and structural data establish that human EB1 is a very stable dimeric protein with a parallel coiled coil. The crystal structure of EB1-C reveals that the coiled-coil-mediated dimerization is essential for the formation of a highly conserved surface patch comprising a deep hydrophobic cavity and two rims, one polar and the other aromatic. The C-terminal partially conserved 19-residue EB1 tails are intrinsically disordered. The high sequence conser-

vation of the EB1-like motif strongly suggests that all EB1 orthologues assemble into dimeric structures as depicted in Figure 7.

The highly conserved surface patch of EB1-C strongly supports a functional selection, which we propose to be driven by binding to APC. Our binding data suggest that (1) an intact EB1-C dimer interface is essential for the interaction, (2) the central deep hydrophobic cavity formed by the highly conserved side chains of helices α1 and α2′ plays a central role in the binding reaction, and (3) EB1-C can simultaneously bind two APC-derived carboxy-terminal 39-mer peptides with equal 5 μM affinity. Remarkably, mutating the Ile2805 and Pro2806 APC residues to serine completely abolishes binding of C-APCp1 to EB1-C, demonstrating the essential role of this dipeptide segment in the interaction. However, the very high dissociation constant obtained for the 17-mer C-APCp2 peptide demonstrates that additional interactions with the surrounding conserved EB1-C surface are needed to increase binding affinity. Consistent with this conclusion, a mutational study targeting Glu211, Glu213, and Asp215 indicates that EB1-C's polar rim (Figure 4B) may also be critical for the formation of the EB1–APC complex (Wen *et al*, 2004).

The extensive presence of low-complexity sequence stretches in C-APC together with the fact that the EB1-binding site is preserved in a short sequence segment (Val2781–Lys2819; Figure 6A) makes an intrinsically disordered structure for the carboxy termini of APC appear very likely. This suggests that the EB1–APC interaction is established between a folded domain and a flexible polypeptide chain segment reminiscent of the one formed between EB1-C and C-APCp1. The deep hydrophobic cavity seen in the EB1-C crystal structure is thus expected to serve as a binding site into which the APC Ile2805 side chain is anchored like the tripeptide segment bound to cavity A (Figure 5). Consistent with this conclusion, mutating Lys220 and Arg222 to alanine, which is expected to compromise the left and right walls, respectively, of the EB1-C cavity (Figures 4B and 5), abolishes the EB1–APC interaction, inhibits stable MT formation *in vivo*, and reduces cell migration (Wen *et al*, 2004). Notably, the APC Ile2805–Pro2806 sequence motif is strictly conserved in the rat and frog APC orthologues (Figure 6A). In the budding yeast APC-related Kar9p molecule, whose carboxy-terminal domain is also predicted to be intrinsically disordered, the isoleucine is conservatively replaced by a leucine residue (Leu510). The isoleucine side chain fits optimally into the cavity but the one of a leucine appears equally suitable. The role of the invariant proline residue may be to restrict the number of possible conformations the polypeptide backbone can assume upon binding.

The moderate but specific affinity of C-APCp1 for EB1-C is consistent with the observed dynamic and transient nature of EB1–APC *in vivo* (Mimori-Kiyosue and Tsukita, 2001). The ~four-fold decreased binding of the phosphorylated C-pAPCp1 peptide suggests that the site encompassing Ser2789 is implicated in the regulation of the interaction. It appears likely that further downregulation of the APC affinity for EB1 is mediated by phosphorylation of additional serine residues present in the sequence segment Val2781–Lys2819 (Trzepacz *et al*, 1997; Askham *et al*, 2000; Bu and Su, 2003). However, Ser2789 is a conserved Cdc2 phosphorylation site (Trzepacz *et al*, 1997) that may play an important role in modulating the association of APC and EB1 during mitosis (Askham *et al*, 2000). Moreover, phosphorylation of Ser2789 inhibits the EB1–APC-promoted MT polymerization activity *in vitro* (Nakamura *et al*, 2001). In *S. cerevisiae*, Cdc28 (the yeast Cdc2 orthologue) phosphorylation of the corresponding conserved Kar9p Ser496 residue is critical for asymmetric loading of the yeast molecule onto MTs at the spindle pole and for proper MT capture and guidance (Liakopoulos *et al*, 2003). In analogy to EB1–APC, immunoprecipitation experiments suggest that the effect of Cdc28 phosphorylation is to inhibit the ability of Kar9p to interact with the EB1 orthologue Bim1p (Liakopoulos *et al*, 2003). Together, these findings support our conclusion that the APC sequence segment Val2781–Lys2819 represents a major interaction site between APC and EB1 *in vivo*. They further suggest that specific C-APC phosphorylation is a mechanism for regulating the EB1–APC complex during the cell cycle.

The structural organization of EB1-C (Figure 7) also rationalizes functional data obtained on the EB1–dynactin/p150^{glued} interaction. A fragmentation analysis suggests that the last two conserved carboxy-terminal EB1 residues, Glu267 and Tyr268, are essential for the association with the p150^{glued} CAP-Gly domain (Bu and Su, 2003). However, a mutational study indicates that both polar rim and hydrophobic cavity also contribute to complex formation (Wen *et al*, 2004). The fact that the APC–EB1 and EB1–dynactin/p150^{glued} interactions appear to be mediated by partially overlapping parts of EB1-C is consistent with the observation that EB1 may form mutually exclusive complexes with these proteins under certain conditions (Askham *et al*, 2002).

In conclusion, our analysis reveals that a central aspect of both interactions, APC–EB1 and EB1–dynactin/p150^{glued}, is the involvement of a flexible polypeptide chain segment and a folded binding site. Such an interaction mode is well suited to recruit different molecular functionalities to a common location without imposing undesired structural constraints on the resulting assemblies. Moreover, as expected from *in vivo* observations, such regulated (e.g., via phosphorylation events) protein–protein interactions provide a basis for understanding the dynamic crosstalk among +TIP proteins at growing MT ends, the anchoring of MT tips to cellular structures such as centrosomes, and the delivery of proteins to the cell periphery (Carvalho *et al*, 2003; Galjart and Perez, 2003).

Materials and methods

Construction of expression plasmids

The EST clone IMAGE:3922022 was used as a template for PCR amplification of the complete coding sequence of the human EB1 gene. The amplified product was ligated into a modified pET-15b (Novagen) bacterial expression vector at the *Bam*HI site. For the EB1-derived fragments, the cloned full-length EB1 cDNA was used as a template for PCR amplification. The PCR products were ligated into the bacterial expression vectors pPEP-T (Brandenberger *et al*, 1996) for CysEB1-Ca, into pHisTrx (Frank *et al*, 2002) for EB1-Cb, and into a modified pET-15b for EB1-C at the *Bam*HI–*Eco*RI sites, respectively. The inserted sequences of all constructs were verified by Sanger dideoxy DNA sequencing.

Protein and peptide preparations

The *Escherichia coli* host strains BL21(DE3) (Stratagene) and JM109(DE3) (Promega) were used for expression. Bacteria were grown at 37°C in LB medium containing 100 mg/l ampicillin.

Bacterial cultures were induced at $OD_{600} = 0.8$ by adding IPTG to 1 mM and incubating at 37°C for 4 h. Affinity purification of the 6xHis-tagged fusion proteins by immobilized metal affinity chromatography on Ni^{2+}-Sepharose (Amersham) was performed under native conditions at room temperature as described in the manufacturer's instructions.

For separation of the recombinant proteins from the N-terminal carrier polypeptides, proteins were dialyzed against thrombin cleavage buffer (20 mM Tris–HCl, pH 8.4, 150 mM NaCl, 2.5 mM $CaCl_2$). Proteolytic cleavage was carried out for 8–24 h at room temperature using human thrombin (Sigma) at a concentration of 5 U/mg recombinant protein. Unexpectedly, nonspecific cleavage was observed for the full-length EB1 protein. N-terminal amino-acid sequencing and mass spectrometric analyses of processed protein fragment bands revealed that cleavage occurred within the EB1 sequence Pro145–Pro161. The processed poypeptides were separated from the oligohistidine containing polypeptide tags by reapplication to immobilized metal affinity columns.

The homogeneity of the recombinant proteins was confirmed by either 15% SDS–PAGE or tricine–SDS–PAGE (Schagger and von Jagow, 1987) and their identities were assessed by mass spectral analyses. The identity of the EB1-Cb fragment was further confirmed by N-terminal sequencing. Protein samples were dialyzed against PBS (5 mM sodium phosphate buffer, pH 7.4, 150 mM NaCl).

The N-acetylated and C-amidated APC-derived peptides were assembled on an automated continuous-flow synthesizer employing standard methods. The purity of the peptides (~95%) was verified by reversed-phase analytical HPLC and their identities were assessed by mass spectral analysis.

Exact concentrations of protein and peptide solutions were determined by tyrosine absorbance at 276 nm in 6 M GuHCl (Edelhoch, 1967).

Biophysical characterization

For CD spectroscopy, protein samples were in PBS. Reducing buffer conditions were obtained by supplementing samples with 1 mM DTT. Far-UV CD spectra and thermal unfolding profiles were recorded on a J-810 spectropolarimeter (Jasco Inc.) equipped with a temperature-controlled quartz cell of 0.1 cm path length. The spectra shown are the averages of five accumulations. The data were evaluated with the Jasco and Sigma Plot (Jandel Scientific) software. A ramping rate of 1°C/min was used to record the thermal unfolding profiles. The apparent midpoints of the transitions, T_m's, were taken as the maximum of the derivative $d[\Theta]_{222}/dT$.

AUC was performed on an Optima XL-A analytical ultracentrifuge (Beckman Instruments) equipped with an An-60ti rotor. The recombinant EB1 molecules were analyzed in PBS and protein concentrations were adjusted to 0.1–0.5 mg/ml in PBS supplemented with 1 mM DTT. Sedimentation velocity experiments were performed at 54 000 r.p.m. in a 12 mm epon double-sector cell. Sedimentation coefficients were corrected to water by the standard procedure (Eason, 1986). Sedimentation equilibrium runs were performed at 15 000 and 21 000 r.p.m. for EB1 and at 36 000 r.p.m. for CysEB1-Ca. For all samples, a partial specific volume of 0.73 ml/g was assumed.

Electron micrographs were taken in a Philips Morgagni TEM operated at 80 kV equipped with a Megaview III CCD camera. Protein samples (0.5 mg/ml) in PBS were supplemented with glycerol to a final concentration of 30%. The samples were subsequently sprayed onto freshly cleaved mica and rotary shadowed in a BA 511 M freeze-etch apparatus (Balzers) with platinum/carbon at an elevation angle of 3–5° (Fowler and Aebi, 1983). It should be noted that the TEM and AUC experiments on full-length EB1 were carried out with the uncleaved 6xHis-tagged protein.

High-sensitivity ITC experiments to assess the interaction between EB1-C and APC-derived peptides were performed at 25°C in PBS using a VP-ITC calorimeter (Microcal Inc., Northampton, MA). For each experiment, the sample cell (volume 1.4 ml) was filled with an ~100 μM EB1-C solution. A 300 μl syringe was filled with an ~1 mM APC peptide solution (present in the same buffer as EB1-C). The reference cell contained water. Typically, 10 μl of APC peptide aliquots from the stirred syringe (305 r.p.m.) were injected 30 times into the sample cell. At each injection, APC peptide was bound to EB1-C, leading to a characteristic heat signal. Integration of the individual calorimeter traces yielded the heat of binding, h_i, of each injection step. The binding isotherms were fitted via a nonlinear least squares minimization method to determine the binding stoichiometry, n, the equilibrium binding constant, K_D, and the apparent change in enthalpy, ΔH^0.

Crystal structure determination

EB1-C crystals grew within 1 week from a 15–20 mg/ml stock solution at 20°C using the sitting drop method. The crystals exhibited space group P21 (no. 4) and were grown using a reservoir solution containing 50 mM sodium citrate at pH 4.0–4.5, 10% PEG 3350, and 4% γ-butyrolactone (Sigma). Data sets were collected using CuKα radiation produced by an Enraf-Nonius FR591 rotating anode generator. A total of 360 rotation images of 0.5° were recorded on a MAR345 imaging plate. The structure of EB1-C was solved by SIRAS using a mercury derivative obtained by overnight soaks of crystals in the presence of 1 mM thiomersal. Iterative rounds of model building and maximum likelihood refinement resulted in a complete 1.54 Å resolution model for the EB1-C dimer. The final model converged at an R/R_{free} of 0.18/0.22 with very good stereochemistry. Data sets and refinement statistics are given in Supplementary Table 1. Figures were prepared with the program PyMOL (De-Lano Scientific LLC, San Carlos, CA, www.pymol.org). The structure of EB1-C has been deposited in the Protein Data Bank (PDB entry 1WU9).

Supplementary data

Supplementary data are available at *The EMBO Journal* Online.

Acknowledgements

We are indebted to Drs Y Barral, D Fitzgerald, RA Kammerer, and D Liakopoulos for insightful discussions, to Dr I Jelesarov for assistance with the ITC experiments, and to A Lustig for performing the AUC analysis. We are grateful to the Interdisciplinary Center for Microscopy of the University of Basel and to the Institute for Molecular Biology and Biophysics of ETH Zürich for access to the TEM and CD spectropolarimeter, respectively. This work was supported by the Swiss National Science Foundation grant #31-64978.01 (to MOS) and by the Eidgenössische Technische Hochschule Zürich grant #TH-42/02-2 (to FKW and MOS).

References

Askham JM, Moncur P, Markham AF, Morrison EE (2000) Regulation and function of the interaction between the APC tumour suppressor protein and EB1. *Oncogene* **19:** 1950–1958

Askham JM, Vaughan KT, Goodson HV, Morrison EE (2002) Evidence that an interaction between EB1 and p150(Glued) is required for the formation and maintenance of a radial microtubule array anchored at the centrosome. *Mol Biol Cell* **13:** 3627–3645

Berrueta L, Kraeft SK, Tirnauer JS, Schuyler SC, Chen LB, Hill DE, Pellman D, Bierer BE (1998) The adenomatous polyposis coli-binding protein EB1 is associated with cytoplasmic and spindle microtubules. *Proc Natl Acad Sci USA* **95:** 10596–10601

Berrueta L, Tirnauer JS, Schuyler SC, Pellman D, Bierer BE (1999) The APC-associated protein EB1 associates with components of the dynactin complex and cytoplasmic dynein intermediate chain. *Curr Biol* **9:** 425–428

Bienz M (2001) Spindles cotton on to junctions, APC and EB1. *Nat Cell Biol* **3:** E67–E68

Brandenberger R, Kammerer RA, Engel J, Chiquet M (1996) Native chick laminin-4 containing the beta 2 chain (s-laminin) promotes motor axon growth. *J Cell Biol* **135:** 1583–1592

Bu W, Su LK (2003) Characterization of functional domains of human EB1 family proteins. *J Biol Chem* **278:** 49721–49731

Busch KE, Hayles J, Nurse P, Brunner D (2004) Tea2p kinesin is involved in spatial microtubule organization by transporting tip1p on microtubules. *Dev Cell* **6:** 831–843

Carvalho P, Tirnauer JS, Pellman D (2003) Surfing on microtubule ends. *Trends Cell Biol* **13:** 229–237

Cohen C, Parry DA (1990) Alpha-helical coiled coils and bundles: how to design an alpha-helical protein. *Proteins* **7:** 1–15

Dikovskaya D, Zumbrunn J, Penman GA, Nathke IS (2001) The adenomatous polyposis coli protein: in the limelight out at the edge. *Trends Cell Biol* **11:** 378–384

Eason R (1986) Centrifugation, a practical approach. In *Analytical Ultracentrifugation*, Rickwood D (ed) pp 251–286. IRL Press: Oxford (UK) and Washington, DC

Edelhoch H (1967) Spectroscopic determination of tryptophan and tyrosine in proteins. *Biochemistry* **6:** 1948–1954

Fodde R, Kuipers J, Rosenberg C, Smits R, Kielman M, Gaspar C, van Es JH, Breukel C, Wiegant J, Giles RH, Clevers H (2001) Mutations in the APC tumour suppressor gene cause chromosomal instability. *Nat Cell Biol* **3:** 433–438

Fowler WE, Aebi U (1983) Preparations of single molecules and supramolecular complexes for high-resolution metal shadowing. *J Ultrastruct Res* **83:** 319–334

Frank S, Schulthess T, Landwehr R, Lustig A, Mini T, Jeno P, Engel J, Kammerer RA (2002) Characterization of the matrilin coiled-coil domains reveals seven novel isoforms. *J Biol Chem* **277:** 19071–19079

Galjart N, Perez F (2003) A plus-end raft to control microtubule dynamics and function. *Curr Opin Cell Biol* **15:** 48–53

Goodson HV, Skube SB, Stalder R, Valetti C, Kreis TE, Morrison EE, Schroer TA (2003) CLIP-170 interacts with dynactin complex and the APC-binding protein EB1 by different mechanisms. *Cell Motil Cytoskeleton* **55:** 156–173

Gundersen GG (2002) Evolutionary conservation of microtubule-capture mechanisms. *Nat Rev Mol Cell Biol* **3:** 296–304

Harbury PB, Zhang T, Kim PS, Alber T (1993) A switch between two-, three-, and four-stranded coiled coils in GCN4 leucine zipper mutants. *Science* **262:** 1401–1407

Hayashi I, Ikura M (2003) Crystal structure of the amino-terminal microtubule-binding domain of end-binding protein 1 (EB1). *J Biol Chem* **278:** 36430–36434

Juwana JP, Henderikx P, Mischo A, Wadle A, Fadle N, Gerlach K, Arends JW, Hoogenboom H, Pfreundschuh M, Renner C (1999) EB/RP gene family encodes tubulin binding proteins. *Int J Cancer* **81:** 275–284

Kusch J, Liakopoulos D, Barral Y (2003) Spindle asymmetry: a compass for the cell. *Trends Cell Biol* **13:** 562–569

Liakopoulos D, Kusch J, Grava S, Vogel J, Barral Y (2003) Asymmetric loading of Kar9 onto spindle poles and microtubules ensures proper spindle alignment. *Cell* **112:** 561–574

Ligon LA, Shelly SS, Tokito M, Holzbaur EL (2003) The microtubule plus-end proteins EB1 and dynactin have differential effects on microtubule polymerization. *Mol Biol Cell* **14:** 1405–1417

Louie RK, Bahmanyar S, Siemers KA, Votin V, Chang P, Stearns T, Nelson WJ, Barth AI (2004) Adenomatous polyposis coli and EB1 localize in close proximity of the mother centriole and EB1 is a functional component of centrosomes. *J Cell Sci* **117:** 1117–1128

Mimori-Kiyosue Y, Shiina N, Tsukita S (2000) The dynamic behavior of the APC-binding protein EB1 on the distal ends of microtubules. *Curr Biol* **10:** 865–868

Mimori-Kiyosue Y, Tsukita S (2001) Where is APC going? *J Cell Biol* **154:** 1105–1109

Nakamura M, Zhou XZ, Lu KP (2001) Critical role for the EB1 and APC interaction in the regulation of microtubule polymerization. *Curr Biol* **11:** 1062–1067

Rehberg M, Gräf R (2002) *Dictyostelium* EB1 is a genuine centrosomal component required for proper spindle formation. *Mol Biol Cell* **13:** 2301–2310

Rogers SL, Rogers GC, Sharp DJ, Vale RD (2002) *Drosophila* EB1 is important for proper assembly, dynamics, and positioning of the mitotic spindle. *J Cell Biol* **158:** 873–884

Rogers SL, Wiedemann U, Hacker U, Turck C, Vale RD (2004) *Drosophila* RhoGEF2 associates with microtubule plus ends in an EB1-dependent manner. *Curr Biol* **14:** 1827–1833

Schagger H, von Jagow G (1987) Tricine–sodium dodecyl sulfate–polyacrylamide gel electrophoresis for the separation of proteins in the range from 1 to 100 kDa. *Anal Biochem* **166:** 368–379

Schroer TA (2001) Microtubules don and doff their caps: dynamic attachments at plus and minus ends. *Curr Opin Cell Biol* **13:** 92–96

Su LK, Burrell M, Hill DE, Gyuris J, Brent R, Wiltshire R, Trent J, Vogelstein B, Kinzler KW (1995) APC binds to the novel protein EB1. *Cancer Res* **55:** 2972–2977

Tirnauer JS, Bierer BE (2000) EB1 proteins regulate microtubule dynamics, cell polarity, and chromosome stability. *J Cell Biol* **149:** 761–766

Trzepacz C, Lowy AM, Kordich JJ, Groden J (1997) Phosphorylation of the tumor suppressor adenomatous polyposis coli (APC) by the cyclin-dependent kinase p34. *J Biol Chem* **272:** 21681–21684

Wen Y, Eng CH, Schmoranzer J, Cabrera-Poch N, Morris EJ, Chen M, Wallar BJ, Alberts AS, Gundersen GG (2004) EB1 and APC bind to mDia to stabilize microtubules downstream of Rho and promote cell migration. *Nat Cell Biol* **6:** 820–830

Table I. Crystallographic data and refinement statistics

	Native data set	Thiomersal derivative data set[g]
Space group	$P2_1$ (No. 4)	$P2_1$ (No. 4)
Cell axes *a*, *b*, *c and* β	31.9Å, 37.3Å, 56.4Å and 105.4°	31.8Å, 37.4Å, 56.5Å and 105.2°
Resolution range (outer shell)	50.0 (1.60-1.54 Å)	25.0 (1.7-1.66 Å)
No. of observed reflections	53616	90244
No. of unique reflections	18705	28522
R_{sym} overall(outer shell) [a]	4.0 %(18.8%)	4.1% (14.7%)
$I/\sigma(I)$ overall(outer shell)	14.8 (5.4)	16.2 (7.5)
Completeness overall(outer shell)	97.4% (90.1%)	95.9%(93.1%)
Phasing power (centric/acentric)[b]	0.90/1.14	
R_{Cullis} (centric/acentric)[c]	0.82/0.77	
Figure-of-merit (centric/acentric)[d]	0.16/0.27	
No. of refined atoms		
protein	1030	
water	119	
R-factor/free *R*-factor[e]	0.18/0.22	
R.m.s.d. bond lengths/bond angles[f]	0.011Å/1.2°	

[a] $R_{sym} = \sum_h \sum_i | I_i(h) - \langle I(h) \rangle | / \sum_h \sum_i I_i(h)$, where $I_i(h)$ and $\langle I(h) \rangle$ are the *i*th and mean measurement of the intensity of reflection *h*.

[b] Phasing power $= \sum F_H^{calc} / \sum | F_{PH}^{obs} - F_{PH}^{calc} |$, where F_H^{calc} is the calculated heavy atom amplitude and F_{PH}^{obs} and F_{PH}^{calc} are the observed and calculated heavy atom derivative structure factor amplitudes, respectively

[c] $R_{Cullis} = \sum | F_{PH}^{obs} \pm F_P^{obs} | - | F_H^{calc} | / \sum | F_{PH}^{obs} - F_P^{obs} |$, where F_{PH}^{obs} is the observed heavy atom derivative structure factor amplitude, F_P^{obs} is the observed native structure factor amplitude, and F_H^{calc} is the calculated heavy atom amplitude

[d] Figure-of-merit $= | \int_\alpha P(\alpha) \exp(i\alpha) d_\alpha / \int_\alpha P(\alpha) d_\alpha |$, with α ranging from 0 to 2π.

[e] $R = \sum | F_P^{obs} - F_P^{calc} | / \sum F_P^{obs}$, where F_P^{obs} and F_P^{calc} are the the observed and calculated structure factor amplitudes, respectively

[f] rmsd, root-mean-square-deviation from the parameter set for ideal stereochemistry (Engh and Huber, 1991)

[g] mercury-binding sites were at cysteine 228

Figure 1

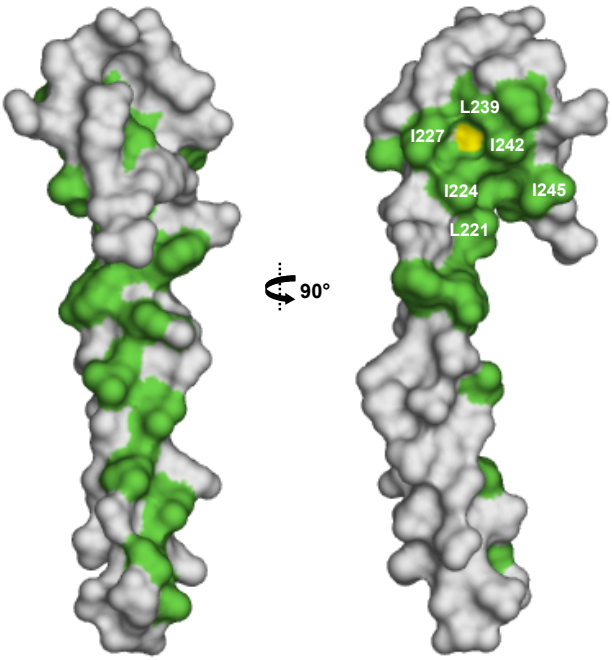

Fig. 1. Monomer A of EB1-C in surface representation. Conserved hydrophobic residue side chains engaged at the dimer interface are highlighted in green. Cys228 is shown in yellow.

SUPPLEMENTARY REFERENCE

Engh RA & Huber R (1991) Accurate bond and angle parameters for X-ray protein structure refinement. *Acta Cryst* **A47:** 392-400

IV. Conclusions and Perspectives

Previous studies establish that stathmin and EB1 are key regulators of microtubule dynamics. Both proteins play an important role in the progression of some forms of cancer in humans. In this thesis, I have investigated detailed structure and function relationship to characterize the tubulin-stathmin and EB1-APC interactions.

Structure-Function Relationship of Tubulin- Stathmin Interaction

The thesis provides the first detailed thermodynamic analysis of the tubulin-stathmin interaction. In general it aims to provide molecular insights into the function of intrinsically disordered proteins and the structural elements regulating the interaction with their ligands/binding partner.

We report that stathmin binds two tubulin subunits with equal affinities under all conditions investigated, in contrast to earlier studies suggesting that the second tubulin subunit is bound distinctly tighter than the first (Larsson *et al.*, 1999;Holmfeldt *et al.*, 2001;Amayed *et al.*, 2002;Segerman *et al.*, 2003). Earlier binding assays required tagging, immobilization, and separation of the different species. I used highly sensitive isothermal titration calorimetry (ITC), in which the binding reaction occurs between two native protein forms free in solution. Our analyses provide evidence for a binary tubulin-stathmin (TS) complex.

These observations suggest possibilities for engineering a stable TS complex. The recently published 3.5 Å resolution X-ray structure of the ternary tubulin-stathmin/RB3 complex (Ravelli *et al.*, 2004) revealed the side-chain conformations of most stathmin/RB3 residues with reasonable reliability. This knowledge offers the prospect of rationally engineering variants of the complex with improved stability and crystallization properties, which can yield better diffracting crystals. The precise binding modes of tubulin-targeting drugs is presently difficult to establish because of the moderate resolution (~3.57 Å) of the currently known structures. A precise knowledge of these interaction modes, is a prerequisite for modelling studies aiming at engineering new antimitotic compounds with improved specificity and activity profiles.

A TS complex may have better crystallization properties than T_2S because the latter complex displays some flexibility at the interface between the two α/β-heterodimers (Ravelli *et al.*, 2004). This flexibility could hinder the growth of well-diffracting crystals. The specific covalent linkage of stathmin to α-tubulin, as well as the introduction of cysteine cross-links and helix/β-hairpin stabilizing interactions, should improve the affinity of stathmin fragment variants for tubulin.

Our thermodynamic data suggest that the hydrophobic effect constitutes the major driving force governing the tubulin-stathmin binding reaction. Based on modelling and sequence alignments of stathmin-protein family members, the predominantly hydrophobic seam of the stathmin helix that faces the two tubulin heterodimers in T_2S can be systematically modified. Bulky hydrophobic amino acids (Val, Ile, Leu, Phe, Trp) could be substituted for existing small or polar residues at promising sites. Thus increasing the stability of tubulin-stathmin complex could yield better-diffracting crystals.

The results described in this thesis provide the structural basis for understanding the down-regulating effects of phosphorylating the four serine residues (Ser16, Ser25, Ser38, and Ser63) of stathmin that are relevant for controlling MT-dynamics during the cell cycle. The protocol for preparing high quality phosphorylated stathmin isoforms in milligram quantities, which I standardized, facilitates their use in other *in vitro* assays designed to understand quantitatively the microtubule dynamics. The results presented in this thesis concerning the binding affinities of several phospho-stathmin isoforms could contribute to constructing a cellular model of microtubule dynamics using computer simulations.

A recent study has shown that stathmin interacts with $p27^{Kip1}$, a protein necessary for regulation of cell migration and cancer progression (Baldassarre *et al.*, 2005). Using an *in vitro* tubulin polymerization assay, Baldassarre *et al.* also showed that $p27^{Kip1}$ interferes with the ability of stathmin to sequester tubulin, leading to increased microtubule polymerization. Certainly, the experimental methods described in this thesis could contribute to very interesting issue of understanding the structural basis for interaction of stathmin and $p27^{Kip1}$.

In conclusion, our results provide new insights into the regulation of microtubule dynamics by stathmin and the role of multisite phosphorylation. Simultaneously, they provide a molecular basis for understanding the consequences of phosphorylating an intrinsically disordered protein. The insights are expected to contribute to the design of therapeutic strategies directed against cancer and other human disorders.

EB1-mediated Interaction Networks

The dynamic crosstalk among +TIP proteins and the observation that EB1 is always localized at growing MT ends suggest that EB1 is involved in the establishment of macromolecular 'plus-end complexes' at MT tips (Schroer, 2001;Galjart and Perez, 2003).

The crystal structure of the EB1-C domain reveals a unique homodimeric structure formed by a coiled coil that folds back at the C-terminal region to form a four-helix bundle. EB1-C is a very stable domain and has a unique fold; the four-helix bundle increases the stability of the coiled coil. Although sequence analysis suggested that EB1 and Bim1p has a coiled-coil domain (Rehberg and Gräf, 2002), the crystal structure is the first direct evidence that EB1 proteins are indeed dimers. Investigating the thermodynamics of the protein folding behaviour of this domain and its binding partners should help unravel the energetics of EB1 mediated interactions.

Although the crystal structure reported in this thesis describes a homodimeric structure, we cannot rule out the possibility that EB1 heterodimers (EB1 can form heterodimers with other EB1 isoforms like RP1, EB2) exist and mediate diverse cargo recognition. The length of the coiled-coil domains, and the residues in the C-terminal domain constituting the hydrophobic core and mediating dimer contacts, are highly conserved across family members. Because each bivalent cargo-binding site is formed from residues contributed by each of the EB1 molecules, heterodimers could confer complex, pair-wise cargo recognition motifs. Thus, the possibility that heterodimers of EB1 can form *in vitro* and within cells merits investigation.

Previous studies suggest that specific C-APC phosphorylation is a mechanism for regulating the EB1-APC complex during cell cycle (Trzepacz *et al.*, 1997;Askham *et al.*, 2000;Bu and Su, 2003). Phosphorylation of the conserved Cdc2 site Ser2789−Lys2792 in C-APC reduces binding four-fold, indicating that the interaction APC−EB1 is post-translationally regulated in

cells. As described in the present thesis, ITC experiments with specific C-APC phosphoisoforms could probe the effects of multi-site phosphorylation of APC.

The conservation of the EB1-C terminal domain extends from vertebrates down to the yeast homologs Bim1 and Mal3. Kar9 is functionally homologous to APC regarding its involvement in microtubule search and capture; however, Kar9 does not have a repeat motif architecture similar to APC/spectraplakins (Miller and Rose, 1998). An unconfirmed study reported a hydrophobic segment of weak homology between regions of Kar9 and the EB1 binding motif (Bienz, 2001). Comparing the molecular basis of the interactions between EB1 and APC and between Bim1 and Kar9 is desirable in order to determine if the sets of factors governing these binding interactions are unique or similar.

Studies from several laboratories have shown that the proteins: $p150^{glued}$, CLASPs, APC and ACF7 are involved in stabilizing a subset of microtubules at specific cellular sites in response to signalling cues. These proteins use EB1-related proteins or CLIPs to target microtubule ends. These observations open up a broad area of structural investigation of the mechanisms permitting a single domain of EB1-C to recognize and bind many different proteins.

The presented study of EB1-APC provides insights into other EB1-mediated protein-protein interactions. Many of these interactions very likely involve a disordered polypeptide and a folded binding site. Detailed understanding of such interactions at the molecular level is of great interest, because they are frequently involved in critical regulatory functions in the cell, in development of cancer and in protein deposition diseases. EB1, very likely constitutes a core element in the spatial organization of +TIP assembly, indicating that further efforts are necessary to determine complexes of EB1 structures and their binding partners. Following this line, I have already solved the crystal structure of the CAP-Gly domain of $p150^{glued}$ alone and also the complex structure of EB1-C with the $p150^{glued}$ CAP-Gly domain at 1.8 Å resolutions. Thus this thesis has also provided a great stimulation for further detailed structural studies of the protein-protein interactions regulating microtubule dynamics. Understanding such complex regulatory networks of protein-protein interactions in a more quantitative fashion will greatly profit from detailed thermodynamic and structural studies of the underlying molecular interactions as presented in this thesis.

V. References

1. Adames NR and Cooper JA (2000) Microtubule interactions with the cell cortex causing nuclear movements in Saccharomyces cerevisiae. *J Cell Biol,* **149,** 863-874.

2. Amayed P, Pantaloni D, and Carlier MF (2002) The effect of stathmin phosphorylation on microtubule assembly depends on tubulin critical concentration. *J Biol Chem,* **277,** 22718-22724.

3. Andersen SS, Ashford AJ, Tournebize R, Gavet O, Sobel A, Hyman AA, and Karsenti E (1997) Mitotic chromatin regulates phosphorylation of Stathmin/Op18. *Nature,* **389,** 640-643.

4. Antonsson B, Kassel DB, Di PG, Lutjens R, Riederer BM, and Grenningloh G (1998) Identification of in vitro phosphorylation sites in the growth cone protein SCG10. Effect Of phosphorylation site mutants on microtubule-destabilizing activity. *J Biol Chem,* **273,** 8439-8446.

5. Askham JM, Moncur P, Markham AF, and Morrison EE (2000) Regulation and function of the interaction between the APC tumour suppressor protein and EB1. *Oncogene,* **19,** 1950-1958.

6. Askham JM, Vaughan KT, Goodson HV, and Morrison EE (2002) Evidence that an interaction between EB1 and p150(Glued) is required for the formation and maintenance of a radial microtubule array anchored at the centrosome. *Mol Biol Cell,* **13,** 3627-3645.

7. Baldassarre G, Belletti B, Nicoloso MS, Schiappacassi M, Vecchione A, Spessotto P, Morrione A, Canzonieri V, and Colombatti A (2005) p27(Kip1)-stathmin interaction influences sarcoma cell migration and invasion. *Cancer Cell,* **7,** 51-63.

8. Belmont LD and Mitchison TJ (1996) Identification of a protein that interacts with tubulin dimers and increases the catastrophe rate of microtubules. *Cell,* **84,** 623-631.

9. Beretta L, Dobransky T, and Sobel A (1993) Multiple phosphorylation of stathmin. Identification of four sites phosphorylated in intact cells and in vitro by cyclic AMP-dependent protein kinase and p34cdc2. *J Biol Chem,* **268,** 20076-20084.

10. Berrueta L, Kraeft SK, Tirnauer JS, Schuyler SC, Chen LB, Hill DE, Pellman D, and Bierer BE (1998) The adenomatous polyposis coli-binding protein EB1 is associated with cytoplasmic and spindle microtubules. *Proc Natl Acad Sci U S A,* **95,** 10596-10601.

11. Berrueta L, Tirnauer JS, Schuyler SC, Pellman D, and Bierer BE (1999) The APC-associated protein EB1 associates with components of the dynactin complex and cytoplasmic dynein intermediate chain. *Curr Biol,* **9,** 425-428.

12. Brattsand G, Roos G, Marklund U, Ueda H, Landberg G, Nanberg E, Sideras P, and Gullberg M (1993) Quantitative analysis of the expression and regulation of an activation-regulated phosphoprotein (oncoprotein 18) in normal and neoplastic cells. *Leukemia,* **7,** 569-579.

13. Brinkley W (1997) Microtubules: a brief historical perspective. *J Struct Biol,* **118,** 84-86.

14. Bu W and Su LK (2003) Characterization of functional domains of human EB1 family proteins. *J Biol Chem,* **278,** 49721-49731.

15. Budde PP, Kumagai A, Dunphy WG, and Heald R (2001) Regulation of Op18 during spindle assembly in Xenopus egg extracts. *J Cell Biol,* **153,** 149-158.

16. Busch KE and Brunner D (2004) The microtubule plus end-tracking proteins mal3p and tip1p cooperate for cell-end targeting of interphase microtubules. *Curr Biol,* **14,** 548-559.

17. Byers B and Goetsch L (1976) A highly ordered ring of membrane-associated filaments in budding yeast. *J Cell Biol,* **69,** 717-721.

18. Carvalho P, Tirnauer JS, and Pellman D (2003) Surfing on microtubule ends. *Trends Cell Biol,* **13,** 229-237.

19. Cassimeris L, Gard D, Tran PT, and Erickson HP (2001) XMAP215 is a long thin molecule that does not increase microtubule stiffness. *J Cell Sci,* **114,** 3025-3033.

20. Charbaut E, Curmi PA, Ozon S, Lachkar S, Redeker V, and Sobel A (2001) Stathmin family proteins display specific molecular and tubulin binding properties. *J Biol Chem,* **276,** 16146-16154.

21. Chen W, Ji J, Xu X, He S, and Ru B (2003) Proteomic comparison between human young and old brains by two-dimensional gel electrophoresis and identification of proteins. *Int J Dev Neurosci,* **21,** 209-216.

22. Chen XP, Yin H, and Huffaker TC (1998) The yeast spindle pole body component Spc72p interacts with Stu2p and is required for proper microtubule assembly. *J Cell Biol,* **141,** 1169-1179.

23. Chretien D, Fuller SD, and Karsenti E (1995) Structure of growing microtubule ends: two-dimensional sheets close into tubes at variable rates. *J Cell Biol,* **129,** 1311-1328.

24. Curmi PA, Gavet O, Charbaut E, Ozon S, Lachkar-Colmerauer S, Manceau V, Siavoshian S, Maucuer A, and Sobel A (1999) Stathmin and its phosphoprotein family: general properties, biochemical and functional interaction with tubulin. *Cell Struct Funct,* **24,** 345-357.

25. Curmi PA, Nogues C, Lachkar S, Carelle N, Gonthier MP, Sobel A, Lidereau R, and Bieche I (2000) Overexpression of stathmin in breast carcinomas points out to highly proliferative tumours. *Br J Cancer,* **82,** 142-150.

26. Dammermann A, Desai A, and Oegema K (2003) The minus end in sight. *Curr Biol,* **13,** R614-R624.

27. Daub H, Gevaert K, Vandekerckhove J, Sobel A, and Hall A (2001) Rac/Cdc42 and p65PAK regulate the microtubule-destabilizing protein stathmin through phosphorylation at serine 16. *J Biol Chem,* **276,** 1677-1680.

28. Desai A and Mitchison TJ (1997) Microtubule polymerization dynamics. *Annu Rev Cell Dev Biol,* **13,** 83-117.

29. Desai A, Verma S, Mitchison TJ, and Walczak CE (1999) Kin I kinesins are microtubule-destabilizing enzymes. *Cell,* **96,** 69-78.

30. Di PG, Antonsson B, Kassel D, Riederer BM, and Grenningloh G (1997) Phosphorylation regulates the microtubule-destabilizing activity of stathmin and its interaction with tubulin. *FEBS Lett,* **416,** 149-152.

31. Diamantopoulos GS, Perez F, Goodson HV, Batelier G, Melki R, Kreis TE, and Rickard JE (1999) Dynamic localization of CLIP-170 to microtubule plus ends is coupled to microtubule assembly. *J Cell Biol,* **144,** 99-112.

32. Downing KH and Nogales E (1998) Tubulin structure: insights into microtubule properties and functions. *Curr Opin Struct Biol,* **8,** 785-791.

33. Endow SA, Kang SJ, Satterwhite LL, Rose MD, Skeen VP, and Salmon ED (1994) Yeast Kar3 is a minus-end microtubule motor protein that destabilizes microtubules preferentially at the minus ends. *EMBO J,* **13,** 2708-2713.

34. Erickson HP and O'Brien ET (1992) Microtubule dynamic instability and GTP hydrolysis. *Annu Rev Biophys Biomol Struct,* **21,** 145-166.

35. Etienne-Manneville S and Hall A (2003) Cdc42 regulates GSK-3beta and adenomatous polyposis coli to control cell polarity. *Nature,* **421,** 753-756.

36. Field CM and Kellogg D (1999) Septins: cytoskeletal polymers or signalling GTPases? *Trends Cell Biol,* **9,** 387-394.

37. Fodde R, Kuipers J, Rosenberg C, Smits R, Kielman M, Gaspar C, van Es JH, Breukel C, Wiegant J, Giles RH, and Clevers H (2001) Mutations in the APC tumour suppressor gene cause chromosomal instability. *Nat Cell Biol,* **3,** 433-438.

38. Friedrich B, Gronberg H, Landstrom M, Gullberg M, and Bergh A (1995) Differentiation-stage specific expression of oncoprotein 18 in human and rat prostatic adenocarcinoma. *Prostate,* **27,** 102-109.

39. Fukunaga K and Miyamoto E (1998) Role of MAP kinase in neurons. *Mol Neurobiol,* **16,** 79-95.

40. Galjart N and Perez F (2003) A plus-end raft to control microtubule dynamics and function. *Curr Opin Cell Biol,* **15,** 48-53.

41. Gigant B, Curmi PA, Martin-Barbey C, Charbaut E, Lachkar S, Lebeau L, Siavoshian S, Sobel A, and Knossow M (2000) The 4 A X-ray structure of a tubulin:stathmin-like domain complex. *Cell,* **102,** 809-816.

42. Green RA and Kaplan KB (2003) Chromosome instability in colorectal tumor cells is associated with defects in microtubule plus-end attachments caused by a dominant mutation in APC. *J Cell Biol,* **163,** 949-961.

43. Green RA, Wollman R, and Kaplan KB (2005) APC and EB1 Function Together in Mitosis to Regulate Spindle Dynamics and Chromosome Alignment. *Mol Biol Cell*.

44. Grenningloh G, Soehrman S, Bondallaz P, Ruchti E, and Cadas H (2004) Role of the microtubule destabilizing proteins SCG10 and stathmin in neuronal growth. *J Neurobiol,* **58,** 60-69.

45. Hayashi I and Ikura M (2003) Crystal structure of the amino-terminal microtubule-binding domain of end-binding protein 1 (EB1). *J Biol Chem,* **278,** 36430-36434.

46. Hayashi I, Wilde A, Mal TK, and Ikura M (2005) Structural Basis for the Activation of Microtubule Assembly by the EB1 and p150(Glued) Complex. *Mol Cell,* **19,** 449-460.

47. Heidemann SR and McIntosh JR (1980) Visualization of the structural polarity of microtubules. *Nature,* **286,** 517-519.

48. Helfand BT, Chang L, and Goldman RD (2004) Intermediate filaments are dynamic and motile elements of cellular architecture. *J Cell Sci,* **117,** 133-141.

49. Herrmann H, Hesse M, Reichenzeller M, Aebi U, and Magin TM (2003) Functional complexity of intermediate filament cytoskeletons: from structure to assembly to gene ablation. *Int Rev Cytol,* **223,** 83-175.

50. Hestermann A and Graf R (2004) The XMAP215-family protein DdCP224 is required for cortical interactions of microtubules. *BMC Cell Biol,* **5,** 24.

51. Holmfeldt P, Larsson N, Segerman B, Howell B, Morabito J, Cassimeris L, and Gullberg M (2001) The catastrophe-promoting activity of ectopic Op18/stathmin is required for disruption of mitotic spindles but not interphase microtubules. *Mol Biol Cell,* **12,** 73-83.

52. Hoogenraad CC, Koekkoek B, Akhmanova A, Krugers H, Dortland B, Miedema M, van AA, Kistler WM, Jaegle M, Koutsourakis M, Van CN, Verhoye M, van der LA, Kaverina I, Grosveld F, De Zeeuw CI, and Galjart N (2002) Targeted mutation of Cyln2 in the Williams syndrome critical region links CLIP-115 haploinsufficiency to neurodevelopmental abnormalities in mice. *Nat Genet,* **32,** 116-127.

53. Horwitz SB, Shen HJ, He L, Dittmar P, Neef R, Chen J, and Schubart UK (1997) The microtubule-destabilizing activity of metablastin (p19) is controlled by phosphorylation. *J Biol Chem,* **272,** 8129-8132.

54. Hosoya H, Ishikawa K, Dohi N, and Marunouchi T (1996) Transcriptional and post-transcriptional regulation of pr22 (Op18) with proliferation control. *Cell Struct Funct,* **21,** 237-243.

55. Howell B, Larsson N, Gullberg M, and Cassimeris L (1999) Dissociation of the tubulin-sequestering and microtubule catastrophe-promoting activities of oncoprotein 18/stathmin. *Mol Biol Cell,* **10,** 105-118.

56. Iancu C, Mistry SJ, Arkin S, and Atweh GF (2000) Taxol and anti-stathmin therapy: a synergistic combination that targets the mitotic spindle. *Cancer Res,* **60,** 3537-3541.

57. Jimbo T, Kawasaki Y, Koyama R, Sato R, Takada S, Haraguchi K, and Akiyama T (2002) Identification of a link between the tumour suppressor APC and the kinesin superfamily. *Nat Cell Biol,* **4,** 323-327.

58. Jourdain L, Curmi P, Sobel A, Pantaloni D, and Carlier MF (1997) Stathmin: a tubulin-sequestering protein which forms a ternary T2S complex with two tubulin molecules. *Biochemistry,* **36,** 10817-10821.

59. Juwana JP, Henderikx P, Mischo A, Wadle A, Fadle N, Gerlach K, Arends JW, Hoogenboom H, Pfreundschuh M, and Renner C (1999) EB/RP gene family encodes tubulin binding proteins. *Int J Cancer,* **81,** 275-284.

60. Kabsch W and Vandekerckhove J (1992) Structure and function of actin. *Annu Rev Biophys Biomol Struct,* **21,** 49-76.

61. Kaplan KB, Burds AA, Swedlow JR, Bekir SS, Sorger PK, and Nathke IS (2001) A role for the Adenomatous Polyposis Coli protein in chromosome segregation. *Nat Cell Biol,* **3,** 429-432.

62. Kim AJ and Endow SA (2000) A kinesin family tree. *J Cell Sci,* **113 Pt 21,** 3681-3682.

63. Kinoshita K, Arnal I, Desai A, Drechsel DN, and Hyman AA (2001) Reconstitution of physiological microtubule dynamics using purified components. *Science,* **294,** 1340-1343.

64. Korenbaum E and Rivero F (2002) Calponin homology domains at a glance. *J Cell Sci,* **115,** 3543-3545.

65. Kosco KA, Pearson CG, Maddox PS, Wang PJ, Adams IR, Salmon ED, Bloom K, and Huffaker TC (2001) Control of microtubule dynamics by Stu2p is essential for spindle orientation and metaphase chromosome alignment in yeast. *Mol Biol Cell,* **12,** 2870-2880.

66. Kull FJ, Sablin EP, Lau R, Fletterick RJ, and Vale RD (1996) Crystal structure of the kinesin motor domain reveals a structural similarity to myosin. *Nature,* **380,** 550-555.

67. Kusch J, Meyer A, Snyder MP, and Barral Y (2002) Microtubule capture by the cleavage apparatus is required for proper spindle positioning in yeast. *Genes Dev,* **16,** 1627-1639.

68. Larsson N, Marklund U, Gradin HM, Brattsand G, and Gullberg M (1997) Control of microtubule dynamics by oncoprotein 18: dissection of the regulatory role of multisite phosphorylation during mitosis. *Mol Cell Biol,* **17,** 5530-5539.

69. Lawler S (1998) Microtubule dynamics: if you need a shrink try stathmin/Op18. *Curr Biol,* **8,** R212-R214.

70. Lee L, Tirnauer JS, Li J, Schuyler SC, Liu JY, and Pellman D (2000) Positioning of the mitotic spindle by a cortical-microtubule capture mechanism. *Science,* **287,** 2260-2262.

71. Li F and Higgs HN (2003) The mouse Formin mDia1 is a potent actin nucleation factor regulated by autoinhibition. *Curr Biol,* **13,** 1335-1340.

72. Liakopoulos D, Kusch J, Grava S, Vogel J, and Barral Y (2003) Asymmetric loading of Kar9 onto spindle poles and microtubules ensures proper spindle alignment. *Cell,* **112,** 561-574.

73. Ligon LA, Shelly SS, Tokito M, and Holzbaur EL (2003) The microtubule plus-end proteins EB1 and dynactin have differential effects on microtubule polymerization. *Mol Biol Cell,* **14,** 1405-1417.

74. Longtine MS and Bi E (2003) Regulation of septin organization and function in yeast. *Trends Cell Biol,* **13,** 403-409.

75. Longtine MS, DeMarini DJ, Valencik ML, Al-Awar OS, Fares H, De VC, and Pringle JR (1996) The septins: roles in cytokinesis and other processes. *Curr Opin Cell Biol,* **8,** 106-119.

76. Louie RK, Bahmanyar S, Siemers KA, Votin V, Chang P, Stearns T, Nelson WJ, and Barth AI (2004) Adenomatous polyposis coli and EB1 localize in close proximity of the mother centriole and EB1 is a functional component of centrosomes. *J Cell Sci,* **117,** 1117-1128.

77. Luduena RF (1998) Multiple forms of tubulin: different gene products and covalent modifications. *Int Rev Cytol,* **178,** 207-275.

78. Luo XN, Mookerjee B, Ferrari A, Mistry S, and Atweh GF (1994) Regulation of phosphoprotein p18 in leukemic cells. Cell cycle regulated phosphorylation by p34cdc2 kinase. *J Biol Chem,* **269,** 10312-10318.

79. Lutjens R, Igarashi M, Pellier V, Blasey H, Di PG, Ruchti E, Pfulg C, Staple JK, Catsicas S, and Grenningloh G (2000) Localization and targeting of SCG10 to the trans-Golgi apparatus and growth cone vesicles. *Eur J Neurosci,* **12,** 2224-2234.

80. Maney T, Hunter AW, Wagenbach M, and Wordeman L (1998) Mitotic centromere-associated kinesin is important for anaphase chromosome segregation. *J Cell Biol,* **142,** 787-801.

81. Marklund U, Larsson N, Gradin HM, Brattsand G, and Gullberg M (1996) Oncoprotein 18 is a phosphorylation-responsive regulator of microtubule dynamics. *EMBO J,* **15,** 5290-5298.

82. Maucuer A, Moreau J, Mechali M, and Sobel A (1993) Stathmin gene family: phylogenetic conservation and developmental regulation in Xenopus. *J Biol Chem,* **268,** 16420-16429.

83. Mayordomo I and Sanz P (2002) The Saccharomyces cerevisiae 14-3-3 protein Bmh2 is required for regulation of the phosphorylation status of Fin1, a novel intermediate filament protein. *Biochem J,* **365,** 51-56.

84. McNally FJ and Thomas S (1998) Katanin is responsible for the M-phase microtubule-severing activity in Xenopus eggs. *Mol Biol Cell,* **9,** 1847-1861.

85. Melander GH, Marklund U, Larsson N, Chatila TA, and Gullberg M (1997) Regulation of microtubule dynamics by Ca2+/calmodulin-dependent kinase IV/Gr-dependent phosphorylation of oncoprotein 18. *Mol Cell Biol,* **17,** 3459-3467.

86. Menendez M, Rivas G, Diaz JF, and Andreu JM (1998) Control of the structural stability of the tubulin dimer by one high affinity bound magnesium ion at nucleotide N-site. *J Biol Chem,* **273,** 167-176.

87. Mickey B and Howard J (1995) Rigidity of microtubules is increased by stabilizing agents. *J Cell Biol,* **130,** 909-917.

88. Mimori-Kiyosue Y, Grigoriev I, Lansbergen G, Sasaki H, Matsui C, Severin F, Galjart N, Grosveld F, Vorobjev I, Tsukita S, and Akhmanova A (2005) CLASP1 and CLASP2 bind to EB1 and regulate microtubule plus-end dynamics at the cell cortex. *J Cell Biol,* **168,** 141-153.

89. Mimori-Kiyosue Y, Shiina N, and Tsukita S (2000) The dynamic behavior of the APC-binding protein EB1 on the distal ends of microtubules. *Curr Biol,* **10,** 865-868.

90. Mitchison T and Kirschner M (1984) Dynamic instability of microtubule growth. *Nature,* **312,** 237-242.

91. Mori N and Morii H (2002) SCG10-related neuronal growth-associated proteins in neural development, plasticity, degeneration, and aging. *J Neurosci Res,* **70,** 264-273.

92. Moritz M and Agard DA (2001) Gamma-tubulin complexes and microtubule nucleation. *Curr Opin Struct Biol,* **11,** 174-181.

93. Muller DR, Schindler P, Towbin H, Wirth U, Voshol H, Hoving S, and Steinmetz MO (2001) Isotope-tagged cross-linking reagents. A new tool in mass spectrometric protein interaction analysis. *Anal Chem,* **73,** 1927-1934.

94. Nakagawa H, Koyama K, Murata Y, Morito M, Akiyama T, and Nakamura Y (2000) EB3, a novel member of the EB1 family preferentially expressed in the central nervous system, binds to a CNS-specific APC homologue. *Oncogene,* **19,** 210-216.

95. Nakamura M, Zhou XZ, and Lu KP (2001) Critical role for the EB1 and APC interaction in the regulation of microtubule polymerization. *Curr Biol,* **11,** 1062-1067.

96. Niethammer P, Bastiaens P, and Karsenti E (2004) Stathmin-tubulin interaction gradients in motile and mitotic cells. *Science,* **303,** 1862-1866.

97. Nogales E, Whittaker M, Milligan RA, and Downing KH (1999) High-resolution model of the microtubule. *Cell,* **96,** 79-88.

98. Nogales E, Wolf SG, and Downing KH (1998) Structure of the alpha beta tubulin dimer by electron crystallography. *Nature,* **391,** 199-203.

99. Ozon S, El MS, and Sobel A (1999) Differential, regional, and cellular expression of the stathmin family transcripts in the adult rat brain. *J Neurosci Res,* **56,** 553-564.

100. Ozon S, Maucuer A, and Sobel A (1997) The stathmin family -- molecular and biological characterization of novel mammalian proteins expressed in the nervous system. *Eur J Biochem,* **248,** 794-806.

101. Palazzo AF, Joseph HL, Chen YJ, Dujardin DL, Alberts AS, Pfister KK, Vallee RB, and Gundersen GG (2001) Cdc42, dynein, and dynactin regulate MTOC reorientation independent of Rho-regulated microtubule stabilization. *Curr Biol,* **11,** 1536-1541.

102. Pereira G and Schiebel E (1997) Centrosome-microtubule nucleation. *J Cell Sci,* **110 (Pt 3),** 295-300.

103. Pierre P, Pepperkok R, and Kreis TE (1994) Molecular characterization of two functional domains of CLIP-170 in vivo. *J Cell Sci,* **107 (Pt 7),** 1909-1920.

104. Pigino G, Paglini G, Ulloa L, Avila J, and Caceres A (1997) Analysis of the expression, distribution and function of cyclin dependent kinase 5 (cdk5) in developing cerebellar macroneurons. *J Cell Sci,* **110 (Pt 2),** 257-270.

105. Popov AV, Pozniakovsky A, Arnal I, Antony C, Ashford AJ, Kinoshita K, Tournebize R, Hyman AA, and Karsenti E (2001) XMAP215 regulates microtubule dynamics through two distinct domains. *EMBO J,* **20,** 397-410.

106. Ravelli RB, Gigant B, Curmi PA, Jourdain I, Lachkar S, Sobel A, and Knossow M (2004) Insight into tubulin regulation from a complex with colchicine and a stathmin-like domain. *Nature,* **428,** 198-202.

107. Rehberg M and Gräf R (2002) Dictyostelium EB1 is a genuine centrosomal component required for proper spindle formation. *Mol Biol Cell,* **13,** 2301-2310.

108. Rickard JE and Kreis TE (1990) Identification of a novel nucleotide-sensitive microtubule-binding protein in HeLa cells. *J Cell Biol,* **110,** 1623-1633.

109. Rogers SL, Rogers GC, Sharp DJ, and Vale RD (2002) Drosophila EB1 is important for proper assembly, dynamics, and positioning of the mitotic spindle. *J Cell Biol,* **158,** 873-884.

110. Roos G, Brattsand G, Landberg G, Marklund U, and Gullberg M (1993) Expression of oncoprotein 18 in human leukemias and lymphomas. *Leukemia,* **7,** 1538-1546.

111. Rosin-Arbesfeld R, Ihrke G, and Bienz M (2001) Actin-dependent membrane association of the APC tumour suppressor in polarized mammalian epithelial cells. *EMBO J,* **20,** 5929-5939.

112. Rowlands DC, Williams A, Jones NA, Guest SS, Reynolds GM, Barber PC, and Brown G (1995) Stathmin expression is a feature of proliferating cells of most, if not all, cell lineages. *Lab Invest,* **72,** 100-113.

113. Sato M, Vardy L, Angel GM, Koonrugsa N, and Toda T (2004) Interdependency of fission yeast Alp14/TOG and coiled coil protein Alp7 in microtubule localization and bipolar spindle formation. *Mol Biol Cell,* **15,** 1609-1622.

114. Saunders W, Hornack D, Lengyel V, and Deng C (1997) The Saccharomyces cerevisiae kinesin-related motor Kar3p acts at preanaphase spindle poles to limit the number and length of cytoplasmic microtubules. *J Cell Biol,* **137,** 417-431.

115. Scheel J, Pierre P, Rickard JE, Diamantopoulos GS, Valetti C, van der Goot FG, Haner M, Aebi U, and Kreis TE (1999) Purification and analysis of authentic CLIP-170 and recombinant fragments. *J Biol Chem,* **274,** 25883-25891.

116. Schuyler SC and Pellman D (2001) Microtubule "plus-end-tracking proteins": The end is just the beginning. *Cell,* **105,** 421-424.

117. Schwartz K, Richards K, and Botstein D (1997) BIM1 encodes a microtubule-binding protein in yeast. *Mol Biol Cell,* **8,** 2677-2691.

118. Segerman B, Holmfeldt P, Morabito J, Cassimeris L, and Gullberg M (2003) Autonomous and phosphorylation-responsive microtubule-regulating activities of the N-terminus of Op18/stathmin. *J Cell Sci,* **116,** 197-205.

119. Sellers JR (1999) Unphosphorylated crossbridges and latch: smooth muscle regulation revisited. *J Muscle Res Cell Motil,* **20,** 347-349.

120. Sells MA, Pfaff A, and Chernoff J (2000) Temporal and spatial distribution of activated Pak1 in fibroblasts. *J Cell Biol,* **151,** 1449-1458.

121. Shiina N, Gotoh Y, Kubomura N, Iwamatsu A, and Nishida E (1994) Microtubule severing by elongation factor 1 alpha. *Science,* **266,** 282-285.

122. Shiina N, Gotoh Y, and Nishida E (1992) A novel homo-oligomeric protein responsible for an MPF-dependent microtubule-severing activity. *EMBO J,* **11,** 4723-4731.

123. Slep KC, Rogers SL, Elliott SL, Ohkura H, Kolodziej PA, and Vale RD (2005) Structural determinants for EB1-mediated recruitment of APC and spectraplakins to the microtubule plus end. *J Cell Biol*.

124. Smith DP, Jones S, Serpell LC, Sunde M, and Radford SE (2003) A systematic investigation into the effect of protein destabilisation on beta 2-microglobulin amyloid formation. *J Mol Biol,* **330,** 943-954.

125. Sobel A (1991) Stathmin: a relay phosphoprotein for multiple signal transduction? *Trends Biochem Sci,* **16,** 301-305.

126. Steinmetz MO, Goldie KN, and Aebi U (1997) A correlative analysis of actin filament assembly, structure, and dynamics. *J Cell Biol,* **138,** 559-574.

127. Steinmetz MO, Kammerer RA, Jahnke W, Goldie KN, Lustig A, and van Oostrum J (2000) Op18/stathmin caps a kinked protofilament-like tubulin tetramer. *EMBO J,* **19,** 572-580.

128. Strelkov SV, Herrmann H, and Aebi U (2003) Molecular architecture of intermediate filaments. *Bioessays,* **25,** 243-251.

129. Stukenberg PT (2003) Mitosis: long-range signals guide microtubules. *Curr Biol,* **13,** R848-R850.

130. Su LK, Burrell M, Hill DE, Gyuris J, Brent R, Wiltshire R, Trent J, Vogelstein B, and Kinzler KW (1995) APC binds to the novel protein EB1. *Cancer Res,* **55,** 2972-2977.

131. Tirnauer JS and Bierer BE (2000) EB1 proteins regulate microtubule dynamics, cell polarity, and chromosome stability. *J Cell Biol,* **149,** 761-766.

132. Tirnauer JS, Canman JC, Salmon ED, and Mitchison TJ (2002a) EB1 targets to kinetochores with attached, polymerizing microtubules. *Mol Biol Cell,* **13,** 4308-4316.

133. Tirnauer JS, Grego S, Salmon ED, and Mitchison TJ (2002b) EB1-microtubule interactions in Xenopus egg extracts: role of EB1 in microtubule stabilization and mechanisms of targeting to microtubules. *Mol Biol Cell,* **13,** 3614-3626.

134. Tirnauer JS, O'Toole E, Berrueta L, Bierer BE, and Pellman D (1999) Yeast Bim1p promotes the G1-specific dynamics of microtubules. *J Cell Biol,* **145,** 993-1007.

135. Tournebize R, Andersen SS, Verde F, Doree M, Karsenti E, and Hyman AA (1997) Distinct roles of PP1 and PP2A-like phosphatases in control of microtubule dynamics during mitosis. *EMBO J,* **16,** 5537-5549.

136. Tournebize R, Popov A, Kinoshita K, Ashford AJ, Rybina S, Pozniakovsky A, Mayer TU, Walczak CE, Karsenti E, and Hyman AA (2000) Control of microtubule dynamics by the antagonistic activities of XMAP215 and XKCM1 in Xenopus egg extracts. *Nat Cell Biol,* **2,** 13-19.

137. Tran PT, Walker RA, and Salmon ED (1997) A metastable intermediate state of microtubule dynamic instability that differs significantly between plus and minus ends. *J Cell Biol,* **138,** 105-117.

138. van BM, Drechsel D, and Hyman A (2003) Stu2p, the budding yeast member of the conserved Dis1/XMAP215 family of microtubule-associated proteins is a plus end-binding microtubule destabilizer. *J Cell Biol,* **161,** 359-369.

139. Vasquez RJ, Gard DL, and Cassimeris L (1999) Phosphorylation by CDK1 regulates XMAP215 function in vitro. *Cell Motil Cytoskeleton,* **43,** 310-321.

140. Walczak CE (2000) Microtubule dynamics and tubulin interacting proteins. *Curr Opin Cell Biol,* **12,** 52-56.

141. Walker RA, Inoue S, and Salmon ED (1989) Asymmetric behavior of severed microtubule ends after ultraviolet-microbeam irradiation of individual microtubules in vitro. *J Cell Biol,* **108,** 931-937.

142. Walker RA, O'Brien ET, Pryer NK, Soboeiro MF, Voter WA, Erickson HP, and Salmon ED (1988) Dynamic instability of individual microtubules analyzed by video light microscopy: rate constants and transition frequencies. *J Cell Biol,* **107,** 1437-1448.

143. Wallon G, Rappsilber J, Mann M, and Serrano L (2000) Model for stathmin/OP18 binding to tubulin. *EMBO J,* **19,** 213-222.

144. Wang HW and Nogales E (2005) Nucleotide-dependent bending flexibility of tubulin regulates microtubule assembly. *Nature,* **435,** 911-915.

145. Waterman-Storer CM and Salmon ED (1998) How microtubules get fluorescent speckles. *Biophys J,* **75,** 2059-2069.

146. Wen Y, Eng CH, Schmoranzer J, Cabrera-Poch N, Morris EJ, Chen M, Wallar BJ, Alberts AS, and Gundersen GG (2004) EB1 and APC bind to mDia to stabilize microtubules downstream of Rho and promote cell migration. *Nat Cell Biol,* **6,** 820-830.

147. Wittmann T, Bokoch GM, and Waterman-Storer CM (2004) Regulation of microtubule destabilizing activity of Op18/stathmin downstream of Rac1. *J Biol Chem,* **279,** 6196-6203.

VI. Acknowledgements

I would like to acknowledge all those who have helped me during my doctoral work. Special thanks to my supervisor, Michel Steinmetz, whose vision created the project, whose focus permitted me to take part, and whose advice kept me on the pathway to completion. Throughout my doctoral work he encouraged me to develop independent thinking and research skills. He continually stimulated my analytical thinking and greatly assisted me in scientific writing.

I am also very grateful for having an exceptional doctoral committee and wish to thank Fritz Winkler, Joachim Seelig and Nikolaus Amrhein for their continual support and encouragement.

I very much appreciate the friendly and supportive working atmosphere provided by the past and present members of Biomolecular Research group. I would like to thank Antonietta Gasperina for being so organized and helpful to introduce me to lab instruments, Dirk Kostrewa for introducing me to X-ray crystallography techniques and John Missimer for critical reading of the thesis.

Finally, I'd like to thank my family. My father and mother were a constant source of support. I'm grateful to my sister and brother for their encouragement and enthusiasm. I'm especially grateful to my wife and best friend, Annapurna, for her patience and for her help in keeping my life in proper perspective and balance.

I extend my gratitude to Swiss National Science Foundation for providing financial support which made this work possible.

VII. Curriculum vitae

Mr. Honnappa Srinivas

Paul Scherrer Institut
Biomolecular Research, Structural Biology
OFLC/106CH-5232 Villigen PSI, Switzerland
Tel.: +41-56-310-4785 / Fax: +41-56-310-5288
e-mail: srinivas.honnappa@psi.ch

PERSONAL INFORMATION:

Nationality: Indian
Date of Birth: 12th May 1975
Place of Birth: Bangalore, India
Civil status: Married

EDUCATION

MSc, in Biochemistry, Basic Science and Humanities College, University of Agricultural Sciences, Bangalore, 2000.

BSc, in Agriculture, University of Agricultural Sciences, Bangalore, 1997.

PROFESSIONAL EXPERIENCE

PhD. Student, Biomolecular Research, Structural Biology, Paul Scherrer Institut, Villigen PSI, Switzerland. 2002 - present.

Research Assistant, under Prof. Avadesh Surolia, Molecular Biophysics Unit, Indian Institute of Science, Bangalore, India. 2001-2002

TEACHING ACTIVITIES

Supervision of Integrated Ph.D students, while working as a Research Assistant in Molecular Biophysics Unit, Indian Institute of Science, Bangalore

---

Phd. Qualifying Exams passed at ETH, Zurich

Biochemistry by Prof. Ari Helenius and Prof. Yves Barral
(30 min oral exam)

Molecular Biology and Biophysics by Prof. Nenad Ban
(30 min oral exam)

LANGUAGE

English: Excellent oral/written

INVITED TALK AND ORAL PRESENTATIONS

2003: Thermodynamics of the Op18/stathmin-tubulin interaction. Cytomeet, 2004, Bern, Switzerland.

2004: Structural insights into the EB1 interaction modes with APC and Dynactin at microtubule ends. 18th Regional Meeting on X-ray Crystallography of Biomacromolecules, 2004, Einsiedeln, Switzerland.

2004: Structural insights into the EB1-APC interaction. EMBL, Heidelberg. (Invited)

LIST OF PUBLICATIONS

Honnappa, S., Jahnke, W., Seelig, J. and Steinmetz M.O. 2005. Control of intrinsically disordered stathmin function by multisite phosphorylation. *Submitted*

Kammerer, R.A., Kostrewa, D., Progias, P., **Honnappa, S**., Avilla, D., Lustig A., Winkler, F.K., Pieters, J. and Steinmetz, M.O. 2005, A conserved trimerization motif controls the topology of short coiled coils. *Proc. Natl. Acad. Sci USA.* **102**, 13891-96.

Honnappa, S., John, C.M., Kostrewa, D., Winkler, F.K. and Steinmetz M.O**.** 2005. Structural insights into the EB1-APC interaction. *EMBO J.* **24**, 261-269.

Honnappa, S., Cutting, B., Jahnke, W., Seelig, J. and Steinmetz M.O. 2003. Thermodynamics of the Op18/stathmin-tubulin interaction. *J. Biol. Chem.* **278**, 38926-38934.

Kapoor, M*****.,**Honnappa, S***., Eaazhisai, K., Gemma, E., Ellgaard, L., Oscarson, S., Helenius, A. and Surolia, A. 2003. Interactions of substrate with calreticulin, an endoplasmic reticulum chaperone. *J. Biol. Chem.* **278**, 6194–6200. (***equally contributed**)
